A Fine Detail Physicochemical Depositional Model for Devonian Organic-Rich Mudstones: A Petrographic Study of the Hare Indian and Canol Formations, Central Mackenzie Valley, Northwest Territories

by

Sara Kimberley Biddle

A thesis submitted in partial fullfillment of the requiremnts for the degree of

Master of Science

Department of Earth and Atmospheric Sciences

University of Alberta

Abstract

The Hare Indian and Canol Formations, making up part of the Horn River Group (HRG) in the Northwest Territories, primarily consist of organic-rich mudstones deposited during the Middle to Late Devonian. The formations were previously considered to represent marine basin fill accumulated in an oxygen starved distal shelf setting, evidenced by the organic-rich character, pyrite content, and lack of macro-scale bioturbation. The depositional model, paleo-oxygenation interpretations, and methods of organic carbon preservation presented in this study are in contrast to previous assumptions of the Horn River Group mudstones. Detailed petrographic sedimentological and ichnological analyses were carried out on thin sections taken from several cored HRG intervals. These organic-rich mudstones contain eight distinct microfacies representing four main sedimentation processes: (1) pelagic suspension settling, (2) plug-like sediment gravity flows, (3) surge and surge-like low density turbidity currents, and (4) debrites. Pelagic suspension settling dominated in distal quiet waters out of the reach of persistent storm influence. Debrites, plug-like flows, and low density turbidite processes represent a continuum, where storm influence is the dominant driver in sediment delivery.

Several morphologically distinct microscopic biogenic-sedimentary structures (*i.e.* ichnofossils) have been identified throughout the HRG mudstones, indicative of sediment pore waters that were at least periodically partially oxygenated. Evaluation of total organic carbon (TOC) content against bioturbation and microfacies interpretation suggest that persistent anoxia was not the dominant factor in organic carbon preservation but is rather a result of a combination of heightened sedimentation and burial rates and possible amplified rates of primary production.

Preface

This thesis is original work by Sara Kimberley Biddle and contains material that has been submitted for publication and has involved collaboration with other researchers. This study was completed in conjunction with Maya LaGrange's PhD thesis and Brette Harris's MSc. thesis, which focus on the geochemical properties and chemostratigraphy of the Canol and Hare Indian Formations, respectively.

A modified version of Chapter 2 has been submitted for publication as:

Biddle, S., LaGrange, M., Harris, B., Fiess, K., Terlaky, V., Macquaker, J., Gingras, M., "A Fine Detail Physiochemical Depositional Model for Devonian Organic-Rich Mudstones: A Petrographic Study of the Hare Indian and Canol Formations, Central Mackenzie Valley, Northwest Territories" in Sedimentary Geology. Data collection, interpretations, and manuscript composition were conducted by myself. Co-authors aided in interpretations, and provided discussion of research, editorial guidance and feedback.

"Possibly many may think that the deposition and consolidation of fine-grained mud must be a very simple matter, and the results of little interest. However, when carefully studied experimentally it is soon found to be so complex a question, and the results dependent on so many variable conditions, that one might feel inclined to abandon the inquiry, were it not that so much of the history of our rocks appears to be written in this language."

-Henry Clifton Sorby, 1908

Acknowledgments

My past three years with the Ichnology Research Group have truly been a life changing experience. I have expanded my geologic knowledge immensely, and made many new friends in the process. I have several people to thank who have contributed in some way to this study, and have made my time at the University of Alberta as exciting and successful as it has been.

First and foremost, I would like to thank my supervisor Murray Gingras. Thank you for taking me on as a Master's student, entrusting me with this project, providing guidance, advice and support throughout this process. Thank you for allowing me the opportunity to travel to many wonderful places, through field work, conferences, and field trips. I would also like to thank George Pemberton, for although it was cut short, the time we spent discussing potential micro-burrows will be cherished memories. Thank you to JP Zonneveld for the many thought-provoking discussions during my time in the lab (whether they were thesis related, or about life in general).

A massive thank you to my teamDEVO crew, Brette Harris and Maya LaGrange, for the countless ways you've helped and supported this project, from collecting all the XRF data, helping cut thin section samples, providing very much appreciated input on this project on a weekly basis. An even bigger thank you for the friendship.

Thank you, Murray Gingras, Maya LaGrange, Brette Harris, Viktor Terlaky and Johnathan Rocheleau for making the 2018 field work season one to remember.

Thank you Patricia Gonzalez for teaching me the ways of the lab microscope and how to take brilliant pictures. Thank you to Marilynn Huff for all the help with the petrography lab microscopes, and always helping when the scopes were being finicky. Thank you to Darrin Molinaro for being my go-to lab helper and saving the day with exam materials and your extensive knowledge of eclass. Thank you Melissa Dillion for all your help near the end of this journey, and for ironing out all the wrinkles in my transition to a PhD.

Thank you to my Ichnology Research Group family for all the laughs both in Edmonton and on field trips: Arzu Acikelli, Waqar Ahmad, Shaliza Ali, Daniel Baker, Scott Botterill, Qi Chen, Chenyang Feng, Carolyn Furlong, Patricia Gonzalez, Brette Harris, Calla Knudson, Maya LaGrange, Skye Lybbert, Scott Melnyk, Reed Meyers, Cole Ross, Chundi Shan, and Sheridan Sigstad. Thank you to Kathryn Fiess, Viktor Terlaky and Johnathan Rocheleau from the Northwest territories Geological Survey for the support and input. Thank you to Joe Macquaker for lending his extensive knowledge of mudstone depositional processes, diagenetic effects, and petrographic expressions. Thank you to Viktor Terlaky for schooling me on all things turbidites.

Thank you Murray Gingras, JP Zonneveld, and Pilar Lecumberri-Sanchez for being on my committee.

I would like to thank Husky Energy, Paramount Resources, and ConocoPhillips for the generous donation of the cores and available thin sections. Thank you to the Northwest Territories geological Survey for providing funding for this project.

Thank you to Kerrie Bann and Stuart Tye for introducing me to the wonderful world of geology.

Finally, I would like to thank the people that have always been there for me. To my parents Kim and Sue Biddle, thank you for the endless love and support throughout my entire life. Thank you to my twin sister, Melissa, for being my roomie since day 1, putting up with all my rants, and always being down for a snack run. To my sister Callie and brother Keifer for providing endless laughs. Thank you to Bailey Tye for the all the unfailing love and support throughout this process and encouraging me from afar. This project would not have been possible without all of you.

Table of Contents

List of Tables

List of Figures

Chapter 1

Introduction

1.1 General Overview

The Middle to Late Devonian of North America was characterized by widespread deposition of organic-rich mud, resulting in units such as the well-known Eagleford Shale, Bakken Formation, and the Western Canadian Sedimentary Basin's Duvernay Formation. Perhaps lesser known is the Horn River Group (HRG) in the Northern Canadian Mainland Sedimentary Basin. The HRG spans the length of the NW to SE trending Mackenzie Mountains and Mackenzie Plain in the Northwest Territories, and is split into the basal Hare Indian Formation, then locally the Ramparts Formation, and the uppermost Canol Formation.

Initial interest in the HRG stemmed from the discovery of a conventional oil field within the Kee Scarp Reef Member of the Ramparts Formation, as a result of oil prospecting during the second world war (Tassonyi, 1969). Imperial oil Corp. developed this northern oilfield at what was to become the community of Norman Wells. The organic rich fine-grained Canol Formation is younger and locally age-equivalent to the Ramparts Formation (Kabanov & Gouwy, 2017), and has been identified as the source rock for the Norman Wells oil field (Snowdon, Brooks, Williams, & Goodarzi, 1987). Recent renewed interest in explorations of the HRG came about with the advent of horizontal drilling and the potential use of the organic rich Canol Formation and Bluefish Member of the Hare Indian Formation as unconventional reservoirs.

1.2 Significance and Rational

Physico-chemical depositional conditions of organic-rich fine-grained sedimentary successions have in the last several decades become a popular topic of detailed petrographic analyses. This is owing to the various roles they play in petroleum systems (*i.e.* variously as sources, and/or unconventional reservoirs). Despite their importance in the petroleum system, mudrocks are still relatively poorly understood.

Conventional interpretations of mudrock depositional settings are typically limited to slow hemipelagic suspension settling in anoxic or euxinic bottom waters. More recent studies have identified small scale (petrographic) primary sedimentary structures in mudstone units that appear plane parallel laminated in hand sample and outcrop (*e.g.* Schieber, 1994, 1998; Abbott, 2000; Schieber, 2007; Macquaker, Bentley, & Bohacs, 2010; Schieber, Southard, & Schimmelmann, 2010). Microbioturbation has also been identified in organic-rich mudstone units (*e.g.* Macquaker & Taylor, 1996; Schieber, 2003; Egenhoff & Fishman, 2013) that were previously thought to preclude burrowing organisms. These findings have revealed that fine-grained deposits are more depositionally dynamic than previously understood, with more complex paleoredox conditions than persistent and pervasive anoxia.

Both the Hare Indian and Canol Formations have not previously been evaluated at the petrographic level, and existing interpretations of paleo-depositional conditions at the sediment-water interface are generalized, even as recent as 2020, into broad categories of stagnant water anoxia/euxinia (Tassonyi, 1969; Kabanov et al., 2020). A lack of heterogeneity at the lithofacies (macroscopic) scale does little to aid in fine-detail interpretations of physico-chemical stresses present at and just below the sediment water interface. The availability of high-quality cored data from Hare Indian and Canol Formations presents a great opportunity to re-evaluate the physico-chemical depositional conditions of these organic rich mudstone units using a contemporary point of view. The wealth of data also allows us to study how trace fossil morphology, abundance, diversity, and other associated characteristics reflect low-oxygen depositional settings, and how these oxygen-related traits can be applied to other fine-grained reservoirs in hopes of estimating extents of depositional oxygenation.

The main goal of this study was to identify small scale fluctuations in both physical and chemical stresses affecting the sediment-water interface at the time of deposition, using petrographic fabric analysis (*e.g.* microscopic ichnological and sedimentological characteristics) in conjunction with existing geochemical proxies. A secondary goal was to further develop criteria for the identification and interpretation of bioturbation in the context of associated physical sedimentary structures, and chemical proxies for seafloor redox conditions.

1.3 Geologic Background

Deposition of Early to Middle Devonian aged strata in the present-day Mackenzie Mountains and Mackenzie Plain occurred on the Western margin of Devonian North America. During this time the area surrounding and including the Mackenzie Plain was split into the northeast Peel Shelf (present day Peel Plain and Peel Plateau), southeast Mackenzie Platform or Mackenzie Shelf (present day Mackenzie Mountains and Mackenzie Plain), northwestern Porcupine Platform (present day Eagle Plain), and southwest Selwyn Basin (present day Slewn Mountains) (Morrow, 2018). The Porcupine platform was separated from the eastern shelves by the N-S trending Richardson Trough (present day Richardson Mountains, along the northern Northwest Territories – Yukon boarder) (Figure 1.1) (Morrow, 2018; Pugh, 1983). The Early to Middle Devonian was characterized by extensive platform reef growth in the shallow warm-water areas of the Mackenzie and Porcupine shelves, with siliciclastic (mainly mudstone) deposition in the deeper Richardson Trough (Morrow, 2018). Middle Devonian strata reflect a shift from this carbonate-dominated stable passive margin deposition and carbonate platform growth on the Mackenzie Shelf, to siliciclastic deposition of the Horn River Group (Tassonyi, 1969; Bassett & Stout, 1967; Morrow, 2018; Muir, 1988; Pugh, 1983; Uyeno, 1979).

The Hume Formation was the final carbonate platform to develop on the Mackenzie Shelf before the onset of deposition of the Horn River Group, and represents what has been interpreted as normal marine platform growth along a low profile shallow water setting (Tassonyi, 1969). Deposition of the HRG began with the Givetian aged Hare Indian Formation, which onlaps the extensive shallow-water platform carbonates of the underlying Hume Formation (Tassonyi, 1969; Bassett & Stout, 1967; Morrow, 2018; Pugh, 1983; Uyeno, 1979). The Hare Indian Formation represents aggradation and westward progradation of a clastic wedge, and is subdivided into the lower organic rich mudstone Bluefish Member and upper argillaceous mudstone

Bell Creek Member. The Hare Indian has previously been described as an extensive mud-delta with thickening mudbanks and shallowing waters northward (Tassonyi, 1969; Kabanov, Fallas, & Deblonde, 2016). Tassonyi (1969) postulated that the relatively thin organic rich unit (Bluefish Member) represented deposition and thinning along the flanks of the mudbanks into deeper poorly oxygenated waters with reduced sedimentation, whereas the calcareous grey mudstone unit (Bell Creek Member) represents thick mud accumulations in more oxygenated waters. Progradation and thick accumulations of Bell Creek mudstone above the Bluefish Member in the Norman Wells area resulted in a shallow water subaqueous high upon which growth of the Late Givetian – Early Frasnian Ramparts carbonate platform initiated (Kabanov & Gouwy, 2017). The Ramparts Formation is subdivided into the lower limestone Ramparts carbonate platform, the middle argillaceous and bituminous Carcajou Member, and the upper limestone Kee Scarp Member (sometimes referred to as the Reef Member) (Dixon, 1984; Kabanov & Gouwy, 2017). Bell Creek sediments thin to the South and West of the Norman Wells area. Contemporaneously with the Ramparts, organic-rich fine-grained Canol Formation accumulated conformably above the thinner Bell Creek Member in areas to the south and west where the Ramparts Formation is non-existent. Continued transgression lead to the Canol Formation onlapping and eventually capping the Kee Scarp reef (and the Carcajou marker in more northern areas where the Kee Scarp was not developed) (Bassett & Stout, 1967; Dixon, 1984; Kabanov & Gouwy, 2017; Muir, 1988; Pyle & Gal, 2016). Late Frasnian progradation of the Imperial Formation siltstones indicate the end of HRG deposition. The units were subsequently deformed during the Late Cretaceous-Paleocene Laramide orogeny (Norris & Yorath, 1981).

1.4 Study Area

The study area for this project is restricted to the southern portion of the Central Mackenzie Valley (also referred to as the Mackenzie Plain) (Figure 1.1) and is bordered by the Franklin Mountains to the East and Mackenzie Mountains to the West. In the Central Mackenzie Valley area are five wells with cored intervals that were used for this study. From NW to SE the wells are ConocoPhillips Loon Creek O-06, ConocoPhillips Mirror Lake N-20, Husky Little Bear N-09, Husky Little Bear H-64, and MGM Shell East Mackay I-78. The southeast corner of the study area is at 64°47' N, 125°43'W (MGM Shell East Mackay I-78 core) and the northwest corner is at 65°05'N, 127°00'W (ConocoPhillips Loon Creek O-06 core).

1.5 Previous Work

1.5.1 Mudstone Petrography

Historical petrographic analyses of mudstone units, or intercalated mudstone beds within coarser-grained units, were commonly confined to crude grainsize and mineralogic composition estimates (Folk, 1960, 1962; Schieber & Zimmerle, 1998). This was owing to the difficulty associated with producing high quality thin sections from such fine-grained rock samples, which easily disaggregated in the preparation process and resultant thin sections generally appeared quite dark due to high clay and organic matter content; and, probably even more so, because of a general lack of interest in these rock types as the focus was on understanding their coarser-grained carbonate and sandstone counterparts (Schieber & Zimmerle, 1998; Schieber, 1989). Since then, preparation techniques of mudstone thin sections have improved significantly and understanding the intricacies of mudstone units has become an economic necessity (*e.g.* owing to the advent of horizontal drilling and their housing of economic metal deposits), leading to a proliferation of petrographic mudstone studies.

Some of the first studies that included a focus on the petrography of previously ignored mudstone units were completed by Folk in 1960 and 1962, where he described in detail the characteristics of the mudstone beds within the Appalachian Tuscarora, Rochester, and McKenzie Formations. In his studies he described the Rochester Shale and "shaley" interbedded intervals in the other formations in terms of grainsize, textural maturity, and mineral composition. Although petrographic analysis of fine-grained rocks has been in use since Folk's work, the use of mudstone microfacies in the same fashion of sandstone lithofacies had lagged behind. The concept of petrographic microfacies was introduced by Brown in 1943 and was first applied to mudstone units by Schieber in 1989 and 1994, where he integrated thin section scale observations of paleontological, sedimentologic and other petrographic features to classify several different facies in seemingly compositionally homogeneous mudstone units. Since then petrographic analysis has become a popular method of mudstone investigation (*e.g.* Cuomo & Bartholomew, 1991; Dawson, 2000; Hart, Macquaker, & Taylor, 2013; Hickey & Henk, 2007; Knapp, McMillan, & Harris, 2017; Konitzer, Davies, Stephenson, & Leng, 2014; Lazar, Bohacs, Macquaker, Schieber, & Demko, 2015; Milliken & Olson, 2017; Newport, Jerrett, Taylor, Hough, & Worden, 2018; Plint, Macquaker, & Varban, 2012; Schieber, 1999, 2001, 1989, 1998, 2007; Soyinka & Slatt, 2008; Wignall, 1989).

The growing popularity of petrographic mudstone analysis has also sparked debate on how to best classify these fine-grained rocks. Conventionally the term "shale" has been employed for most fine-grained outcrops and cores that showed any fissility, while "mudstone" was reserved for more blocky units. However, upon detailed petrographic inspection these units can be quite heterogeneous. The dichotomy between macroscale homogeneity and microscale heterogeneity makes naming of such units tricky. Earlier petrographic studies used compositional variation as the main variable to categorize fine-grained rocks. Schieber (1989) proposed assessing texture and fabric characteristics in conjunction with compositional variation to differentiate between compositionally identical units, similar to how textural and fabric classifications are critical in carbonate units (compositionally homogenous). More recent proposals on mudstone nomenclature suggest using a root term based on grain size, and modified by variety of petrographically identifiable features such as bedding character, mineralogic composition, biogenic components, and alteration features (Lazar et al., 2015; Macquaker & Adams, 2003). This is in contrast to macroscale mudstone naming schemes that may employ colour, organic content, mechanical properties, silt content, carbonate content, and visible sedimentary structures (Schieber, 1989). If conventional naming schemes were to be employed, most individual microfacies would be classified into the same broad lithofacies (*e.g.* Schieber, 1989).

1.5.2 Mudstone Depositional Processes

The conditions leading to accumulation of fine-grained sediments are conventionally understood to be deposition in quiescent or low energy settings. The limited depth of wave penetration in deep marine waters, such as those in distal shelf positions, has led to the generally accepted assumption that ancient shelfal sediments were deposited in such quiescent low energy settings. The parallel laminated nature of such mudstone units at macroscales seemingly confirmed this assumption.

Advancements in analytical techniques (*e.g.* high-powered slow-motion cameras used to capture results of flume experiments, SEM imaging for analysis of matrix compositions) have sparked a re-thinking of the depositional processes responsible for such marine fine-grained mudstone units. Flume experiments have led to the identification of unidirectional ripples forming from homogenous kaolinite clay suspensions (Schieber, Southard, & Thaisen, 2007), micro-scale rip-up clasts forming from semi-consolidated clay (Schieber et al., 2010), and several types of low-density sediment gravity flows forming thin beds composed of clay and silt (Baas, Best, Peakall, & Wang, 2009; Sumner, Talling, & Amy, 2009). Petrographic analysis of several mudstone units has revealed the presence of seemingly plane parallel laminae that thin and swell - interpreted as the result of variable bed load deposition under bottom currents (Schieber, 2009), lenticular fabrics identical to the rip-up clasts described in flume experiments (Plint et al., 2012; Schieber et al., 2010; Ulmer-Scholle, Scholle, Schieber, & Raine, 2014), scour surfaces and normally graded beds indicating increased bottom current energies and waning flow deposition (*e.g.* Ulmer-Scholle et al., 2014), and micro-scale lag deposits (Egenhoff & Fishman, 2013; Schieber & Zimmerle, 1998; Schieber, 1994), wave-enhanced sediment gravity flows (Macquaker, Bentley, & Bohacs, 2010), and tempestites (Abbott, 2000). All of these features seemingly contradict previous notions of shelfal muds forming form quiescent suspension settling depositional processes.

1.5.3 Low Oxygen Ichnology and Paleoredox Proxies

Previous attempts to define paleo-oxygenation levels have employed sediment colour to mark oxidation boundaries (Lyle, 1983), foraminifera characteristics (Harman, 1964), and geochemical analyses including: carbon-sulfur ratios (Berner & Raiswell, 1983), sulfur isotopes (Gautier, 1986), and rare element concentrations (Anderson, Lehuray, Fleisher, & Murray, 1989). Although each of these methods have their strengths, ichnological analysis, as a proxy for paleo-oxygenation, is one of the most accurate ways to define both relative magnitudes and temporal extents of oxygenation events. This is because benthic organisms act as in situ records of basin conditions.

Previous well-cited studies evaluating the employment of ichnological characteristics as paleoredox proxies have resulted in the identification of four separate biofacies that are inherently linked to dissolved oxygen content of the bottom waters (aerobic, dysaerobic, anaerobic, and anoxic) (Rhoads & Morse, 1971; Byers, 1977). The quantitative boundaries of available dissolved oxygen (DO2) for each biofacies are as follows: >1.0 mL/L = aerobic (oxic), 0.1 – 1.0 mL/L = dysaerobic (dysoxic), 0.0 - 0.1 mL/L = anerobic (dysoxic), and 0.0 mL/L anoxic (Byers, 1977; Rhoads & Morse, 1971). The general consensus is that with declining rates of DO2, infaunal organism body size, ichnogenera diversity, depth of burrow penetration, and bioturbation intensity all decline (Rhoads & Morse, 1971; Rhoads, 1975; Byers, 1977; Bromley & Ekdale, 1984; Savrda & Bottjer, 1984, 1986, 1987; Bottjer & Savrda, 1990; Bromley, 1996; Gingras, MacEachern, & Dashtgard, 2011). No bioturbation is present under anoxic and/or euxinic conditions, due to the respiratory requirements of the burrowing organisms. These previous studies have utilized tiering or burrow cross cutting relationships, depth of burrow penetration, and burrow size to elucidate relative paleo-oxygenation (Ekdale, Muller, & Novak, 1984; Savrda & Bottjer, 1986, 1987).

These particular studies have been widely cited and used to interpret the paleoredox conditions of many clastic rocks. However, these studies only take into account identified macroscopic burrows. A gap in knowledge currently exists between these paleoredox interpretations associated with such macroscopic burrows, and paleoredox conditions associated with burrows constructed by microscopic organisms.

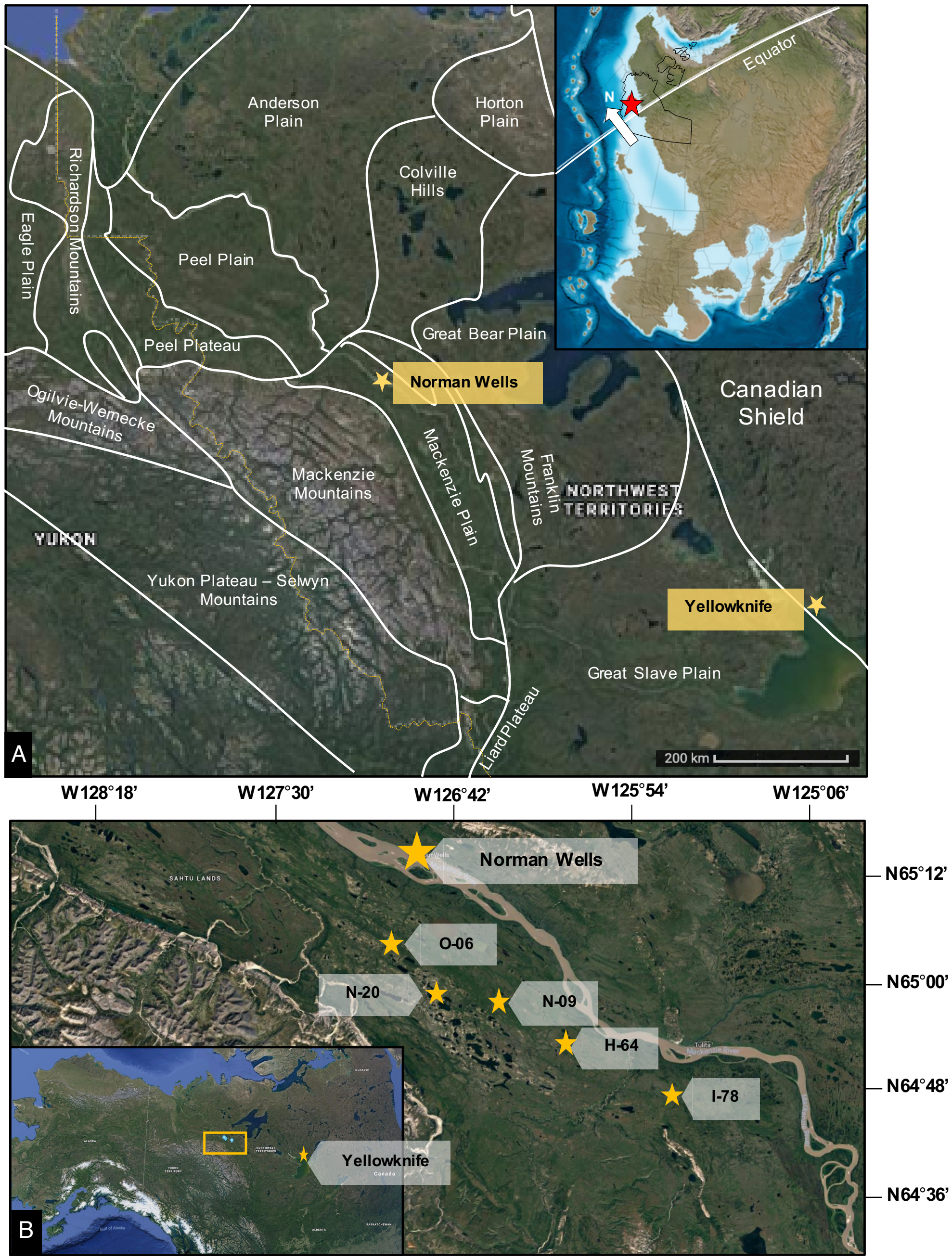

Figure 1.1: Study area in the Central Mackenzie Valley, Northwest Territories, Canada. (A) Physiographic regions in the Northwest Territories (adapted from (Morrow, 2018). Upper left corner shows paleogeographic map of study area (NWT outlined in black); map available through deeptimemaps.com (Blakey). (B) Core locations within the Central Mackenzie Valley/along the Mackenzie Plain. Images modified from Google Maps.

Chapter 2

A Fine Detail Physiochemical Depositional Model for Devonian Organic-Rich Mudstones: A Petrographic Study of the Hare Indian and Canol Formations, Central Mackenzie Valley, Northwest Territories

2.1 Introduction

Physio-chemical depositional conditions of ancient marine organic-rich fine-grained sedimentary successions have in the last several decades become a popular topic of detailed petrographic analyses, owing to the various roles they play in petroleum systems (*i.e.* variously as sources, and/or unconventional reservoirs) (Macquaker, Taylor, & Gawthorpe, 2007; Macquaker, Bentley, & Bohacs, 2010; Aplin & Macquaker, 2011; Ghadeer & Macquaker, 2011; Schieber, 2011; Plint et al., 2012; Egenhoff & Fishman, 2013). This stems from their inherent small-scale (millimeter to sub-millimeter) variability associated with being thin bedded, laminated, and altered by bioturbation and diagenesis. Despite their importance in the petroleum system mudrocks are still relatively poorly understood. Conventional interpretations are typically limited to slow hemipelagic suspension settling in oxygen depleted bottom waters. More recent studies have identified small scale (petrographic) primary sedimentary structures and features in mudstones that appear plane parallel laminated in hand sample and outcrop, including low-angle ripple foresets (Schieber, Southard, & Thaisen, 2007), intrabasinal rip-up clasts (Schieber et al., 2010), sub-millimeter thick scour and lag deposits (Schieber, 1994; Schieber & Zimmerle, 1998), wave-enhanced sediment gravity flows (Macquaker, Bentley, & Bohacs, 2010), intercalated clay-dominated and silt-dominated ripple features (Yawar & Schieber, 2017), normally graded sub-centimeter laminae (Ghadeer & Macquaker, 2011), and tempestites (Abbott, 2000). Such findings have revealed that fine-grained deposits are more depositionally dynamic than previously understood. As well, microbioturbation has been identified in organic-rich mudstones (*e.g.* Macquaker & Taylor, 1996; Egenhoff & Fishman, 2013) that were previously thought to preclude endobenthic animals, and Dashtgard et al. (2015) and Dashtgard and MacEachern (2016) found a lack of macrobenthic organisms in modern-day shelfal muds with only slightly reduced oxygenation. Together these findings indicate more complex paleoredox conditions than persistent and pervasive anoxia for the deposition of seemingly unbioturbated organic-rich mudstone units.

The identification of bioturbation in mudrocks is exceedingly important. In marine settings, penetrative bioturbation is only produced by animals. There are other organisms that can move on top of sediments, such as motile protists (Matz, Frank, Marshall, Widder, & Johnsen, 2008), but they lack the musculature to move through sediment. So, bioturbation can be taken as direct evidence of the presence dissolved oxygen in the bottom waters. In other words, the presence or absence of bioturbation and the size of the trace makers should provide a very useful proxy for identifying the lowermost limits of oxygenation at the sea floor. A significant problem in identifying bioturbation is discriminating bioturbate texture from other types of soft-sediment deformation. Using petrographic observations from the mudstone-dominated Hare Indian and Canol formations, in the Northwest Territories of Canada, this paper aims to further develop criteria for the identification and interpretation of bioturbation in the context of associated physical sedimentary structures. Additionally, comparisons between identified biogenic characteristics, geochemical proxies, and total organic carbon contents are analysed for potential merit in elucidating seafloor paleoredox conditions and estimating TOC trends. This paper identifies the physical and biogenic structures for which the highest degree of confidence is associated (*i.e.* examples where an interpretation of a sedimentary feature as a trace fossil is parsimonious). Using the ichnological dataset, we thereby identify small-scale fluctuations in both the physical and chemical conditions at and just below the sediment-water interface during the deposition of organic-rich mudstones in the Middle to Late Devonian Canol and Hare Indian Formations.

Some of the largest oil and gas producing zones in North America are fine-grained organic-rich mudstones (*e.g.* the Eagle Ford Shale in Texas and the Niobrara Formation in Colorado). Both the Canol Formation and the Bluefish Member of the Hare Indian Formation are organic-rich siliceous mudstones that have the potential to be economically viable unconventional reservoirs (*e.g.* Fraser, Allen, Lane, & Reyes, 2011). Current oil-in-place estimates for the Canol Formation and Bluefish Member are 144.825 and 46.346 billion barrels respectively (NTGS and NEB, 2015). Because of their economic significance, it is important to understand the nuances of these fine-grained hydrocarbon resources and how they form.

2.2 Geological Background

The Horn River Group (HRG) in the Central Mackenzie Valley of the Northwest Territories (Canada) represents late Givetian to early Frasnian deposition (Uyeno, 1979), and includes the Hare Indian, Ramparts, and Canol Formations (Figure 2.1). The Hare Indian and Canol Formations are organic-rich mudstones, whereas the Ramparts Formation consists predominantly of limestone. All three formations are considered to represent deposition along a passive continental margin distal shelf (shelf-slope transition), atop the Mackenzie Platform (Bassett & Stout, 1967; Pugh, 1983; Muir, 1988), and were subsequently deformed during the Late Cretaceous-Paleocene Laramide orogeny (Norris & Yorath, 1981).

The Hare Indian Formation, which represents westward progradation and aggradation of a clastic wedge, is subdivided into the lower dark grey mudstone Bluefish Member and upper gray mudstone Bell Creek Member. A drowning unconformity separates the Bluefish Member from the underlying Hume Formation, a limestone unit comprising carbonate platform deposits (Muir, Wong, & Wendte, 1985). The Bell Creek Member is thought to represent deltaic influence, resulting in thickening mudbanks and shallowing waters northward (*e.g.* Kabanov, Fallas, & Deblonde, 2016). The overlying lower Ramparts Formation consists of limestone and is interpreted to be carbonate platform deposits. The platform developed above the Bell Creek sediments under localized shallow-water. The upper Ramparts comprises patch reef complexes, and is known as the Kee Scarp Reef complex (Dixon, 1984). Limestones of the Ramparts Formation are not present in the study area. The lower Canol Formation mudstones are coeval with the Ramparts carbonates, representing fine-grained basinal deposition (Pyle & Gal, 2016).

Continued transgression lead to the Canol Formation sediments onlapping and eventually overlying the Ramparts Formation (Muir, 1988; Dixon, 1984). Late Frasnian progradation of the Imperial Formation siltstones indicate the end of HRG deposition.

The Ramparts carbonate platform and overlying Kee Scarp Reef act as the reservoir in the conventional Normal Wells oil pool. The organic-rich mudstones of the Canol Formation are thought to be the source of oil for the pool (Snowdon et al., 1987).

2.3 Study Area

The study area for this project is restricted to the southern portion of the Central Mackenzie Valley (also referred to as the Mackenzie Plain) (Figure 2.2) and is bordered by the Franklin Mountains to the East and Mackenzie Mountains to the West. In the Central Mackenzie Valley area are five wells with cored intervals that were used for this study. From NW to SE the wells are ConocoPhillips Loon Creek O-06, ConocoPhillips Mirror Lake N-20, Husky Little Bear N-09, Husky Little Bear H-64, and MGM Shell East Mackay I-78. The southeast corner of the study area is at 64°47' N, 125°43'W (MGM Shell East Mackay I-78 core) and the northwest corner is at 65°05'N, 127°00'W (ConocoPhillips Loon Creek O-06 core).

2.4 Methods

The descriptions and interpretations for the Horn River Group depositional model presented herein are the result of detailed ichnological and sedimentological petrographic analyses. Petrographic analysis is one of the best methods to study organic rich mudstones, which owing to their very fine grain size (<62.5 μm), absence of lithologic contrast, and dark colour, inherently lack macroscopically discernible sedimentological features and bioturbation. Analysis was carried out on 243 thin sections taken from five drill cores made available by Husky Energy (Little Bear N-09 and H-64), ConocoPhillips (Mirror Lake N-20 and Loon Creek O-06), and Paramount Energy (MGM Shell East MacKay I-78). Thin sections were cut extra-thin (approximately 20 μm thickness), to best show the sedimentary fabric of fine-grained organic-rich samples. Some thin sections from the N-09 and H-64 (Husky Little Bear cores) were cut as wedges, thinning from 30 µm to 0 µm laterally; a choice made by Husky to best show fine detail sedimentary fabrics, without being obscured completely by opaque organic matter. Textural attributes of the thin sections at 20x, 100x, and 600x were described and photographed using a Nikon Eclipse 50i POL microscope and Nikon DS Fi1 camera. Sedimentological structures such as mineralogy, grain-size distribution, small-scale sedimentary features such as bedding and laminae, and early diagenetic features such as pyrite habit and carbonate character were noted. Percentage comparison tables were used to visually estimate the percentages of sand, silt, and clay. Biogenic features such as bioturbation intensities (measured as percentage of sediment that has been biogenically reworked, *e.g.* 0-100%) (A. M. Taylor & Goldring, 1993), ichnofossil morphotypes present (diversity), and burrow size (diameter), as well as microfossil elements including type, composition, and abundance were also noted. The microfacies present were described using the nomenclature scheme of Lazar et al., (2015).

A Zeiss Sigma 300 VP-FESEM scanning electron microscope (SEM) was used on both polished and unpolished uncovered thin sections and core fragment samples, to observe variations in microfacies microtextural elements and grain relationships (*e.g.* clay platelet arrangements). Molybdenum and vanadium concentration data were collected at 10 cm intervals (where possible) using a Niton XL3t portable x-ray fluorescence (XRF) analyzer gun, with analysis times of 180 seconds. Three standards (USGS brush creek shale, an in-house standard for the Canol Formation, and SiO2) were run every 10th sample during XRF data collection for quality control. Prior to XRF data collection, the cores were cleaned with water to remove surface residue. Total organic carbon data for the N-09 and I-78 cores were collected by Core Laboratories using the GRI (Gas Research Institute) crushed shale method and by Weatherford Laboratories using Rock-eval pyrolysis, respectively. Ichnological data in the form of bioturbation intensity (in percent), burrow diameter size, trace fossil diversity, and size-diversity index (SDI), was compared to both molybdenum and vanadium bulk composition (ppm) and enrichment factors (EFX = (X/Al) sample /(X/Al) average shale). In this study, the Post-Archean Australian Average Shale (PASS) (S. R. Taylor & McLennan, 1985) was used as the average sample in EF calculations because the HRG intervals in question are mudstone units. Enrichment factors >1 represent samples enriched relative to the average, and <1 represents elemental depletion (Tribovillard, Algeo, Lyons, & Riboulleau, 2006).

2.5 Results

2.5.1 Ichnology

Earlier works on the HRG units have reported limited instances of bioturbation (*e.g.* Kabanov, Fallas, & Deblonde, 2016; Kabanov, Gouwy, Lawrence, Weleschuk, & Chan, 2016). It was previously thought that the mudstones only yield pelagic fauna, and are devoid of epi- and in-faunal trace fossils (Williams, 1983). Inspection of available thin sections shows biogenic reworking, with varying trace fossil morphology, abundance, and diversity. All burrows described in this study were first and foremost identified in the thin sections during petrographic analysis, however, photographic enhancement of the darker colored clay-rich lithosomes does show enhanced evidence for biogenic reworking in some thin sections (e.g. Figures 9B, C). Burrow outlines in all figures (e.g. Figures 4, 5, 9, 11) were done with the intent to be as objective as possible, only outlining and counting the most obvious features as potential burrows.

Identifying microbioturbation in organic-rich fine-grained sediments has several challenges. Defects during the manufacturing of thin sections (scratches, grain-plucking, and bubbles within the epoxy), differential compaction of the sedimentary rock (around micro-concretions, fecal pellets, and intraclastic aggregates), and dewatering structures could all be wrongly interpreted as microscopic trace fossils. A lack of lithologic contrast within the sediments, substantial compaction volumes of water-rich muds (up to 90%) and significant diagenetic alteration may act to obscure any existing micro-burrows. Despite these challenges, five morphologically distinct micro-burrow types are identified in the HRG sediments and are classified by their morphological attributes (*i.e.* burrow orientation, fill type, presence or absence of burrow linings). Methods of micro-tracefossil identification are outlined in Figure 2.3. A morphological classification scheme is presented herein, as the identified traces do not fit in to any accepted trace fossil classification schemes.

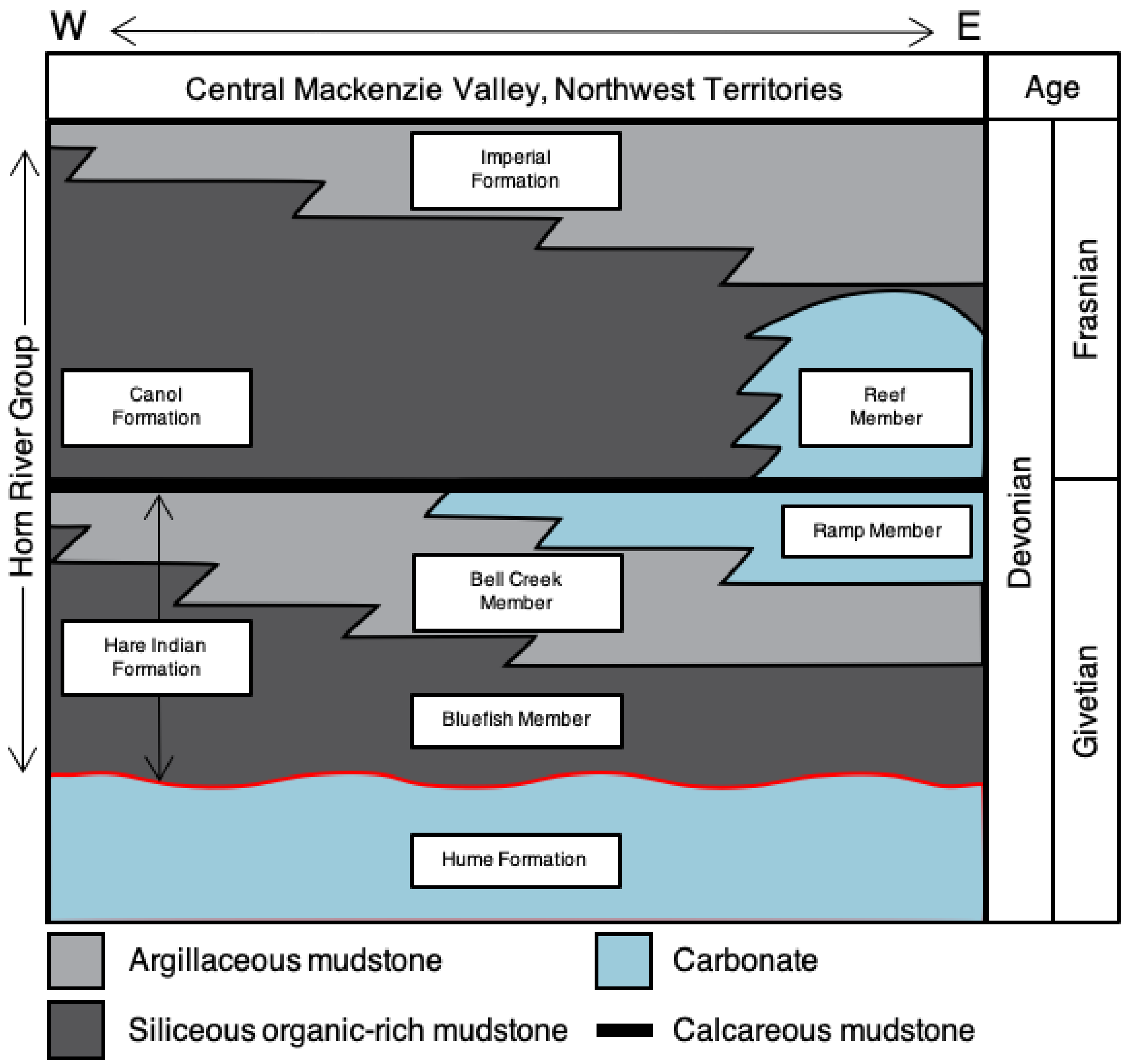

Figure 2.1: Chronostratigraphic cross-section of the Middle to Late Devonian Horn River Group running west to east through the Norman Wells area (modified from LaGrange et al., 2019).

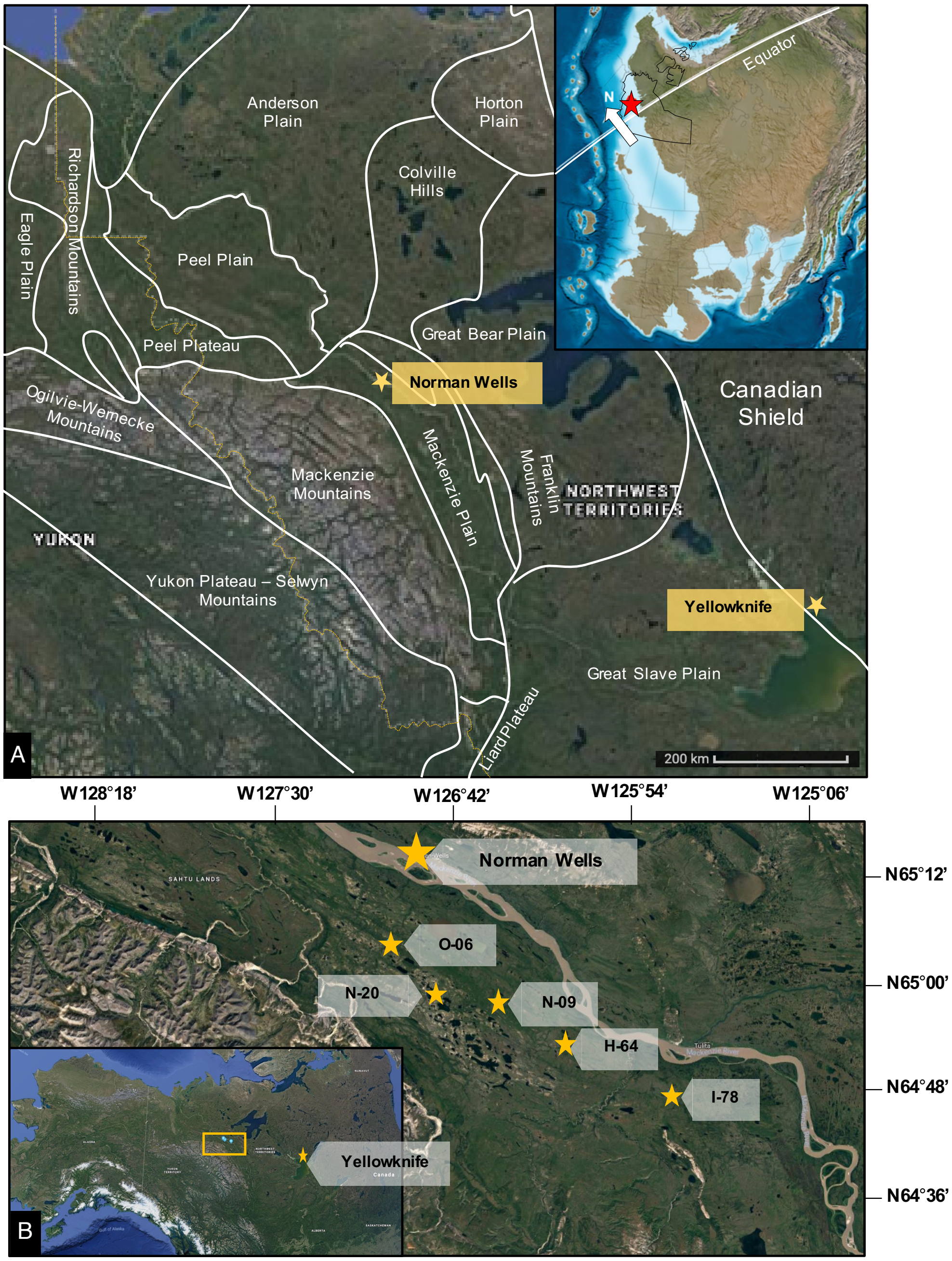

Figure 2.2: Study area in the Central Mackenzie Valley, Northwest Territories, Canada. (A) Physiographic regions in the Northwest Territories (adapted from (Morrow, 2018). Upper left corner shows paleogeographic map of study area (NWT outlined in black); map available through deeptimemaps.com (Blakey). (B) Core locations within the Central Mackenzie Valley/along the Mackenzie Plain. Images modified from Google Maps.

	Sedimentary Feature	Interpretation
1	**Vertical or horizontal structures that disrupt laminae**	Discontinuous horizontal homogenization along bedding planes, representing sinuosity or oblique cuts through horizontal trace fossils
2	**Paired parallel strings of aligned grains**	Pseudo-linings created by grain-selective feeding or migration of coarse-grained fraction to burrow margins during burrow construction
3	**Circular, sinuous, or punctuated lighter-colored zones**	Biogenic homogenization of ingested sediment and preferential removal of darker-colored organic matter
4	**Focussed authigenic alteration**	Selective or preferential pyritization or calcification of tubes/burrow structures

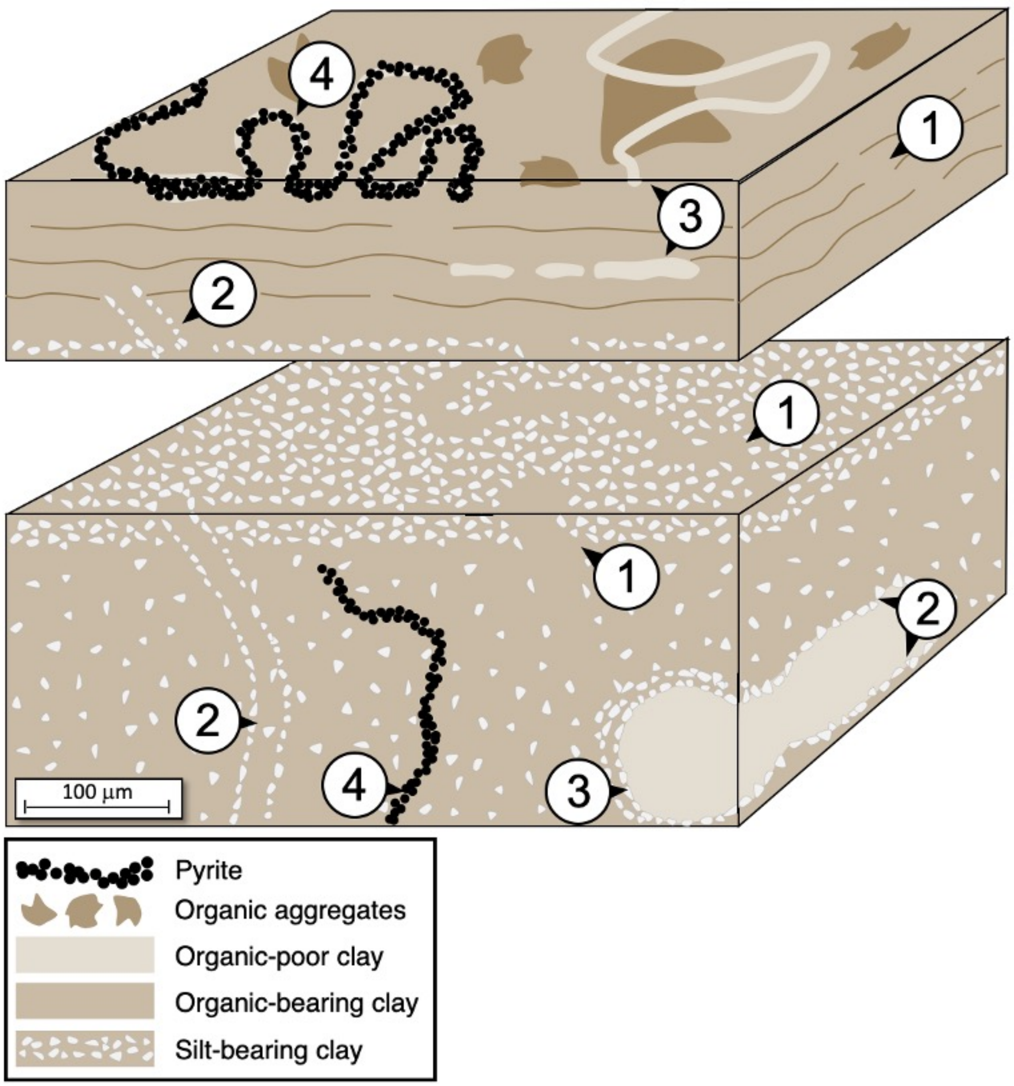

Figure 2.3: Table of sedimentary characteristics used to identify microburrows in thin section and block diagram illustration of recognition characteristics of meiofaunal microburrows in fine-grained clay-dominated ancient sediments. Labels 1-4 correspond to the listed identification features.

Bioturbated sediments in thin section are recognized by disturbances of the laminated sediment, including vertical interruptions in horizontal laminae (where the disturbances can be traced as continuous vertical features below, through, and above the laminae; Figures 2.4A, B; 2.5B, C), discontinuous horizontal homogenization along bedding planes (representing sinuosity or oblique cuts through horizontal trace fossils) (Figure 2.4G, H), vertically or horizontally aligned outsized grains, paired parallel strings of grains interpreted as linings (Figure 2.5E, F), and general sediment homogenization. Most putative trace fossils are more easily identified in silt-rich sediments, where there is enhanced lithologic contrast between undisturbed matrix sediments containing relatively high proportions of silt-sized grains and burrow fills which are generally devoid of silt-sized grains (*i.e.* contain a preferential clay fill).

Two vertical and inclined burrow types were identified (Figure 2.4). The first is classified as inclined-to-vertical unlined meniscate backfilled trace fossils, with diameters ranging from 20 – 60 μm m (Figure 2.4A, B). These burrows display inclined or vertical orientations with respect to bedding and show an organized meniscate backfill. They are distinguished from matrix sediments by vertical interruptions of horizontal lamination, and by the concave nature of the meniscate backfill. The second vertical trace fossil type is an escape trace (fugichnia) (Figure 2.4C, D), resulting from the upward movement of an organism in response to rapid sedimentation (Bromley, 1996). Fugichnia is the only burrow type classified by ethological nomenclature and is identified by the downward warping laminae in otherwise undisturbed sediments. Fugichnia range from 50 – 100 μm m in diameter. Both vertical trace fossil types are rare, and only identified in a handful of samples.

Two burrow types are horizontal burrows and are classified as (1) lined burrows (Figure 2.4E, F) and (2) unlined burrows (Figure 2.4G, H). Both horizontal burrow types have the same diameter range of 50 – 120 μm. In the lined variants, linings are thin (<10 μm thick) and dark in colour. Linings are composed of tangentially aligned and compressed clays and organic matter originating from the host sediment and are often pyritized. In some cases, concentric linings are preserved (Figure 2.4E, F). Both burrow types appear to be unbranching, have homogenized fill, and are characteristically lighter in colour than the host sediment.

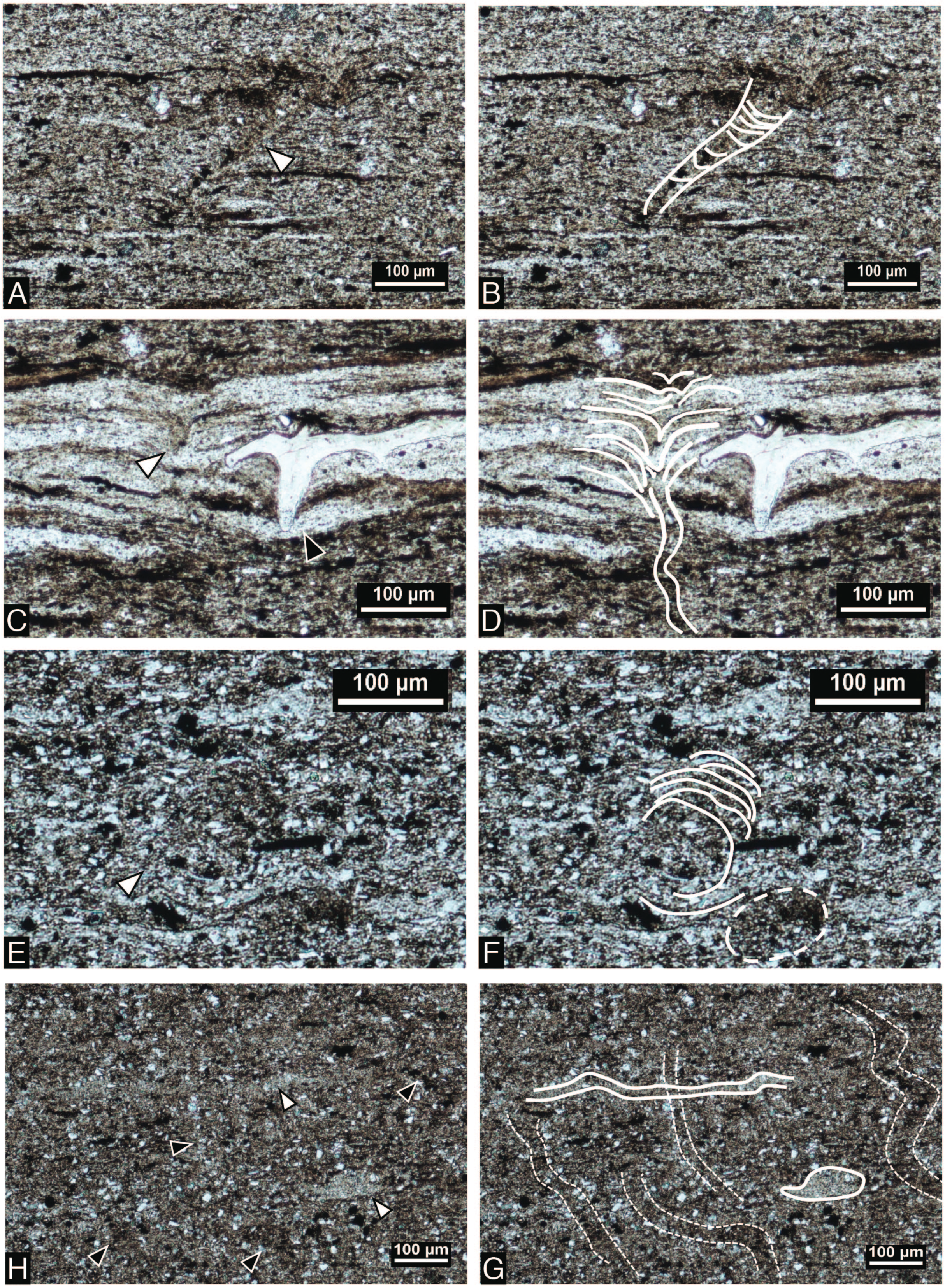

A
100 μm
B
100 μm
C
100 μm
D
100 μm
E
100 μm
F
100 μm
H
100 μm
G
100 μm

Figure 2.4: Photomicrographs of micro-trace fossils identified in HRG mudstones. All photomicrographs are perpendicular to bedding. (A) inclined-to-vertical unlined meniscate backfilled trace (white arrow) (N-09 1692.58 m). (B) Tracing of the burrow in (A). (C) Fugichnia (white arrow) next to a conodont fragment (black arrow) (N-09 1692.58 m). (D) Tracing of fugichnia in (C). (E) Cross section of a concentrically lined horizontal burrow (white arrow) (N-09 1703.54 m). (F) Tracing of the concentric linings in (E). (G) Longitudinal slice (upper white arrow) and cross section (lower white arrow) through two unlined burrows. Sinuous shafts are dictated by black arrows (N-09 1670.87 m). (H) Tracings of burrows in (G).

The final and most abundant burrow type is classified as small sinuous burrows (Figure 2.5). These burrows can be vertical (Figure 2.5A – D) or horizontal (Figure 2.5E – H) and are characterized by sinuous unbranching burrows (primarily horizontal) and shafts (primarily vertical) with a preferential clay infill or backfill (silt-sized detrital grains or aggregates are selectively omitted). Burrow diameters range from 15 – 50 μm. These sinuous burrows are most easily recognized in sediment with higher concentrations of detrital silt grains, where the silt-sized particles are shunted toward the outer margins of the burrow creating the illusion of a silt lining. These burrows are generally darker than the surrounding matrix due to an increase in the concentration of pyrite within the trace. These burrows are similar to, if not the same, as the Phycosiphon incertum type B burrows identified by Egenhoff and Fishman (2013), and are similar to the "pyritic trails" described by Schieber (2003, pg. 5).

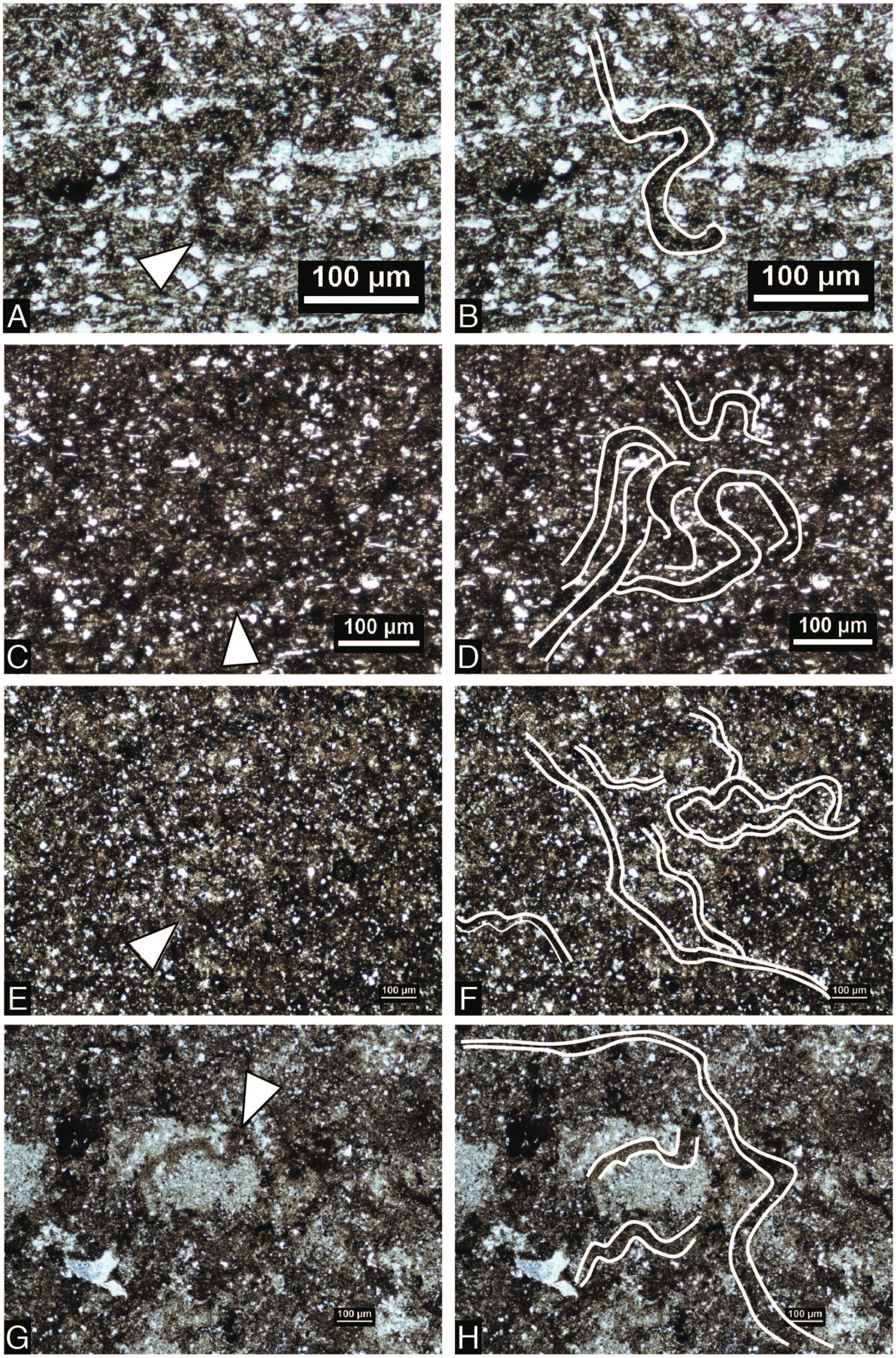
100 µm
A
100 µm
B
100 µm
C
100 µm
D
100 µm
E
100 µm
F
100 µm
G
100 µm
H

Figure 2.5: Photomicrographs of sinuous burrows within HRG mudstones. (A) Well-defined sinuous shaft (white arrow) with clear clay fill (N-09 1701.91 m). (B) Outline of the burrow in (A). (C) Several horisontal and vertical sinuous burrows within a silt-bearing claystone (one such trace denoted by arrow) (H-64 1229.84 m). (D) Outline of traces in (C). (E) Sinuous burrows along a bedding plane in a silt-bearing claystone. Arrow points to an obvious relatively straight burrow (H-64 1232.84 m). (F) Outline of the burrows in (E). (G) Sinuous burrow (arrow) cross cutting an intraclast (lighter coloured diffuse structure) along a bedding plane (I-78 1846.00 m). (H) outline of burrows in (G).

Sediments of the HRG exhibit a range of bioturbation intensities, with degrees of biogenic reworking fluctuating between different microfacies, within the same microfacies at different elevations, and even at the millimeter scale within individual microfacies occurrences (as observed in individual sections). Bioturbation intensities range from 0% to 100% and are relatively the highest in the Canol Formation when compared to the Hare Indian Formation and, where data is available, the overlying Imperial Formation.

2.5.2 Microfacies

Eight distinct microfacies have been defined based on a variety of petrographic parameters, including grain size distribution, composition, bedding characteristics and bioturbation intensities. The microfacies are: (1) Homogenous-looking radiolarian-rich siliceous fine mudstone, (2) homogeneous dolomitized argillaceous fine mudstone, (3) discontinuous wavy-parallel to homogenous-looking argillaceous fine mudstone, (4) rarely bioturbated discontinuous wavy-parallel silt-bearing fine mudstone, (5) bioturbated discontinuous wavy-parallel to homogenous-looking silt-bearing fine mudstone, (6) bioturbated discontinuous planar parallel to continuous wavy non-parallel laminated argillaceous-siliceous medium mudstone, (7) fossiliferous discontinuous to continuous wavy-parallel argillaceous fine mudstone, and (8) intraclast rich discontinuous planar parallel argillaceous fine mudstone. Microfacies characteristics are outlined in Table 2.1, microfossil data is outlined in Figure 2.6, and core photographs of each microfacies are shown in Figure 2.7. The microfacies naming scheme was developed from the terminology and classification nomenclature outlined by Lazar et al., (2015) (Figure 2.8), with a continuum classification ranging from fine mudstone (fMs), through medium mudstone (mMs), to coarse mudstone (cMs). Terms "dominated" refers to sediments composed of <90% of a constituent, "rich" refers to sediments containing 50-90% of a constituent, "bearing" refers to sediments having 10-50% of a constituent, and "poor" referring to <10% (following Macquaker & Adams, 2003).

Table 2.1: Microfacies identified in the Horn River Group mudstones.

PRIMARY SEDIMENTAION MECHANISM	MICROFACIES	NAME	TOC%	DESCRIPTION	INTERPRETATION
(S1) Pelagic suspension settling	**MF1**	**Homogenous-looking radiolarian-rich siliceous fMs**	No Data	>70% siliceous radiolarian tests and spines Commonly intercalated with thin microbial mats and argillaceous fMs beds (MF3) BI: 0% Can be recrystalized to carbonate or partially pyritized	Pelagic suspension settling in quiescent oxygen starved bottom waters during proliferation pulses
(S2) Plug-like flow dominated	**MF2**	**Homogenous-looking dolomitized argillaceous fMs**	Range: 2.2 – 4.7 **Median: 2.43**	>20% early diagenetic dolomite, most commonly ferroan rhombic dolomite <5% detrital silt Sedimentary structures and bioturbation cannot be identified due to pervasive dolomitization Rare tentaculitid fossils	Rare laminar plug-like sedimen gravity flows with long residen times, associated with poorly oxygenated sediment pore waters
	MF3	**Discontinuous wavy parallel to homogenous-looking argillaceous fMs**	1.4 – 5.7 **4.20**	<5% detrital silt Wavy-crenulated fabric Rare intraclasts BI: 0-40% Body fossils: radiolarians, conodonts, tentaculitids Diagenetic dolomite and rare euhedral pyrite	Sedimentation is dominated by plug-like flows with some low density surge and surge-like turbidity flows, associated with poorly oxygenated pore waters
	MF4	**Rarely bioturbated discontinuous wavy parallel silt-bearing fMs**	2.9 – 6.8 **4.10**	5 – 30% detrital silt Unlaminated to weakly plane parallel laminated Absent to common intraclasts rare microbial mats BI: <10% Body fossils: conodonts, agglutinated foraminifers, radiolarians, tentaculitids Common diagenetic dolomite and calcite	A mix of plug-like flows and lov density turbidity flows with poorly oxygenated sediment pore waters
(S3) Combined surge/surge-like turbidity currents, plug-like flows, and debrites	**MF5**	**Bioturbated discontinuous wavy parallel silt-bearing fMs**	3.8 – 8.7 **5.42**	5 - 30% detrital silt Rare to common intraclasts Planar to wavy laminated BI: 10-100% Body fossils: conodonts, radiolarians Diagenetic dolomite	A mix of plug-like flows and lov density turbidity flows with increased carrying capacity, associated with partially oxygenated pore waters
	MF6	**Bioturbated discontinuous planar parallel to continuous wavy non-parallel argillaceous—siliceous mMs**	4.8 – 7.7 **5.48**	>30% detrital silt grains Common intraclasts Detrital clay deposited as silt-sized clay aggregates Primary sedimentary features: undulatory scour surfaces, detrital silt and intraclast lags, normally graded silt-to-clay beds, low amplitude current ripples BI: 20-100% Body fossils: conodonts, radiolarians, agglutinated foraminifers, tentaculitids	Sedimentation dominated by surge and surge-like low densit turbidity flows, with intermitte plug-like flows, and partially oxygenated pore waters
	MF7	**Fossiliferous discontinuous to continuous wavy parallel argillaceous fMs**	5.3 – 7.7 **5.50**	10 - 100% tentaculitid fossil shells Shells are generally intact, some are fragmented Fossils are sporadic throughout (matrix supported) and/or concentrated along isolated bedding planes (grain supported) Contains bioclastic graded bedding (coarse fossil beds fining upwards to detrital clay beds) BI: 0-20%	Sedimentation represented by mixture of debrites, plug-like flows, and surge-like turbidity currents, with an oxygenated overlying water column, and subject to intense storm reworking
(S4) Proximal plug-like flows	**MF8**	**Intraclast-rich discontinuous planar parallel argillaceous fMs**	3.3 – 4.2 **4.10**	>30% Intraclasts 0 – 30% detrital silt Graded bedding, thin distal low density turbidites, and rare soft sediment deformation BI: 0-20% Body fossils: conodonts, radiolarians	Persistent plug-like flows occurring in a proximal setting where intraclasts are continuously generated

Body Fossil Type

	Radiolarians	*Conodonts*	*Tentaculitids*	*Agglutinated Foraminifers*	*Undefined microfossils*
MF1	100	0.0	0.0	6.3	0.0
MF2	5.0	15.0	35.0	10.0	0.0
MF3	21.0	21.0	2.6	18.4	13.2
MF4	24.2	24.2	18.2	15.2	6.1
MF5	12.0	28.0	16.0	20.0	32.0
MF6	4.3	43.0	17.4	26.1	13.0
MF7	0.0	5.0	100	0.0	0.0
MF8	12.0	36.0	4.0	0.0	12.0

Number of thin sections (%) in each MF containing microfossils: 90-100%, 80-89.9%, 70-79.9%, 60-69.9%, 50-59.9%, 40-49.9%, 30-39.9%, 20-29.9%, 10-19.9%, 0-9.9%

Figure 2.6: Heat map showing microfossils present within the individual microfacies. Expressed as percent of thin sections within a given microfacies found to contain at least 1 microfossil of a particular type. Map only shows if a particular microfossil was identified in a thin section, and its corresponding microfacies; not the actual abundance of each particular microfossil type within each microfacies.

Homogenous-Looking Radiolarian-Rich Siliceous Fine Mudstone (MF1)

The homogenous-looking radiolarian-rich siliceous fine mudstone microfacies (also referred to as radiolarites) (Figure 2.9) is characterized by beds and laminae made of up of >70% radiolarian tests in a sparse detrital clay matrix. Detrital silt-sized grains are absent. Individual radiolarian tests range from 50-100 μm in diameter and are generally partially compacted (ovate shape as opposed to retaining original sphericity), dissolved (have diffuse margins), and recrystallized. Tests can also be partially pyritized. Unfortunately, there was no available TOC data for this microfacies.

Radiolarian-rich bed thicknesses range from 250 μm to >3 cm (greater than the size of the thin section). Primary sedimentary features are difficult to identify due to partial dissolution and recrystallization. Remnant bedding planes can be identified in some radiolarian-rich beds (Figure 2.9A). Some radiolarian-rich deposits may be microstylolized or have thin crenulated microbial mat features within the radiolarian-rich beds/laminae or at microfacies contacts. Relatively large allochthonous radiolarian-rich deposit rip-up clasts can be seen in the N-09 core, held together by microbial mat fragments (Figure 2.9E).

Bioturbation is difficult to recognize due to the alteration of the dominant siliceous component, however some micro-burrows are obvious (arrows Figure 2.9B). Bioturbation intensities based on identified micro-burrows appear to be <10%.

Radiolarian-rich fMs is the least common microfacies throughout the Canol and are absent in the Hare Indian formation intervals. They occur only in conjunction with the homogenous-looking fine mudstones (MF3) with sharp contacts (Figure 2.9E).

Homogenous-Looking Dolomitic Argillaceous Fine Mudstone (MF2)

The homogenous-looking dolomitic argillaceous fine mudstone microfacies (Figure 2.10) is characterized by a high degree of dolomitization, ranging from 20% to 90% alteration, within a clay dominated matrix. Detrital quartz silt is present throughout the matrix in trace concentrations (<5%). Dolomite crystal sizes range from <10 μm to 150 μm, and crystals are mainly rhombic. Potassium ferricyanide stanning (blue stain) confirms that it is most commonly ferroan dolomite. Dolomite generally occurs in uniform concentrations, but some instances of this microfacies show gradation from minor dolomitization to pervasive dolomitization over several millimeters of elevation change. The colour of this microfacies under plane polarized light ranges depending on the type of stain used (potassium ferricyanide or alizarin red), the thickness of the thin section (thick cut thin sections appear darker) and the TOC content (ranges from 2.2 to 4.7%). Overall the argillaceous matrix appears moderate reddish-brown to very dusky red (dark-brown), while dolomite appears either transparent or light-blue, with colours based on the Munsell rock-colour classifications (*Geological Rock Color Chart*, 2009).

Primary sedimentary and biogenetic features are obscured by dolomitization. Remnant intraclasts can be seen in some cases (*e.g.* arrow in Figure 2.10D). This microfacies can be associated with fossiliferous zones, but bioclastic debris is mostly sparse. In some instances fossil fragments are pyritized and exhibit bedding-oblique or bedding-perpendicular orientations within the sediments (Figure 2.10D).

Discontinuous Wavy Parallel to Homogenous-Looking Argillaceous Fine Mudstone (MF3)

The discontinuous wavy parallel to homogenous-looking argillaceous fine mudstone microfacies (Figure 2.11) is unbedded to weakly-bedded at the petrographic level. In hand sample and at low magnification (20x) this microfacies appears planar parallel laminated. The wavy appearance is only visible at high powered magnifications (100x) and is best seen in instances with abundant elongate organic matter (Figure 2.11D). This microfacies is dominantly argillaceous, with rare detrital silt-sized quartz grains (<5%). The elongate organic matter is oriented parallel to bedding and is common to abundant throughout, and intraclasts are rare. Siliceous radiolarian tests are common throughout, while other micro-organism body fossils are rare (*e.g.* calcite tentaculitids and phosphatic conodonts). Micro-organism body fossils can be partially to entirely pyritized (Figure 2.11D). Framboidal pyrite is disseminated throughout the matrix but authigenic large (<100 μm) crystals of pyrite are rare throughout the microfacies. Horizontal discontinuous pyritized laminae are also present in some instances. In rare instances sand-sized carbonate nodules and irregular carbonate growths are present. This microfacies appears reddish-brown to very dusky red (dark brown) depending on the thickness of the thin section and TOC content (ranges from 1.4 – 5.7%).

Primary sedimentary structures are subtle owing to the fine grain size and lack of lithologic contrast. Bedding contacts are difficult to identify. Laminae are thin (<1 mm) and composed of a random (homogenous-appearing) distribution of clay and silt grains. Biogenic reworking can be hard to distinguish, again due to the clay-rich matrix and lack of lithologic contrast. However, burrows are most easily identified through the alignment of detrital silt along the burrow margins. Bioturbation intensities are less than 40%. Identified ichnofossil morphotypes include sinuous dark trails, tubular unlined and tubular lined burrows.

This microfacies was found to occur intercalated with the radiolarian-rich fMs (MF1), the dolomitized fMs (MF2), the silt-bearing fMs (MF4 and 5), and the fossiliferous fMs (MF7).

Rarely Bioturbated Discontinuous Wavy-Parallel Argillaceous Fine Mudstone (MF4)

The rarely bioturbated discontinuous wavy-parallel argillaceous fine mudstone microfacies (Figure 2.12) has a slight wavy appearance at high magnification (10x) and appears unbedded to weakly planar parallel bedded at low magnification (2x) and in hand sample. These mudstones contain between 5% to 30% silt-sized detrital grains (mainly quartz and some micas). The silt-sized grains are randomly distributed throughout the individual laminae. Intraclast are absent to common. Fossil fragments are rare throughout, and include calcite tentaculitids, phosphatic conodonts, and siliceous radiolarians. This microfacies can be partially dolomitized, where alteration is limited to about 10% of the surface area of thin sections. This microfacies appears reddish-brown to very dusky red (dark brown) depending on the thickness of the thin section and TOC content (ranges from 2.9 – 6.8%).

The lack of lithologic contrast in these clay-dominated thin sections makes identification of primary structures difficult. Bedding orientation is clearly denoted by preferential orientation of the elongate intraclasts (Figure 2.12A), organic matter, detrital micas, and the presence of horizontal preferentially framboidally pyritized discontinuous horizons. Bedding/laminae contacts are not always obvious, but in some cases normal grading can be identified (Figure 2.12F). Less than 30% of the sediment has been biogenically reworked in this microfacies. Elongate organic matter, when present, appears generally undisturbed (*e.g.* horizontal whispy black stringers in Figure 2.12B). The absence of lithologic contrast and poorly defined bedding contacts may play a role in obscuring true intensities of biogenic reworking.

This rarely bioturbated fMs microfacies occurs in conjunction with other microfacies of similar or slightly variable composition (MF2, 3 and 5).

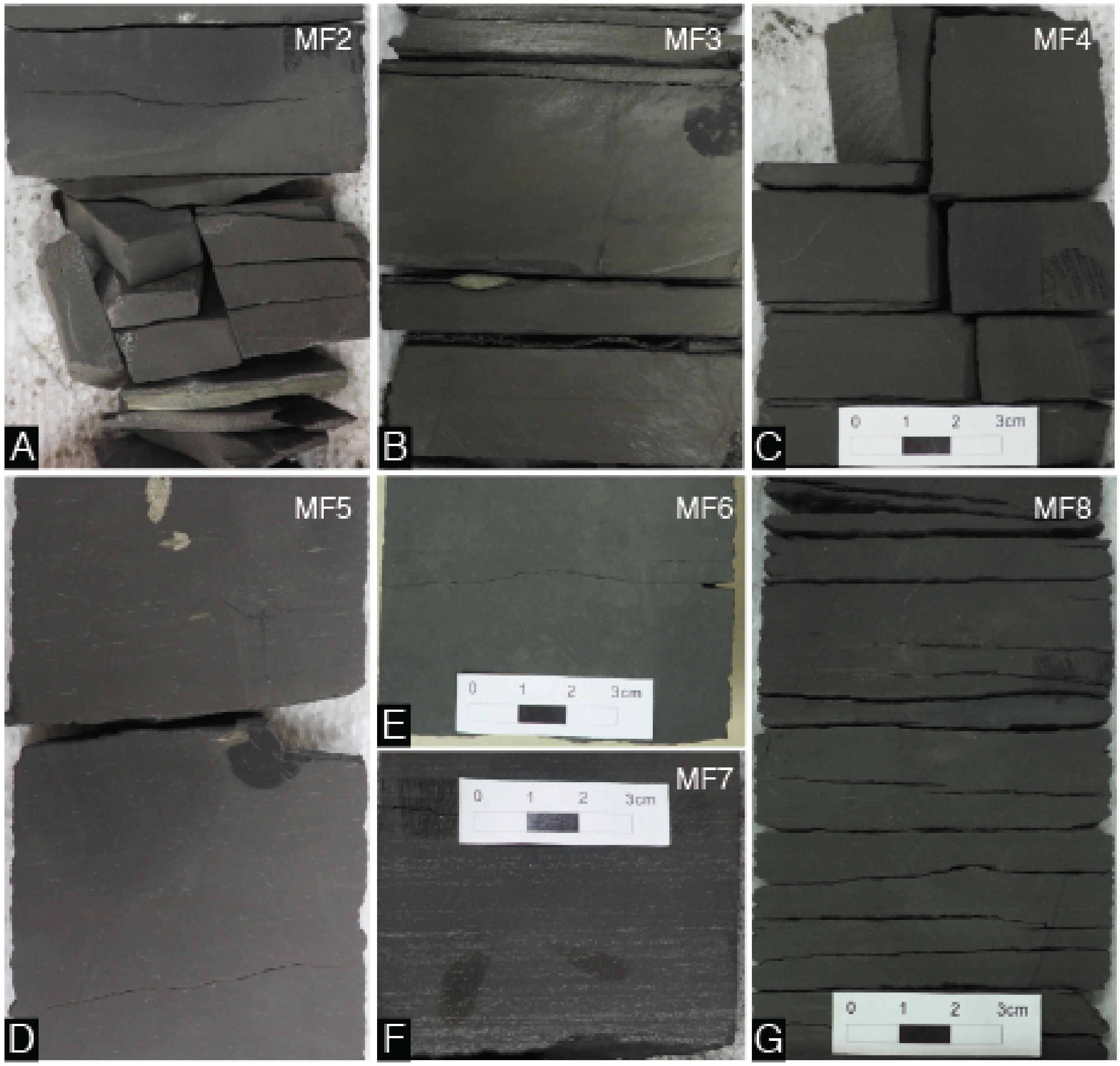

Figure 2.7: Core photographs of each microfacies. A) Homogenous-looking dolomitic argillaceous fine mudstone (MF2). N-09 1754.68 m. B) Discontinuous wavy parallel to homogenous looking fine mudstone (MF3). I-78 1841.17 m. C) Rarely bioturbated discontinuous wavy parallel argillaceous fine mudstone (MF4). N-09 1736.63 m. D) Bioturbated discontinuous to wavy parallel argillaceous fine mudstone (MF5).H-64 1294.23 m. E) Bioturbated discontinuous planar parallel to conttinuous wavy non-parallel argillaceous-siliceous medium mudstone (MF6). I-78 1822.40 m. F) Fossiliferous discontinuous to continuous wavy parallel argillaceous fine mudstone (MF7). N-09 1777.43 m. G) Intraclast rich discontinuous planar parallel argillaceous fine mudstone. I-78 1812.42 m. All core diameters are 7 cm across. No photographs of the homogenous-looking radiolarian-rich siliceous fine mudstone (MF1) were taken (all core elevations of MF1 identified in thin section were missing).

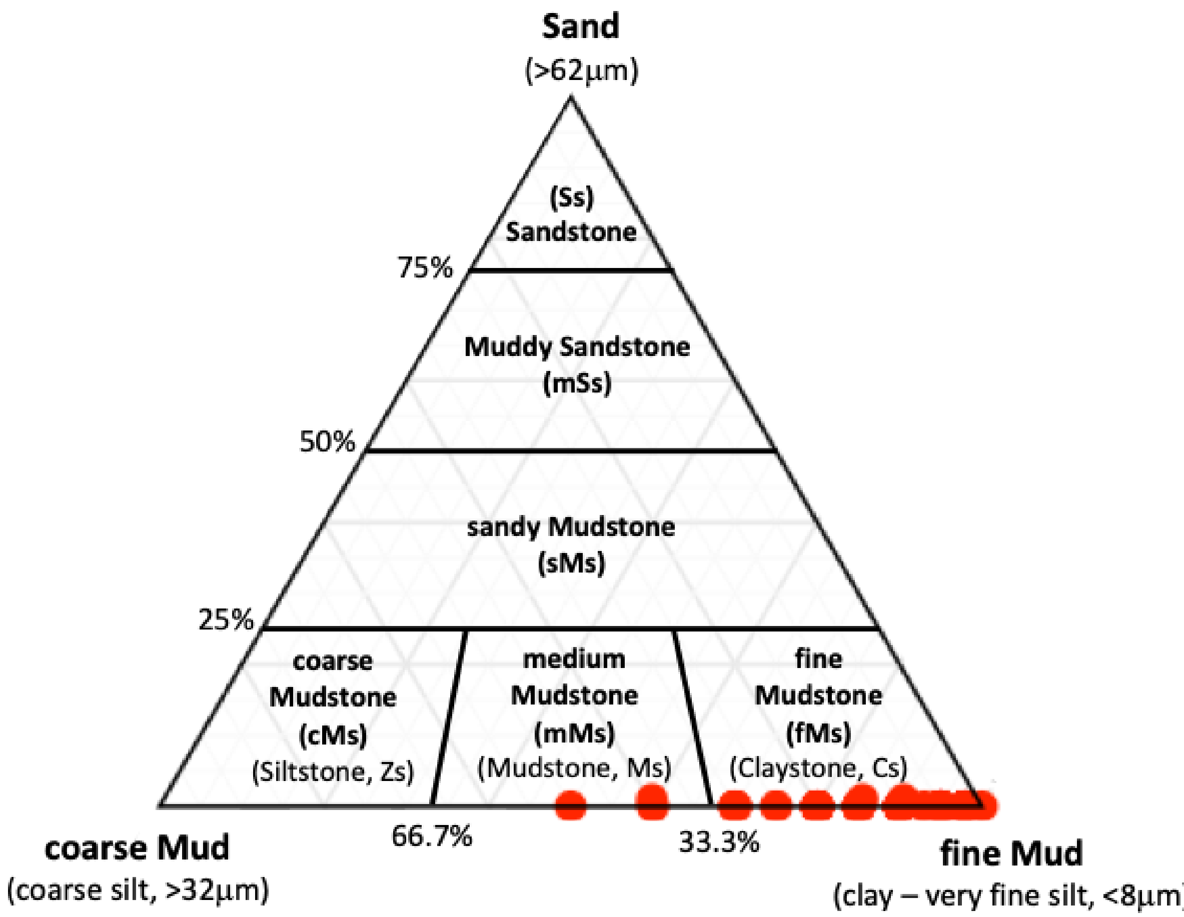

Figure 2.8: Nomenclature of fine-grained rocks. Red dots indicate samples in this study. Figure modified from (Lazar et al., 2015).

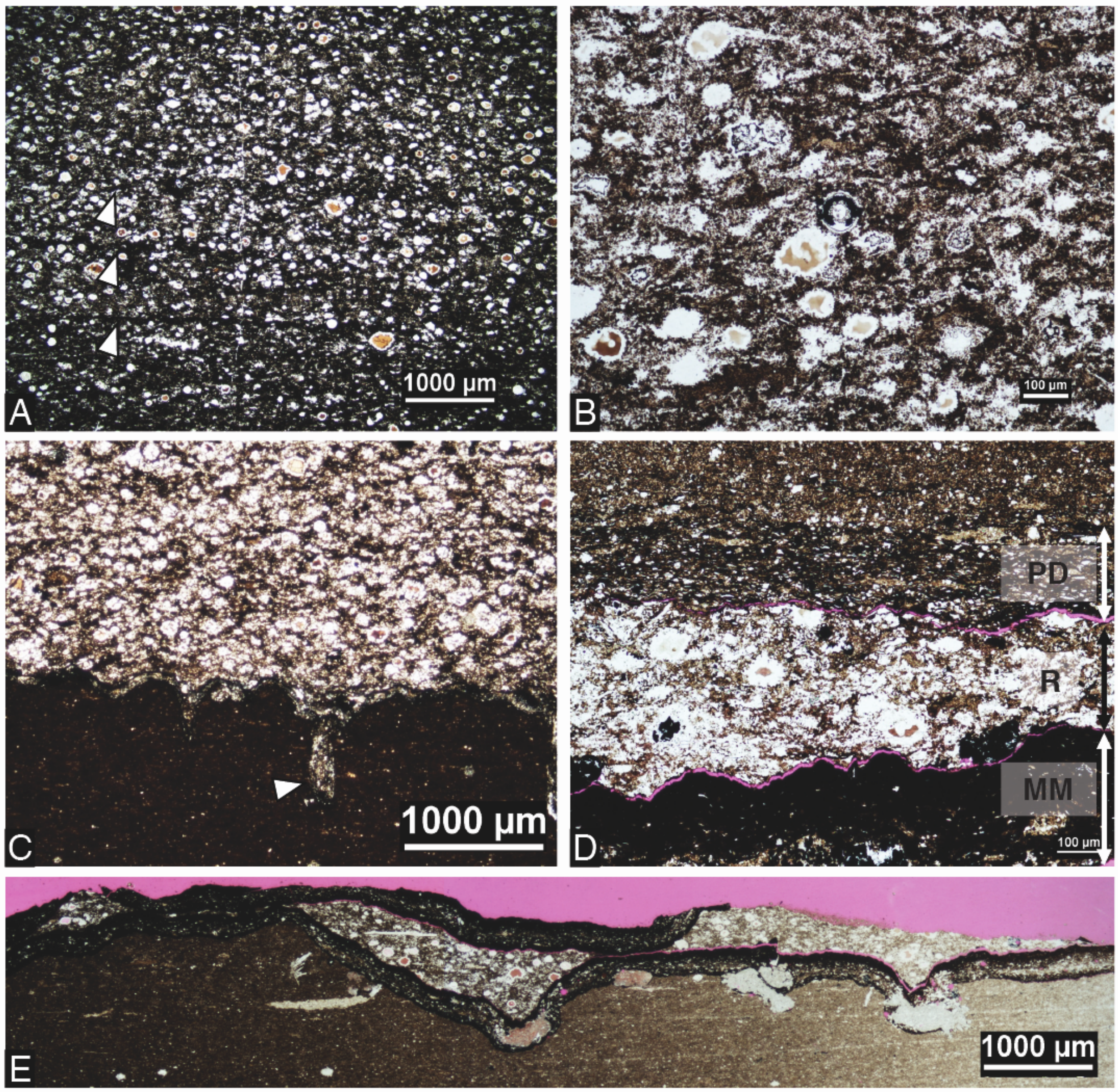

Figure 2.9: Photomicrographs of radiolarian-rich deposits (MF1). (A) Recrystallized and partially dissolved radiolarian-rich deposit. Faint bedding planes can be seen throughout (arrows) possibly representing thin microbial mat features. A sinuous vertical burrow is right-side lined (dashed with line) (H-64 1186.69 m). (B) Silicified radiolarian-rich bed with a singular partially pyritized test in the center (H-64 1186.69 m). (C) Contact between an overlying radiolarian-rich bed and underlying fine mudstone. The unique structure of this contact may represent a stylolitized surface or a thin microbial mat (thin black structure, arrow) between the two lithologies (N-20 1998.78 m). (D) Thin radiolarian-rich deposit (R) overlying a cohesive microbial mat (MM) and capped by a carbonaceous-argillaceous laminae (CA) (N-09 1725.83 m). (E) Radiolarian-rich deposit encased between two microbial mat layers. The variable thickness of the encased radiolarian-rich deposit, and the identical thicknesses of the upper and lower microbial mats may indicate that this feature represents a ripped-up and folded over mat encasing a pre-erosional overlying radiolarian-rich unit. Similar features are described and illustrated in Schieber (1999).

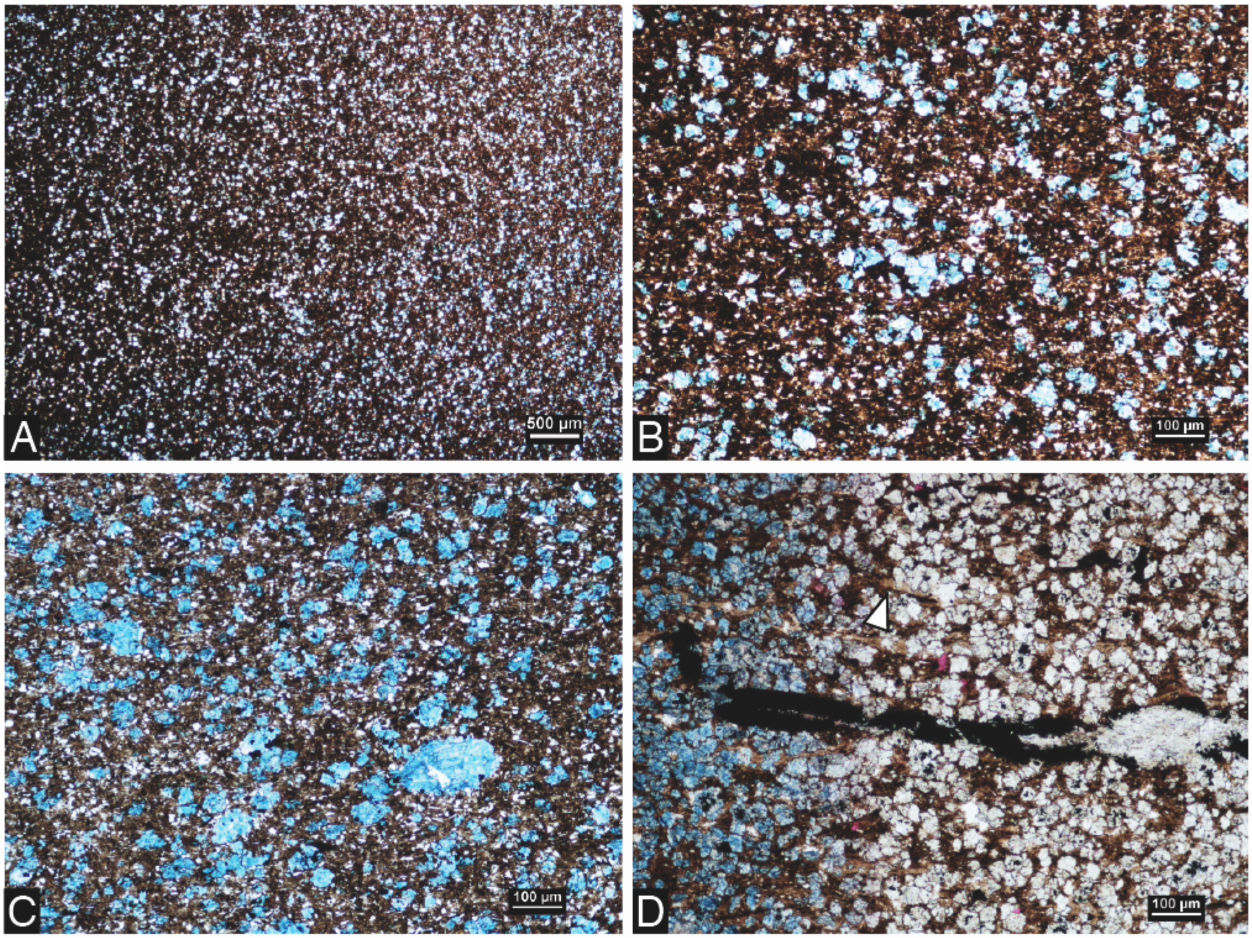

Figure 2.10: Photomicrographs of homogenous-looking dolomitic argillaceous fine mudstones. A) Heavily dolomitized claystone, with ferroan dolomite (blue staining). No primary sedimentary features are preserved (N-09 1754.68 m). B) Clay dominated matrix with some detrital silt (bright spots). Rhombic dolomitization is represented by the blue-stained crystals (N-09 1754.68 m). C) Microcrystalline dolomite (blue stained) within a clay dominated matrix. A possible dolomite replaced microfossil test may be present in the lower right corner (relatively large lenticular dolomite crystal) (N-09 1749.21 m). D) Partially pyritized tentaculitid fragment infilled with ferroan dolomite, within a dolomitized claystone. Can see remnant intraclasts (arrow). Image is half stained with potassium ferricyanide (left hand side) (N-09 1816.92 m).

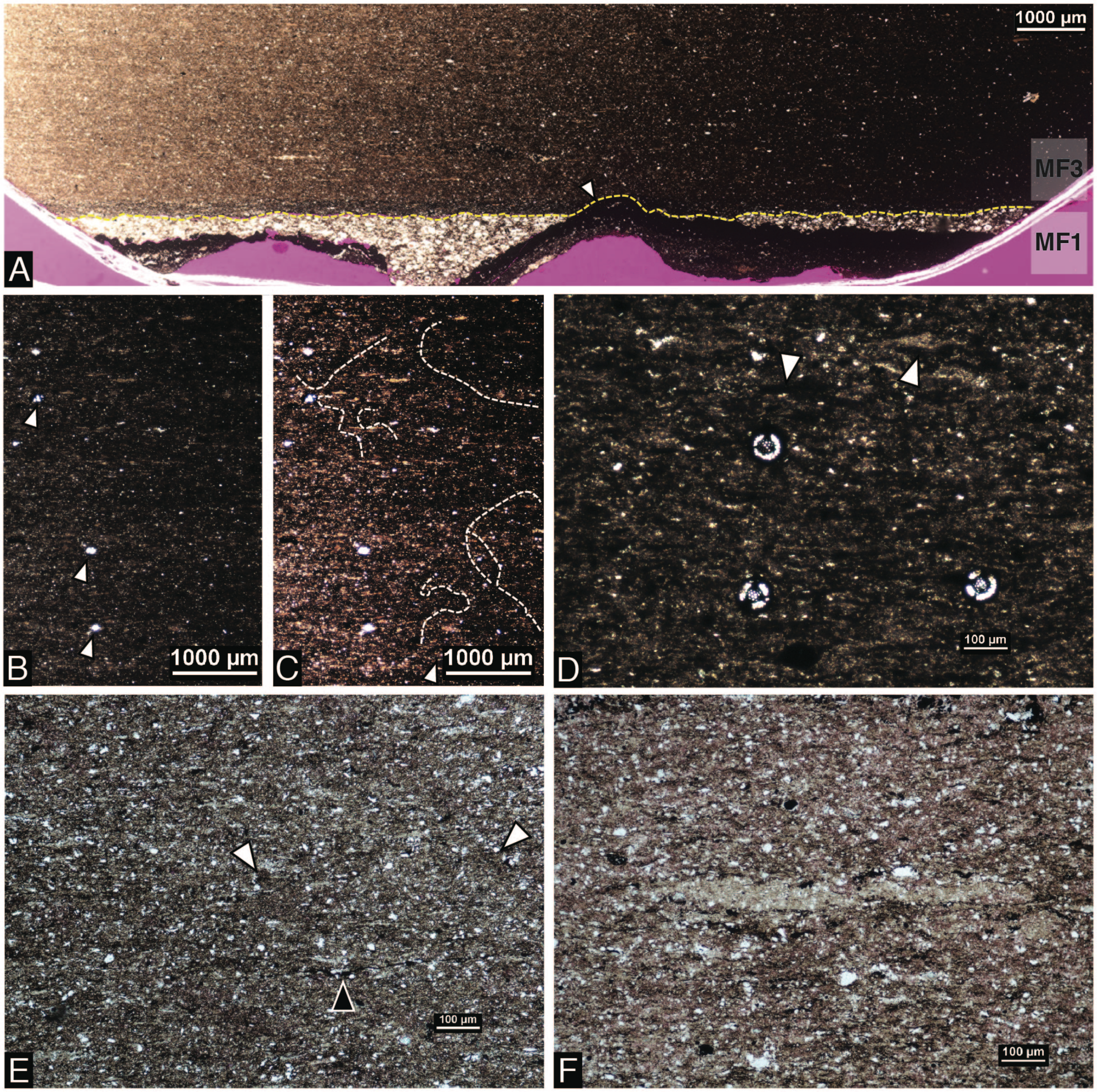

Figure 2.11: Photomicrographs of the radiolarian-rich microfacies (MF3). (A) Thin section scan showing an erosional contact (yellow dashed line) between a lower radiolarian-rich unit (below contact) and MF3 above. An undulatory erosion-resistant microbial mat (arrow) underlies the radiolarian-rich layer in areas where radiolarian tests have not been eroded (black undulatory feature). Close-up image of the same area is shown in Figure 6D (N-09 1725.83m). (B) Thin section photo showing the unbedded character of the microfacies, with radiolarians dispersed throughout (arrows) (N-09 1728.62 m). (C) Same photo as B, with brightness enhanced to better see bioturbation. Apparent burrows are right-side outlined (white dashed outlines). Several un-outlined burrows are present as well. (D) Claystone with 3 well preserved radiolarian tests. Phytodetritus is abundant in the background (arrows) (N-20 1966.16 m). (E) Partially homogenized claystone with burrows (white arrows). Black arrow points towards phytodetritus (N-09 1734.54 m). (F) Intraclast (center) with elongate stringers of phytodetritus throughout (N-09 1724.50 m).

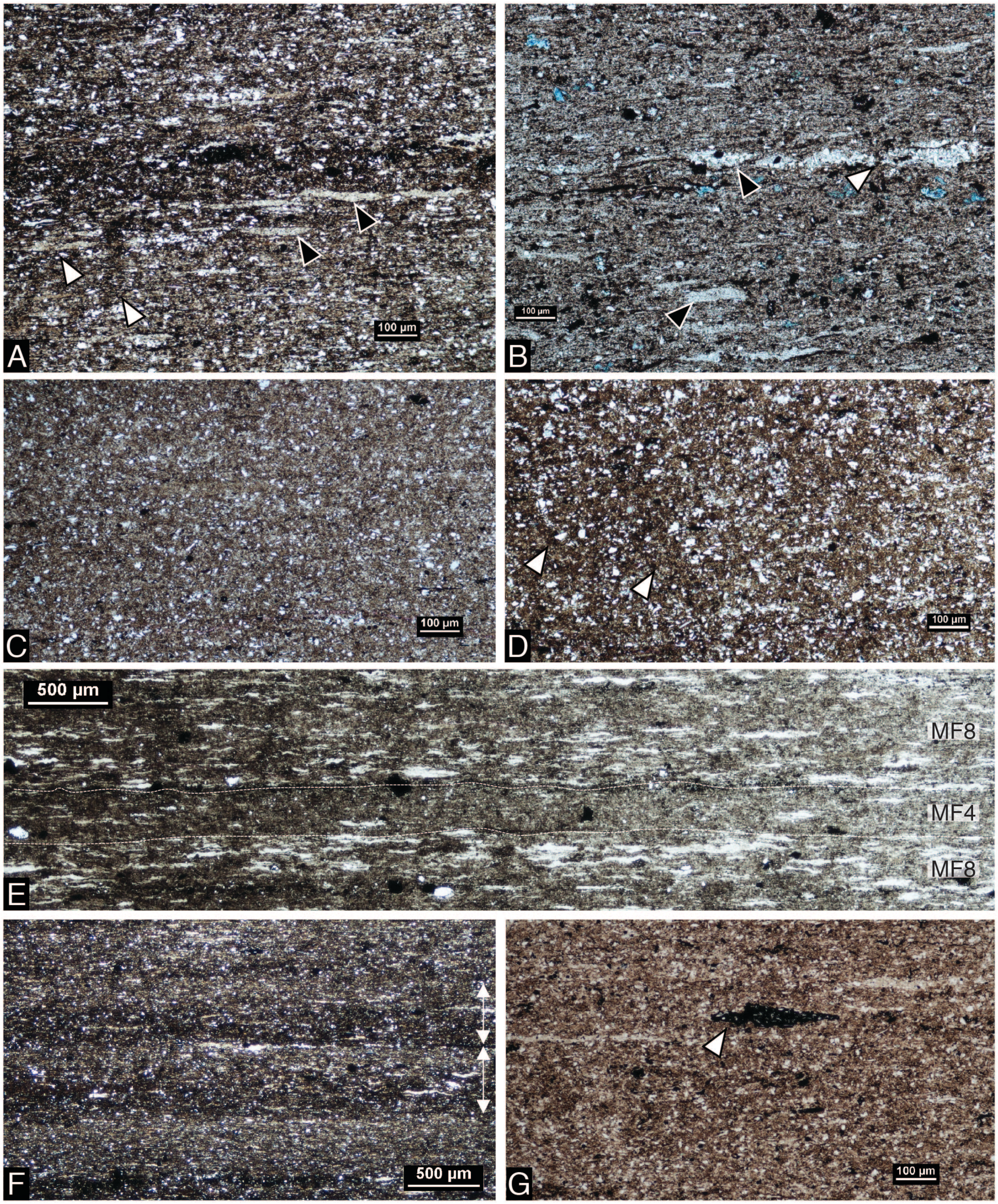
A
100 µm
B
100 µm
C
100 µm
D
100 µm
500 µm
MF8
MF4
MF8
E
F
500 µm
G
100 µm

Figure 2.12: Photomicrographs of rarely bioturbated silt-bearing fine mudstone (A, B) and bioturbated silt-bearing fine mudstone (C, D). (A) Poorly bioturbated silty mudstone with an intraclast rich laminae (center). Sinuous shafts in lower left corner are dictated by arrows (N-09 1736.63 m). (B) Silty mudstone with abundant phytodetritus and common ferroan dolomite (blue). Intraclast lag near center. Sinuous shaft interrupting intraclast lag is shown by arrow (N-09 1699.77 m). (C) Biogenically homogenized silty mudstone. No primary sedimentary features remain (H-64 1294.23 m). (D) Biogenically homogenized silty claystone with some diffuse sinuous burrows preserved (arrows) (N-09 1747.35 m). (E) Photomicrograph showing a thin low density turbidite layer (MF4) punctuating intraclast-rich laminae (MF8) (N-09 1706.58 m). (F) Stacked normally graded laminae (double ended arrows) with phytodetritus, silt, and intraclast-bearing bases fining upwards into clay tops (N-20 1978.32 m). (H) Clay-dominated massive appearing laminae with a microbial mat rip-up fragment (arrow) (N-20 1710.08 m).

Bioturbated Discontinuous Wavy Parallel to Homogenous-Looking Argillaceous Fine Mudstone (MF5)

The bioturbated discontinuous wavy parallel to homogenous-looking argillaceous fine mudstone microfacies (Figure 2.12C and D) is nearly compositionally identical to the rarely bioturbated variant (MF4). This bioturbated silt-bearing fMs is composed of 5-30% detrital silt grains (typically quartz), rare to common intraclasts, and rare elongate organic detritus. Preferentially framboidally pyritized horizons are less common, less continuous, and thinner than in the unbioturbated counterpart. These mudstones can be partially dolomitized, with alteration up to 10% of thin section surface areas. This microfacies appears reddish-brown to (very dusky red (dark brown) in colour depending on the thickness of the thin section and TOC content (which ranges between 3.8 – 8.7%).

The general lack of lithological contrast, especially when paired with biogenic homogenization, makes accurate identification of primary sedimentary structures incredibly difficult. Faint remnant bedding planes of thin (< 1 mm) plane parallel laminae can be seen in some instances (Figure 2.12C). Silt grains are randomly dispersed throughout individual laminae. Bioturbation intensities range from 30% to 100%, with the most common trace belonging to the sinuous burrows.

This microfacies is most often associated with the lesser bioturbated variant (MF4) but has been identified as discrete layers within the medium mudstone microfacies (MF6) and the intraclast-rich microfacies (MF8) (Figure 2.12E).

Bioturbated Discontinuous Planar Parallel to Continuous Wavy Non-Parallel Argillaceous-siliceous Medium Mudstone (MF6)

The bioturbated discontinuous planar parallel to continuous wavy non-parallel argillaceous-siliceous medium mudstone microfacies (Figure 2.13) consists of >30% detrital fine- and medium-silt-sized grains, and has the coarsest-grained detrital fraction of all identified microfacies. Silt is typically quartz but in rare instances can be mica (Figure 2.13F) and carbonate (Figure 2.13A). Intraclasts are rare to common throughout and can consist entirely of clay, or be silt dominated (Figure 2.13A). Calcite tentaculitid fossil shell material, phosphatic fragments (likely conodonts), and radiolarians are rare to common and can be partially pyritized. This microfacies is characteristically very dusky red (dark brown) in colour owing to a high organic content, with TOC's ranging from 4.8 to 7.7%.

The medium mudstone microfacies displays several primary sedimentary bedforms including undulatory scour surfaces, detrital silt and intraclastic lags (Figure 2.13B), and graded bedding (typically normally graded but in rare instances inverse grading is present).

Bioturbation intensities range from 20% to 80% reworking by area. Sinuous dark trails with detrital silt bordering their margins are easy to spot throughout this microfacies (Figure 2.13B, C). Detrital silt lags show vertical disruptions attributed to the burrowing of organism redistributing the coarser fraction (Figure 2.13B, C). Tubular unlined burrows were also identified.

The medium mudstone microfacies can be found intercalated with other compositionally similar silt-bearing microfacies (MF4 and 5).

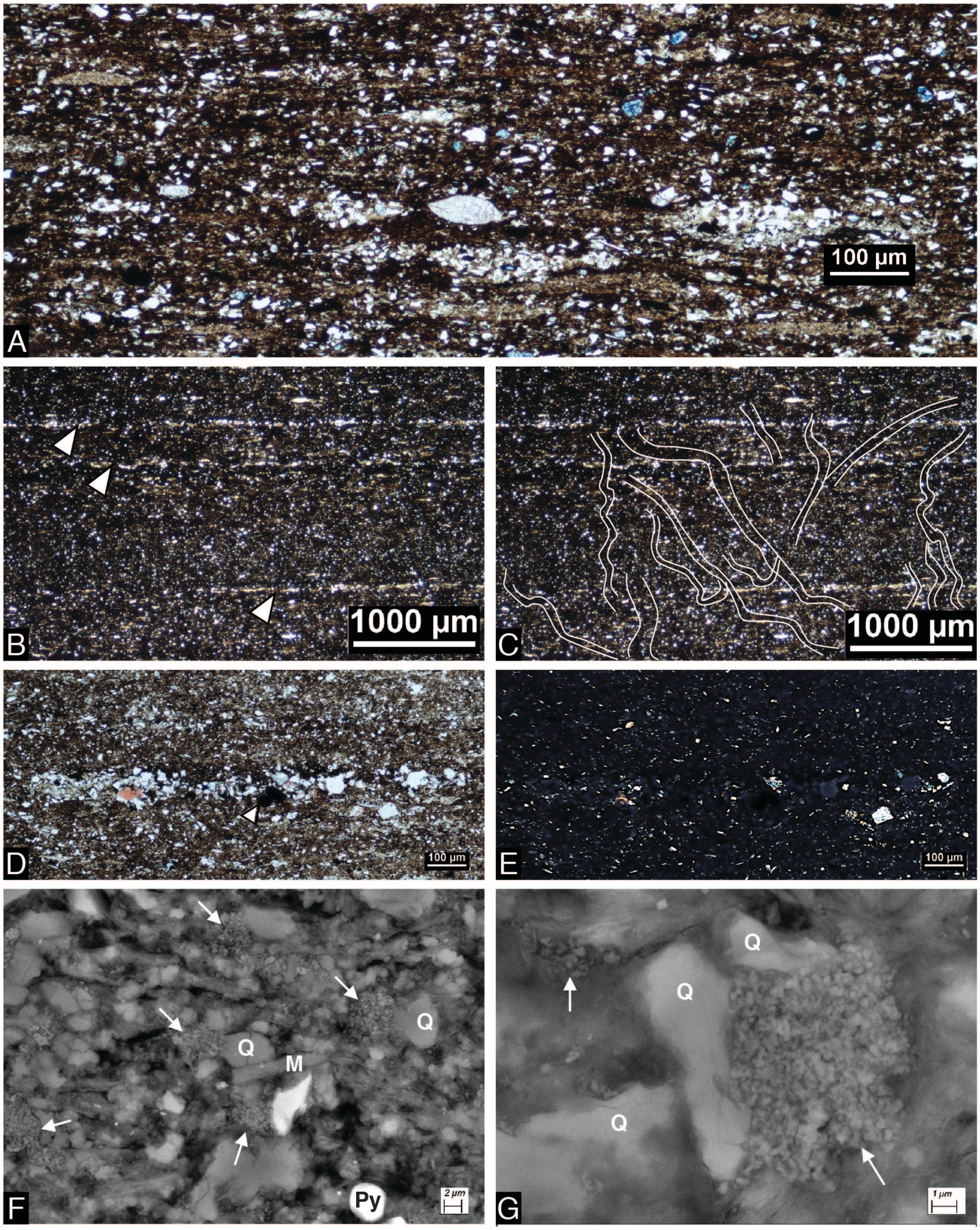
100 µm
A
B
1000 µm
C
1000 µm
D
100 µm
E
100 µm
F
Q
Q
M
Py
2 µm
G
Q
Q
Q
1 µm

Figure 2.13: Photomicrographs (A – E) and scanning electron microprobe (SEM) photos (F and G) of the mudstone microfacies (MF6). (A) Photomicrograph showing coarse-silt-composition of a medium mudstone with abundant silt-rich intraclasts and a relatively large calcified microfossil (center) (I-78 1822.40 m). (B) Thin discontinuous silt lags spanning the width of the thin section (arrows). Discontinuities are the result of biogenic reworking (N-09 1785.74 m). (C) Outlined sinuous shaft burrows in A. (D) Thin detrital silt laminae showing sub-angular roundness and poor sorting of grains. Calcite fragment (pink) and transported pyrite clasts (arrow) are also present. Poor sorting and diverse composition of laminae suggests a thin sediment gravity flow (N-09 1785.74 m). (E) Image in (C) under cross polars (XPL) showing variable grain composition (N-09 1785.74 m). (F) SEM photograph of a mudstone showing detrital quartz (Q) and micas (M), with pyrite framboids (Py). Detrital clays are present as clay aggregates (arrows) (I-78 1827.40 m). (G) SEM close up photographs of a clay aggregate (arrows) surrounded by detrital quartz (Q) (I-78 1827.40 m).

Fossiliferous Discontinuous to Continuous Wavy Parallel Argillaceous Fine Mudstone (MF7)

The fossiliferous discontinuous to continuous wavy parallel argillaceous fine mudstone microfacies (Figure 2.14) is characterized by compositionally homogenous skeletal assemblages of calcite tentaculitid fossils, comprising 10 – 100% of the sediment fraction, in a clay matrix. This includes intact, reworked, and/or fragmented fossil shell material. The fossiliferous mudstones can be 1) matrix supported with fossil fragments sporadically distributed throughout the sediments (Figure 2.14A-C) or 2) allochem supported (matrix-poor) with tentaculitids concentrated within individual fossil-rich bioclastic beds/laminae and along bed planes (Figure 2.14D, E). Tentaculitid shells are composed of calcite (pink when stained with alizarin red, Figure 2.14A-C). Dolomitization and pyritization of calcite shells and shell interiors is common (Figure 2.14A-C). Intragranular fill in matrix-poor layers is typically calcite cement (Figure 2.14E), with some diagenetic kaolinite and pyrite. The fossiliferous microfacies ranges in colour depending on the amount of argillaceous matrix (the more matrix the darker the colour), the type of carbonate stain used, thickness of the thin section (thicker cut thin sections appear darker), and TOC content (ranges between 5.3 – 7.7%). The argillaceous matrix is generally very dusk red (dark brown) and the carbonated components are either transparent, light blue, or pink.

Fossil fragments in matrix-supported layers are oriented parallel to bedding (Figure 2.14A), whereas allochem-supported layers have a random orientation of fossils (parallel, inclined, and oblique to bedding) (Figure 2.14E). Normal grading is common of allochem-supported layers, where large randomly oriented fossil fragments layers grade upwards into clay matrix supported fossiliferous claystones with small bedding parallel oriented fossil fragments (Figure 2.14E). Allochem-supported layers can also be structureless and composed of fragmented or crushed shell debris (Figure 2.14D). Such beds/laminae have undulatory bases and commonly occur in stacked successions of variable thickness. Some heavily calcified fossiliferous beds and laminae are associated with cone-in-come structures. Bioturbation intensities are low within this microfacies, ranging from 0-20%.

Fossiliferous mudstones occur seldom throughout the Canol Formation but dominate in the Bluefish Member. They can be found in conjunction with the dolomitized fMs (MF2) and the silt-poor fMs (MF3).

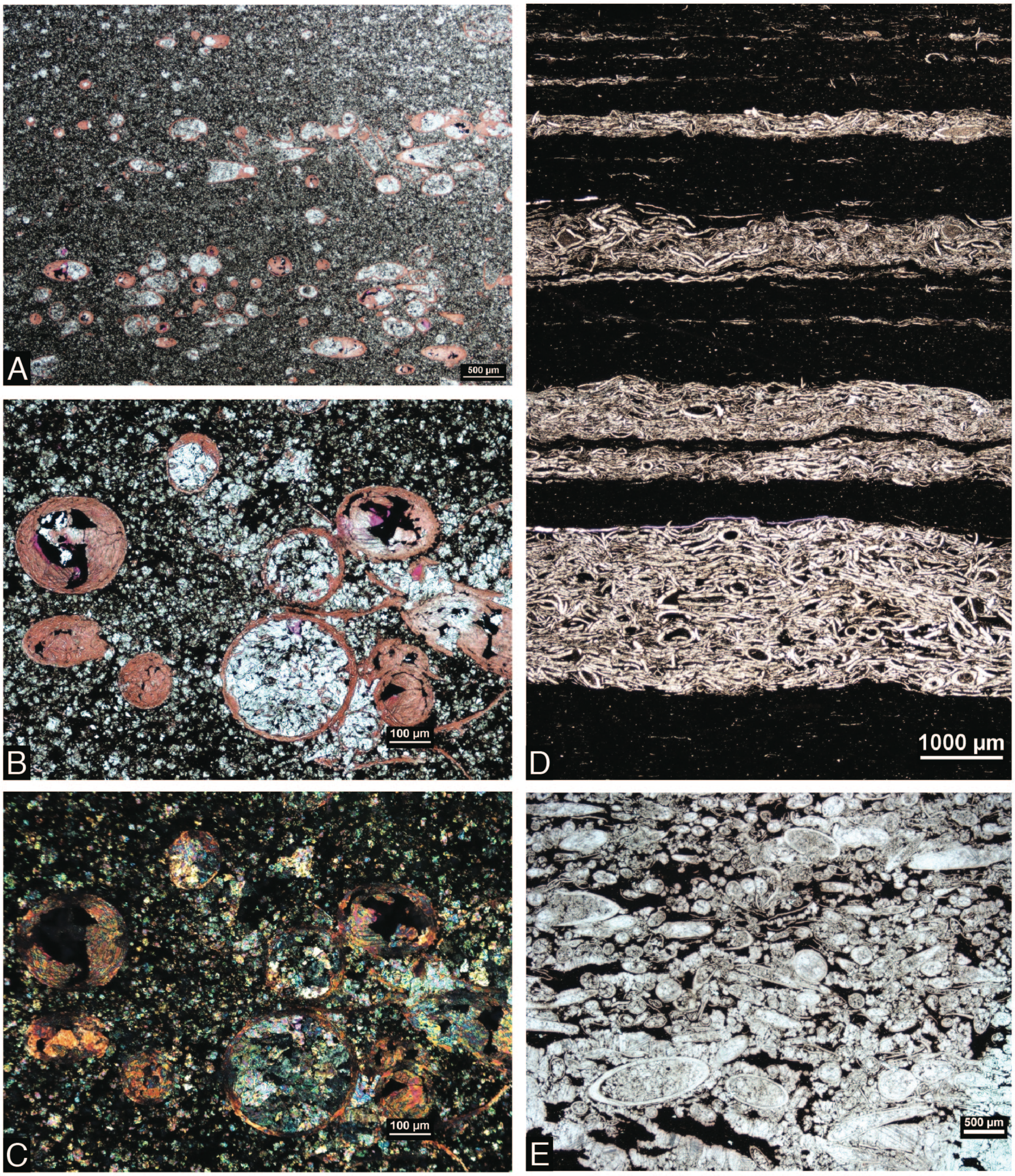
A
500 µm
B
100 µm
C
100 µm
D
1000 µm
E
500 µm

Figure 2.14: Photomicrographs of the fossiliferous mudstone microfacies (MF7). (A) Photomicrograph of a matrix supported fossiliferous mudstone with calcite (pink) tentaculitid shells and early diagenetic dolomitization (unstained) of fossil chamber interiors (pre-compactional). Clay matrix has undergone significant dolomitization (N-09 1777.48 m). (B) Close up photo of calcite tentaculitid fossils and dolomitized interiors in (A) (N-09 1777.48 m). (C) Photograph in (B) under crossed polars (XPL) (N-09 1777.48 m). (D) Stacked winnowed tentaculitid fossil lags punctuated by claystones (N-20 2092.95 m). (E) Normally graded matrix poor tentaculitid layer. Fossils likely underwent pre-compactional dolomitization of shell interiors prior to being re-mobilized (I-78 1953.30 m).

Intraclast-Rich Discontinuous Planar Parallel Argillaceous Fine Mudstone (MF8)

The intraclast-rich discontinuous planar parallel argillaceous fine mudstone microfacies (Figure 2.15) consists of sediments made up of more than 30% intraclasts by area, with both clay-dominated and silt-bearing intraclast compositions. This microfacies has detrital quartz silt content ranging from 0 to 40%. In mudstones where the matrix is clay-dominated, clay intraclasts are the dominant type; whereas mudstones with increased silt content support silt-bearing intraclasts. Elongate organic matter is common to abundant (Figure 2.15D). Fossil shell material is rare within this microfacies; only a handful of conodonts and tentaculitid fragments were identified. This microfacies has a range of diagenetic alterations. Framboidal pyrite can be prevalent throughout (Figure 2.15D), and it is common for this microfacies to be moderately dolomitized (Figure 2.15A, B, D, E). Intraclast-rich mudstones range in colour from light brown to very dusky red (dark brown) depending on intraclast abundance (the more intraclasts the lighter the colour), thickness of the cut thin section, and TOC content (ranges from 3.3 – 4.2%).

The intraclast rich microfacies shows planar parallel bedding at both low (20x) and high (100x) magnifications (Figure 2.15A and E). Individual laminae are comprised of an unsorted homogenous-appearing distribution of intraclasts throughout an argillaceous matrix. Some normally graded laminae with intraclastic bases fining upwards to clay drapes (Figure 2.15E) have been identified. This microfacies is the only microfacies identified as having soft sediment deformation (Figure 2.15B). Intraclast-rich mudstones are poorly bioturbated with bioturbation intensities ranging from 0-20%. When bioturbated, organisms appear to avoid burrowing into or through individual clasts, tending to travel along clast margins (Figure 2.15H).

Clay-dominated intraclast-rich mudstones are present throughout the Horn River Group, but almost totally define the Bell Creek Member. Silt-bearing intraclast-rich mudstones are exclusive to the upper portion of the Canol Formation.

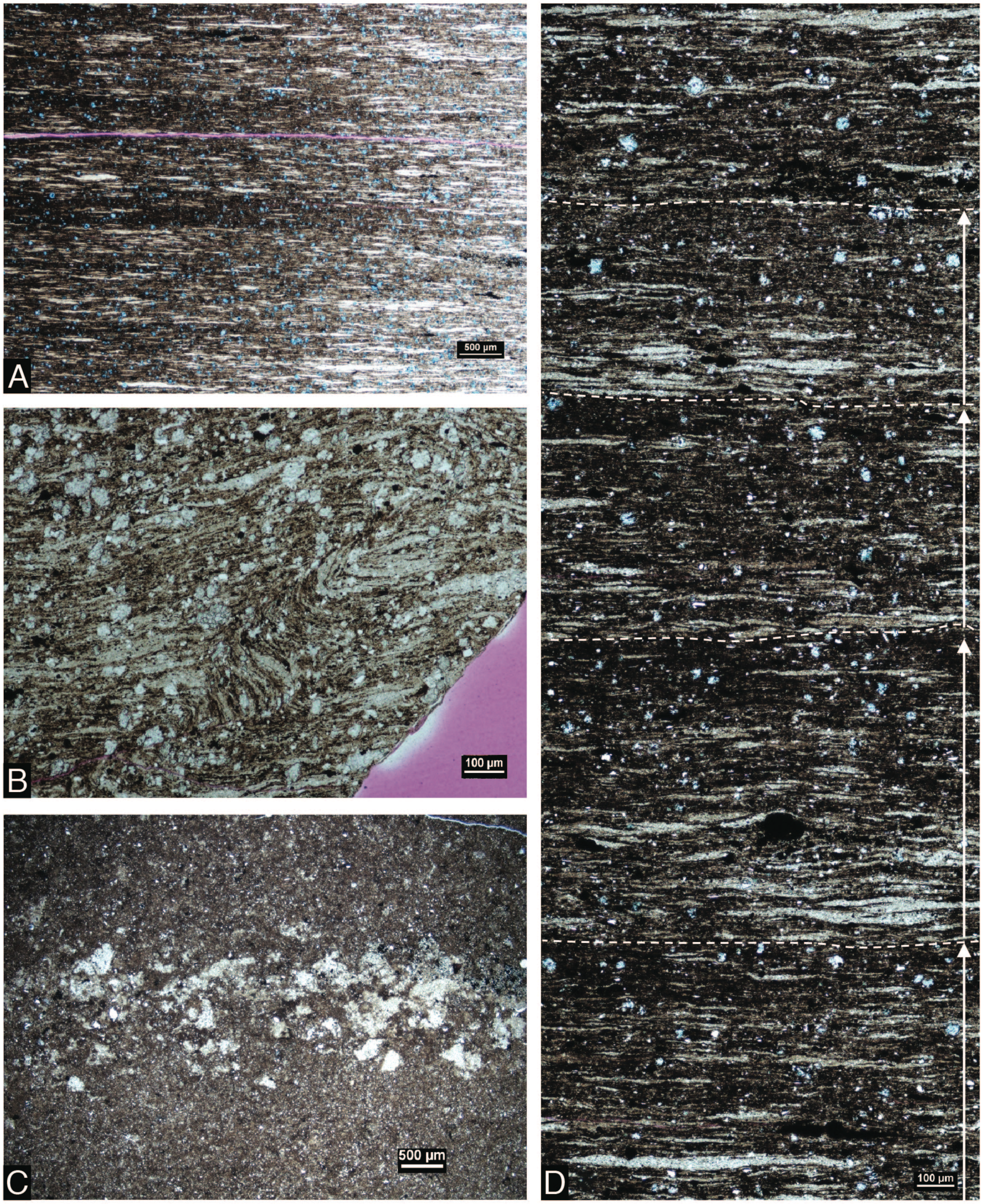
500 µm
A
100 µm
B
500 µm
C
100 µm
D

Figure 2.15: Photomicrographs of intraclast-rich mudstones (MF8). (A) Photomicrograph showing variable intraclast abundance within individual laminae. Diagenetic ferroan dolomite is present throughout (blue) (H-64 1273.90 m). (B) Synsedimentary recumbent folding of an intraclast-rich claystone. Diagenetic dolomite is present throughout (sand-sized crystals) (H-64 1275.38 m). (C) Oblique bedding plane view of an intraclast covered surface. Intraclasts show the compacted remnants of their original spherical morphology (I-78 1846.00 m). (D) Stacked intraclast-rich normally graded laminae. laminae have intraclast rich bases fining up to clay dominated tops. Photo shows 4 laminae (arrows) with bedding planes outlined by punctuated lines (N-09 1807.35 m).

2.6 Discussion and Interpretation

2.6.1 Micro-bioturbation

The small sinuous burrows and both lined and unlined burrows are interpreted to be the result of migrating deposit feeding organisms (fodinichnia). This is consistent with the sinuous unbranching burrow morphologies and lack of sufficiently thick and ridged burrow linings. Thick and ridged burrow linings are typically found in dwelling structures to prevent sediment collapse, but are unnecessary in deposit feeding structures and are therefore poorly developed (Bromley, 1996). The apparent silt linings associated with these burrow morphologies (such as those seen in Figure 2.5E and F) is a relict of grains concentrating at the burrow margin as the animal moves through the sediment, or the result of grain-selective feeding, where clay particles and organic matter are preferentially ingested. The concentric linings that can be seen in some lined burrows (Figure 2.4E, F) are interpreted to be the result of continuous compaction of the surrounding sediment perpendicular to the length of the burrow as the burrowing organism moved and fed (Bromley, 1996). The lighter colour and homogenous infill of both tubular burrow trace fossil types stems from the mining of host sediment and digestion of organic matter by the organisms, as well as differential diagenetic mineralization of burrow infills as a product of organic matter removal (Savrda, 2007).

Trace fossils in the silt-poor and silt-bearing fine mudstone microfacies (MF3, 4 and 5) can be difficult to identify through conventional petrographic techniques. This is likely in-part because burrowing in soft, soupy substrates, results in poorly defined burrow margins that subsequently undergo intense compaction (*e.g.* Lobza & Schieber, 1999). However, photographic enhancement of the darker coloured clay-rich lithosomes does show increased evidence for biogenic reworking (*e.g.* Figure 2.11B and C).

The preservation of burrow morphologies in silt-bearing sediments (MF4 – 8) without the presence of burrow linings is attributed to deposit feeding within semi-consolidated muds rather than soft soup ground muds (Schieber, 2003; Gingras et al., 2011). As well, the detrital silt-grain fraction of the sediments may act to increase sedimentary resistance to compaction. This enhanced cohesiveness associated with higher concentrations of silt may also enhance the preservation of burrow morphology.

The preferential pyritization of thin burrow linings and burrow fills is interpreted to stem from pre-compaction early diagenetic pyritization of the organic mucus sheaths associated with the burrow margins and linings (Bromley, 1996; Savrda & Bottjer, 1984; Thomsen & Vorren, 1984; Schieber, 2002; Macquaker & Taylor, 1996). Such early diagenetic pyritization of organic linings and burrow fills promoted the preservation of the burrows, making them resistant to compaction and significant deformation. This preservation via pyritization mechanism has been noted in several previous studies of macro-scale burrows (*e.g.* Baird, 1978; Yeun Ahn & Babcock, 2012). Although it is likely that Fe-rich burrow linings are the result of amorphous iron oxide precipitation at the burrow margin (*c.f.* Gingras, Zonneveld, & Konhauser, 2014), the precipitate may act as a permeability barrier that buffers H2S diffusing from the sediment.

The very low diversity and exceptionally small size of the identified trace fossils (Figures 2.4 and 2.5) likely reflects the lowest limit of sustainable body size for the trace making organisms in response to severely low dissolved oxygen concentrations in pore waters. Such organism body size is interpreted as facultative diminution, whereby for the organism to survive in such an oxygen stressed environment they require large surface area to volume ratios, achieved by decreasing overall body size in order to diffuse the maximum amount of oxygen across their membranes (Gingras et al., 2011). When looking at trace fossil statistics at the petrographic level, especially in mudstones, measured burrow diameters will reflect some level of compactional deformation (*e.g.* Lobza & Schieber, 1999). As well, the orientation of the slice through the burrow may result in incorrect measurements. Just as with trace fossil diversity counts, the burrow size statistics from this study are based on the most obvious (best preserved) burrows that happen to be present in the small thin section sample area, which likely does not capture the full diversity and size range of all trace fossil types. Due of the aforementioned difficulties associated with evaluating burrow size and diversity, size-diversity indexes (SDI) (*c.f.* Gingras et al., 2011) have no sound statistical value.

The identification of bioturbation within the Horn River Group sediments indicates that persistent bottom water anoxia was at the very best, episodic during deposition of these organic-rich mudstones. However, the microscopic burrow sizes (maximum diameters of 150 μm) coupled with the low diversity suite of morphotypes (a maximum of five trace fossil types) also indicate that bottom waters and sediment pore waters were not sufficiently oxygenated to support and sustain a range of benthic deposit feeders that could achieve macro-scale body sizes (Gingras et al., 2011; Bromley & Ekdale, 1984; Savrda & Bottjer, 1987; Wignall, 1991). The presence of bioturbation with a microscopic low diversity suite signifies extreme dysoxia, likely at the lower limit of hospitable conditions (approaching 0.0 mL/L O2).

It is also possible that the amount of identified bioturbation in these mudstones is only a fraction of that actually present. As previously mentioned, a lack of lithologic contrast, especially within the darker clay-rich lithosomes, makes confident identification of micro-burrows difficult (*e.g.* Figure 2.11B, C). Furthermore, evidence of near-surface early diagenetic cementation of the highly reactive argillaceous HRG sediments, in the form of well-preserved uncompacted radiolaria tests (Figure 2.11C), uncompacted clay floccules, and differential compaction around larger carbonate nodules and minus-porosity cement (porosity present prior to cementation, visible as irregular cementation throughout clay matrix or intergranular between intraclasts (Milliken & Olson, 2017)), may have influenced meiofaunal organism's ability to penetrate the sediments.

The most common criticism of petrographic microbioturbation studies is why, definitively, these microscopic features are meiofaunal trace fossils and not some form of soft sediment deformation or defects within the thin section (*i.e.* Schieber, 2014 on Egenhoff and Fishman, 2013). Perhaps the best argument in favour of a biogenic origin is the nature of the burrow fill. Burrow fills differ not only in composition, where preferential clay fills reflect particular meiofaunal feeding strategies, but also in colour. Burrows are generally lighter in colour than the surrounding matrix, reflecting consumption and removal of available organic matter and variable diagenetic mineralization within burrow structures (Savrda, 2007). In contrast, burrow infills can appear darker in colour than the surrounding matrix when mucus sheaths of burrow linings and margins have been preferentially pyritized (Bromley, 1996; Savrda & Bottjer, 1984; Thomsen & Vorren, 1984; Schieber, 2002). Removal of organic matter and preferential pyritization of soft sediment deformation structures is not as likely. Although de-watering can result in preferential removal of certain hydraulically equivalent grains (*e.g.* larger organic grains and smaller lithic grains), which in turn can lead to preferential fill compositions, recognition of the sinuosity of these structures is key. The sinuosity argument in favour of trace fossils over soft sediment deformation is especially evident in plan view. Soft sediment deformation structures, such as dewatering structures, are expected to take the path of least resistance (i.e. approximately straight vertical paths). The proposed biogenic features documented in both bedding perpendicular and bedding parallel thin sections show that these features are almost always sinuous (excluding the inclined to vertical unlined meniscate backfilled burrows). In some instances, we observed trace fossils that double-back on themselves, and others are n-shaped (*e.g.* Figure 2.5D) — morphologies unexpected with soft sediment deformation structures. As well, the unlined circular to elliptical cross sections in elevation views with infill differing from the matrix (Figure 2.4G, H) are difficult to reconcile with most mechanical deformation processes and are best ascribed to bioturbation or at the very least peloidal features.

The argument has been made that similar burrow features (*e.g.* those described by Egenhoff and Fishman, 2013) are the result of defects produced during thin section preparation: i.e. the reported clay infill of micro-burrows may actually result from grain plucking during preparation of petrographic sections (Schieber, 2014). The HRG thin sections show these burrow types over a range of thin section thicknesses and matrix compositions. Although burrows are best seen in siltier sediments with greater lithologic contrast (*e.g.* Figure 2.5A-F), they are also present in wedge-cut (30 μm – 0 μm) silt-poor claystone thin sections (*e.g.* Figure 2.5G, H) where such grain plucking can be readily identified. Furthermore, during SEM analysis no evidence of grain plucking from the upper surface of thin sections was identified.

Potential organisms responsible for the micro-burrows identified in this study include polychaetes, copepods, benthic foraminifera, and nematodes. Small (150 - 800 μm) surface deposit feeding polychaetes have been identified in modern-day severely dysoxic (<0.2 mL/L O2) marine settings (Cuomo & Bartholomew, 1991; Levin, 2003), and benthic meiofaunal copepods have been noted, although rarely, in modern oxygen depleted sediments (Giere, 2009; Löhr & Kennedy, 2015). Small (<500 μm) benthic burrowing agglutinated foraminifers have been found in modern dysoxic marine bottom waters (Bernhard et al., 2003), and have been identified in other North American Devonian organic-rich mudstones (Schieber, 1999). Sulfide-adapted meiofaunal (50 – 75 μm) nematodes have also been cited as potential trace-makers in poorly oxygenated and partially sulfidic sediments (Schieber, 2014; Giere, 2009; Löhr & Kennedy, 2015; Pike, Bernhard, Moreton, & Butler, 2001).

2.6.2 Microfacies Depositional Environments

Homogenous-looking radiolarian-rich siliceous fine mudstone (MF1)

Geologists, *e.g.* Bohacs et al., (2005) and Egenhoff and Fishman (2013), commonly argue that radiolarian-rich mudstones (sometimes referred to as radiolarites) (Figure 2.9A - D) are deposited typically in depositional settings away from the effects of clastic dilution commonly towards the end of sediment transport paths. The dominance of biogenic-derived radiolarian tests over detrital sediment fraction indicates a paucity in input of allochthonous material to the depositional setting (Aplin & Macquaker, 2011; Egenhoff & Fishman, 2013).

The lack of primary sedimentary features and structures in radiolarian-rich deposits that would indicate bedload sediment transport processes (*e.g.* ripple laminae) likely reflects mass suspension settling of radiolaria from proliferation pulses in response to planktonic blooms (*c.f.* Egenhoff & Fishman, 2013). Such blooms may be associated with increased nutrient influx accompanying seasonality and/or upwelling (Aplin & Macquaker, 2011; Racki & Cordey, 2000; Jonk, Potma, Bohacs, Advocate, & Starich, 2014). Although there is evidence for some bioturbation within the radiolarian-rich microfacies (Figure 2.9A), there is not enough to attribute the structureless nature of the radiolairites to complete biogenic homogenization. For example opal-A dissolution and associated dewatering and compaction may contribute to the homogenous appearance.

The radiolarian-rich microfacies is the only microfacies associated with benthic microbial mats (cohesive carbonaceous interbeds, *e.g.* Figure 2.9A, C, D and Figure 2.11A). Evidence of the distinctive cohesive behaviour of microbial mats is revealed as microbial-mat encased radiolarian-rich fMs clasts; reflected as a carbonaceous units (presumed microbial mat) of uniform thickness completely encasing a radiolarian-rich deposit of variable thickness. The mechanisms behind formation of such a clast are interpreted as similar to the "rolled up mat" features illustrated by Schieber (1999, Fig. 3). In the HRG case, erosion of an overlying radiolarian-rich fMs and underlying microbial mat caused the mat to lift and flip over on itself (encasing the overlying radiolarian-rich deposit), eventually tearing away from the remainder of the original mat structure, and thus allowing it to be transported as a single clast. Evidence of microbial mat sediment stabilization is shown in Figure 8A, where a microbial mat of uniform thickness (dark carbonaceous layer) has 'captured' the overlying radiolarian-rich fMs deposit, preventing the individual radiolaria from settling into the presumed water-rich muds below. Differential loading of the radiolarian-rich deposit is obvious when looking at the thickness of the deposit, as the thicker sections have sunken further into the underlying muds. Without the mat stabilization, settling radiolarians would have sunken into the water rich muds until reaching a semi-consolidated depth, where they would then begin to concentrate, or potentially even form ball and pillow structures (Schieber, 2007; Schieber, Bose, et al., 2007). Similar mat features have been interpreted to have formed in relatively quiet settings with absent to episodic sedimentation (Schieber, 1986). Preservation of microbial mat features requires low dissolved oxygen concentrations, which inhibits both oxidative break-down of organic matter and limits degrees of bioturbation which would otherwise destroy mat features (Schieber, 1986). Microbial mats can also be sites of significant sulfur cycling, which can lead to calcium phosphate precipitation in the presence of free hydrogen sulfide (K. G. Taylor & Macquaker, 2011; Macquaker, Taylor, Keller, & Polya, 2014); another process which may be acting to preserve these mat features.

Radiolarian-bearing argillaceous fMs laminae (MF3) that alternate with radiolarian-rich fMs (MF1) show erosive scour at their base (*e.g.* Figure 2.9E, 2.11A), and microbial mat colonization at their tops (Figure 2.9D). These two features indicate elevated depositional energies of these argillaceous laminae (with bottom current velocities high enough to erode coarse-silt to fine-grained sand sized radiolarian tests), followed by prolonged periods of non-deposition allowing for mat colonization. The erosive nature of these units indicate that they are event deposits, while the radiolarian-rich deposits are likely events in and of themselves in response to proliferation pulses.

The generally uncompacted nature of the radiolarians (*e.g.* Figure 2.9B and 2.11D) indicates that recrystallization and infilling of radiolarian tests to chert, or in rare instances calcite, occurred prior to compaction during early diagenesis (Hart et al., 2013; Milliken & Olson, 2017; Fishman, Egenhoff, Boehlke, & Lowers, 2015). The absence of significant bioturbation, the preservation of carbonaceous microbial mat structures, and the inferred early diagenetic cementation in the radiolarian-rich microfacies are all indicators of still bottom waters with low dissolved oxygen concentrations (Egenhoff & Fishman, 2013).

Homogenous-looking Dolomitized Argillaceous Fine Mudstone (MF2)

Dolomite within the dolomitized fine mudstone microfacies is interpreted as post-depositional (diagenetic) on the basis of clear alteration of previously deposited detrital elements, such as intraclastic aggregates (Figure 2.10D), remnant bedding planes, and the presence of some well-formed microscopic ferroan dolomite rhombs. As well, dolomite rich layers have diffuse upper and lower margins as opposed to the discrete bedding planes that would be expected to be present in allochthonous carbonate silt beds (Schieber, 2007). An early diagenetic origin (pre-compactional) is interpreted for the dolomite in this microfacies, as it forms minus-cement porosity within rare fossil fragments which otherwise would have been crushed during compaction (*e.g.* Figure 2.10D) (Pyle, Gal, & Fiess, 2014).

Diagenetic dolomite, both as rhombs and microcrystals, is associated with post-depositional alteration of organic-rich mudstones via microbial sulfate reduction at or near the sediment surface (*e.g.* Baumgartner et al., 2006; Hickey & Henk, 2007; Macquaker et al., 2007). Ferroan dolomite, when it forms in early diagenesis, is considered to be an anoxic mineral that forms under strongly reducing conditions (Schieber, 1999; Macquaker et al., 2007) commonly in association with methanogenesis (*e.g.* Irwin, Curtis, & Coleman, 1977). Therefore, organic-rich heavily dolomitized sediments are interpreted to represent slow sediment accumulation rates under poorly oxygenated regimes combined with long residence times at the sea floor (Aplin & Macquaker, 2011; Hickey & Henk, 2007; Raiswell, 1971), conditions that allow for the byproducts of anaerobic bacterial reactions to accumulate and form early diagenetic iron-bearing dolomite (Hickey & Henk, 2007).

Discontinuous Wavy Parallel to Homogenous-looking Argillaceous Fine Mudstone (MF3)

This argillaceous fine mudstone microfacies contains only rare and sporadically distributed fine-silt grains (Figure 2.11), likely indicating deposition near the end of the sediment transport path. Similar to the detrital silt grains, radiolarian and conodont microfossils occur dispersed throughout the sediments as opposed to concentrated along specific bedding planes (*e.g.* Figure 2.11B vs. Figure 2.14D). The apparent structureless nature and random distribution of coarser-grained components may indicate that these sub-millimeter clay-dominated laminae represent short-lived sediment gravity flows. Such flows result in a massive-appearing mix of clay, clay aggregates, silt grains, and microfossils; similar to the laminar flow plug-like beds described by Baas et al., (2009) and Sumner et al., (2009). In these flows, larger grains are kept in suspension due to incorporation into relatively large clay floccules (Yawar & Schieber, 2017), and/or due to hindered settling mechanisms as a result of increased grain-grain interaction and cohesion (Baas et al., 2009; Sumner et al., 2009). It is likely that these plug-like flows originated from re-suspension of unconsolidated water-rich shelfal muds in response to wave agitation during storms (Prior et al., 1989; Plint et al., 2012), forming flows that can travel along shallow slope gradients (Mulder & Alexander, 2001). These plug-like flows can develop from pre-curser turbidity currents, if the concentration of suspended sediment is increased as the flow travels (Baas et al., 2009; Sumner et al., 2009).

The lack of significant lithologic contrast and obvious bedding planes within this microfacies makes accurate identification of physical sedimentary structures, just as with biogenic structures, difficult. Instances where significant lithologic contrast exists, erosive bedding contacts are obvious (*e.g.* radiolarian-rich fMs interlaminated with MF3, Figure 2.11A) – providing evidence for possible erosive sediment gravity flow heads and subsequent sediment deposition from an associated plug flow.

The amorphous organic matter in this microfacies (Figure 2.11D) is interpreted to be phytodetritus (aggregates of organic matter, detrital sediment, and micro-organism tests). In modern settings, phytodetritus is delivered to the sediment surface through suspension settling processes (Macquaker, Keller, & Davies, 2010). Phytodetritus was likely incorporated into the low-density turbidity flows and subsequently compacted forming elongate stringers (*e.g.* Figure 2.11E). The wavy appearance of these argillaceous fine mudstones at high magnifications (10x) may reflect differential compaction of this phytodetritus around silt-sized quartz grains, pre-compaction cemented silt-sized clay aggregates (*e.g.* Figure 2.13F and G), or compacted burrow infills. Biogenic pelagic elements such as radiolarians, conodonts, and carbonate fossils indicate the presence of an overlying oxygenated water column (Dawson, 2000), whereas rare and difficult to see micro-burrows (Figure 2.11B and C) indicate partial oxygenation of the sediments.

Rarely Bioturbated Discontinuous Wavy Parallel Silt-bearing Fine Mudstones (MF4) and Bioturbated Discontinuous Wavy Parallel to Homogenous-looking Silt-bearing Fine Mudstones (MF5)

The two silt-bearing fine mudstone microfacies (rarely bioturbated and bioturbated) (Figure 2.12A, B) have similar depositional process indicators as the argillaceous fine mudstone microfacies (MF3). The increase in detrital silt content is interpreted to indicate increased proximity to the sediment input source or an increase in flow competency associated with a steepening basin floor gradient (Mulder & Alexander, 2001; Borcovsky et al., 2017). The random dispersal of detrital quartz silt, radiolarian tests, and other rare microfossil debris within the clay-dominated matrix is interpreted to be the result of the same plug-like flows discussed for MF3. In conjunction with this, MF4 and MF5 also occurs as discrete homogenous-looking laminae in other microfacies (Figure 2.12E). Similar discrete beds/laminae in other mudstones have been interpreted as storm deposits (Egenhoff & Fishman, 2013). Sub-millimeter stacked graded laminae can be seen in some cases (Figure 2.12F), fining upwards from phytodetritus and intraclast rich bases to homogenized clay tops, indicating deposition from waning flow. These thin fine-grained graded laminae are interpreted to be the result of surge and surge-like turbidity currents, where flow is turbulent throughout the thickness of the flow, and grain to grain interaction is rare (Mulder & Alexander, 2001). Mulder and Alexander (2001) described these surge and surge-like turbidity flows as fine-grained (typically not transporting grain sizes larger than sand) where particles are kept in suspension from the upward component of fluid turbulence, forming normally graded beds as sediment settles gently as a result of flow cessation.

The rare to common sub-millimeter sized intraclasts (Figure 2.12A and B, black arrows) throughout signify proximal erosion of previously deposited sediments, induced by increased bottom-current energies (Schieber et al., 2010). These small intraclasts were likely entrained in the suspension of the plug-like flows that dominated the deposition of this microfacies. The intraclasts were then transported within the flow to a more distal basin position. Microbial mat rip-up fragments (Figure 2.15G) are also incorporated into some laminae, another indication of erosive bottom currents and relatively high competency flows along the sediment water interface.

Common diagenetic dolomitization indicates intermittent sedimentation, allowing the same anaerobic byproducts to build up that characterize the heavily dolomitized microfacies (Schieber, 1999; Aplin & Macquaker, 2011; Hickey & Henk, 2007; Macquaker et al., 2007). Low intensities or absence of biogenic reworking, and low diversity and occurrence of benthic microfossils (agglutinated foraminifers) in the rarely burrowed microfacies are consistent with deposition under severely dysoxic to anoxic bottom waters. The interpreted laminar plug-like flow and turbidity surge flow sedimentation processes for this microfacies may lead to the idea that low degrees of biogenic reworking is the result of increased rates of sediment accumulation, however the pervasive bioturbation of similar laminae in MF5 (discussed below) strengthen the interpretation that the rarely bioturbated laminae are rather the result of poor oxygenation. Overall, the rarely bioturbated silt-bearing fine mudstone microfacies represents repeated laminar and/or turbid sediment gravity flows, resulting in thin deposits accumulating under oxygen-starved bottom waters.

The bioturbated silt-bearing fine mudstone microfacies (MF5) (Figure 2.12C, D) is interpreted to be the more proximal expression of MF4. Enhanced water mixing from strong bottom currents is interpreted to have facilitated more intense biogenic reworking, due to increased concentrations of dissolved oxygen brought in by the flows, when compared to the flow strength interpreted for MF4. Stronger bottom currents and associated carrying capacity is interpreted to stem from increased shoreline proximity and enhanced storm influence when compared to the rarely bioturbated microfacies.

Bioturbated discontinuous Planar Parallel to Continuous Wavy Non-parallel Argillaceous-siliceous Medium Mudstones (MF6)

The argillaceous-siliceous medium mudstones microfacies (Figure 2.13) is the coarsest grained of all microfacies identified in the Hare Indian and Canol Formations within the study area. The increase in detrital silt content reflects deposition in a proximal high energy setting associated with increased volumes of coarse-grained detrital material. Although a large fraction of the detrital sediment occurs as clay, its presence predominantly as clay-aggregate grains (identified through SEM analysis of both fractured core rock samples and thin sections; Figure 2.13F and G) with hydrodynamic properties similar to that of individual detrital silt grains indicates that deposition of such clays likely occurred under heightened depositional energy and sediment input (Aplin & Macquaker, 2011; Plint et al., 2012).

Discontinuous planar silt laminae (Figure 2.13B and C) are the result of bedload transportation via traction currents. Some such features are the result of recurrent increased bottom-current energies leading to a winnowing of the clay fraction, leaving behind concentrations of detrital silt as thin lag deposits (Schieber, Southard, & Thaisen, 2007; Schieber & Zimmerle, 1998; Egenhoff & Fishman, 2013; Wignall, 1989; Konitzer et al., 2014). More recently, Yawar and Schieber (2017) have experimentally shown that interlaminated discontinuous silt and clay fabrics can result from concomitant migrating of silt-dominated and clay-dominated ripples, where an interfingering of thin veneers left behind during migration leads to intercalation of silt and clay laminae. Furthermore, Schieber et al. (2007) suggested slightly inclined to apparent plane parallel lamination may be the result of compacted migrating floccule ripples deposited under steady-state flow, and therefore apparent planar silt laminae represent flattened low-angle ripple foresets. In many cases the differences between thin silt lags and possible ripple forests are difficult to distinguish, and their presence is simply taken to represent episodes of increased bottom-current energy. Clay and silt-bearing clay intraclasts throughout the mudstone microfacies indicate up-dip erosion and associated high-competency flows. Normally graded laminae are an indication of episodic waning flow, likely forming from surge and surge-like flows linked to storm processes (Mulder & Alexander, 2001). Intercalated thinly laminated (<0.5 mm) silt-poor layers therefore represent intermittent lower-competency plug-like or surge-like flows resulting from smaller storms than those responsible for the normally graded laminae.

Increased intensities of bioturbation and subsequent destruction of some primary sedimentary structures (Figure 2.13B) stems from increased oxygenation associated with enhanced water column mixing. Storm influence is interpreted as intermittent, allowing enough time for sediment colonization between events. Overall, the argillaceous-siliceous medium mudstone microfacies is considered to be the result of episodic suspension settling from low-density, surge and surge-like turbidity flows under heightened but variable bottom-current energies. Such an increase in bottom current energy is interpreted to stem from deposition in a more proximal setting relative to the previously described microfacies.

Fossiliferous Discontinuous to Continuous Wavy Parallel Argillaceous Fine Mudstone (MF7)

The fossiliferous argillaceous fine mudstone microfacies (Figure 2.14) is characterized by the presence of high volumes of tentaculitids; calcareous conical pelagic organisms that were common throughout the Devonian (Filipiak and Jarzynka, 2009). Sediments containing such compositionally homogenous calcareous skeletal debris could be the result of (1) suspension fallout in quiescent depositional settings with an overlying oxygenated water column, or (2) re-sedimentation via storms, debris flows, and turbidites in settings associated with increased bottom-current energy (Hickey & Henk, 2007). Two layer types dominated this microfacies: clay matrix supported layers and allochem supported layers.

The bimodal size contrast between the carbonate fossil shells and the argillaceous clay matrix in matrix-supported fossil bearing layers (Figure 2.14A – C), coupled with the lack of any obvious primary sedimentary structures, could be interpreted as a result of tentaculitid suspension fall-out, where tests settled into argillaceous sea floor sediments (Egenhoff & Fishman, 2013; Konitzer et al., 2014). If these relatively large shells were to have settled into the soupy water-rich fine-grained deposits you would expect shells to concentrate more evenly along remnant bedding planes. However, the random dispersal of tentaculitids throughout individual beds/laminae and variable concentrations of tentaculitids between deposits (Figure 2.14A), together coupled with the bedding parallel but random orientation of conical tests rather suggests deposition from a high-competency collapsing plug flow (Baas et al., 2009; Sumner et al., 2009). Such flows are likely distal storm influence (Wignall, 1989; Konitzer et al., 2014).

The presence of tentaculitids suggests the existence of an overlying oxygenated water column with sufficient dissolved oxygen to support a pelagic biomass. Waters directly near the sediment-water interface were poorly oxygenated, resulting in early diagenetic precipitation of ferroan dolomite and an absence of high rates of biogenic sediment reworking. The absence of microfossils (specifically benthic foraminifers) within the thin sections of this facies, other than the obvious tentaculitids (Figure 2.6) further confirm the interpretation of poorly oxygenated bottom-waters.

Allochem-supported fossiliferous deposits (Figure 2.14D and E) are composed of relatively large tentaculitid shells when compared to tentaculitids of matrix supported deposits (Figure 2.14A). These units signify increased competency of bottom-current activity. Matrix-poor ungraded and fragmented fossiliferous layers (Figure 2.14D) are interpreted to be the result of debrite deposition, where high-cohesion flows did not allow for suspension settling, preferential orientation, or sorting of any kind (Sumner et al., 2009). These layers may also represent post-depositional increased bottom-current energies leading to winnowed shell lags overlying undulatory erosion/scour surfaces (Figure 2.14D) (Egenhoff & Fishman, 2013; Knapp et al., 2017). Normally graded bioclastic beds and laminae (Figure 2.14E) are interpreted to represent waning current energies and suspension settling from surge and/or surge-like low density turbidite flows (Muir, 1988; Baas et al., 2009; Sumner et al., 2009; Konitzer et al., 2014; Knapp et al., 2017). The fossil fraction of the allochem-supported deposits is more commonly intact as opposed to fragmented, indicating very short transport paths (Egenhoff & Fishman, 2013). Authigenic carbonates in the form of intergranular and intragranular cements may be a testament to either intermittent slow fair-weather suspension settling rates or long wait times between recurrent storm activity.

Intraclastic-Rich Discontinuous Planar Parallel Argillaceous Fine Mudstone (MF8)

Intraclast-rich argillaceous fine mudstone (MF8) (Figure 2.15) is interpreted to be the most proximal microfacies and is the result of constant bed load transport of silt and sand-sized intraclastic clay aggregates. A general absence of incorporated organic matter and pyrite framboids in the intraclasts is interpreted to reflect persistent bottom current energy that supplied a constant source of intraclasts and clay floccules from more proximal and oxygenated settings. Minimum bottom-current energies required to erode and transport such intraclasts are estimated at 16 cm/s (Schieber et al., 2010). The consistent distribution of intraclasts throughout this microfacies suggests that these relatively high-energy bottom currents were either; (1) temporally and laterally consistent, or (2) intermittent with low energy suspension settled material being re-transported upon resumption of current flow, likely linked to storm processes.

These sediments dominate the Bell Creek Member of the Hare Indian Formation and are interpreted to represent some extent of deltaic influence, which would have provided the increase in slope gradient, constant down-slope hyperpycnal bottom-current flow, and sediment input necessary for such continuous intraclast generation. As well, proximity to a deltaic setting would provide the depositional topography along the deltaic slope to allow for localized sediment slippage and compaction resulting in the synsedimentary recumbent micro-folding and faulting due to slope-toe failure (Figure 2.15B) (Wignall, 1989; Tyson, 1986). Storm influence is also reflected in low density turbidite laminae (MF3) and stacked graded laminae (Figure 2.15D) produced from waning bottom-current flow (Wignall, 1989). Bottom waters were likely partially oxygenated due to constant bottom-current flow, but bioturbation rates are low – possibly owing to rapid sedimentation rates not allowing time for colonization.

2.6.3 Depositional Model

Petrographic analysis of the Horn River Group mudstones reveals a physically dynamic depositional setting (Figure 12) that is in stark contrast to the hemipelagic suspension settling in quiescent anoxic waters that were previously proposed (Muir, 1988). Storm-generated laminar plug-like flows, surge and surge-like turbidity flows, and even small debrites dominated more proximal settings rich in intraclastic aggregates and coarse-grained allochems. Re-suspension of unconsolidated mud during storm-wave agitation lead to the formation of low density turbidites and plug-like flows in distal settings, recognized as thin (<1 mm thick) normally graded laminae and sharp based and occasionally undulatory homogeneous deposits, respectively (Figure 2.11A, Figure 2.12E and F).

Four primary depositional mechanism associations have been identified through the microfacies analysis, and in order of increasing proximity to the paleo-shoreline they are: 1) pelagic suspension settling association (S1); 2) plug-like flow-dominated association (S2); 3) combined proximal low-density turbidite (surge and surge-like flows), plug-like flow, and debrite association (S3); 4) and proximal plug-like flow association (S4) (Table 2.1).

The suspension settling association (S1, MF1) is the result of pelagic suspension settling in distal shelf and further basinward (slope, deep basin floor) areas with low detrital sediment input, reduced storm influence and few bottom currents (Egenhoff & Fishman, 2013; Knapp et al., 2017; Faugères & Mulder, 2011). Anoxic pore waters may have developed in radiolarian-rich fMs deposits associated with proliferation events due to oxygen consumption from degradation of high volumes of organic matter (Fishman et al., 2015).

The plug-like flow dominated association (S2, MF2-4) is the result of sedimentation from fine-grained flows generated from storm-wave re-suspension of unconsolidated water-rich muds also in relatively distal shelf settings. Uncommon intraclasts and low amounts of detrital silt point towards bottom current energies too low to generate flows with high enough competency to support a coarse-grained fraction. Sedimentation is interpreted as episodic and infrequent, allowing the buildup of anaerobic by-products and their resultant minerals (*e.g.* carbonate and pyrite). Sediment pore waters are interpreted to straddle the dysoxic-anoxic transition, reflected in low bioturbation intensities, low benthic microfossil abundance, and the presence of diagenetic dolomite and common pyrite framboids.

The combined low density turbidite dominated association (S3, MF5 - 7) is interpreted to be the result of storm reworking and subsequent turbulent (surge/surge-like), laminar (plug-like), and cohesive (debrite) sediment delivery in more proximal or more heavily storm influenced shelf settings than that of S1 and S2. Intense storm activity is recorded in the relatively thick fossil shell lags of MF7. Lower energy storms are recorded in laminae with rare intraclasts (MF5), and the distal effects of storms are recorded as low density turbidites fine mudstone laminae. The overlying water column is interpreted to have been partially oxygenated, reflected in the large carbonate fossil sizes, and sediment pore waters were likely partially oxygenated, reflected as increased bioturbation intensities and increased benthic microfossil abundance when compared to S1 and S2.

The proximal plug-like flow-dominated association (S4, MF8) is the result of persistent, high-energy erosive bottom currents, in a proximal shelf setting (generating large numbers of intraclasts), possibly associated with the distal deposits of a delta.

Almost every microfacies identified shows some evidence of storm-generated sediment delivery processes. Thus, sedimentation during the deposition of the HRG mudstones is interpreted to be dominantly storm generated and episodic along a proximal to distal continental shelf.

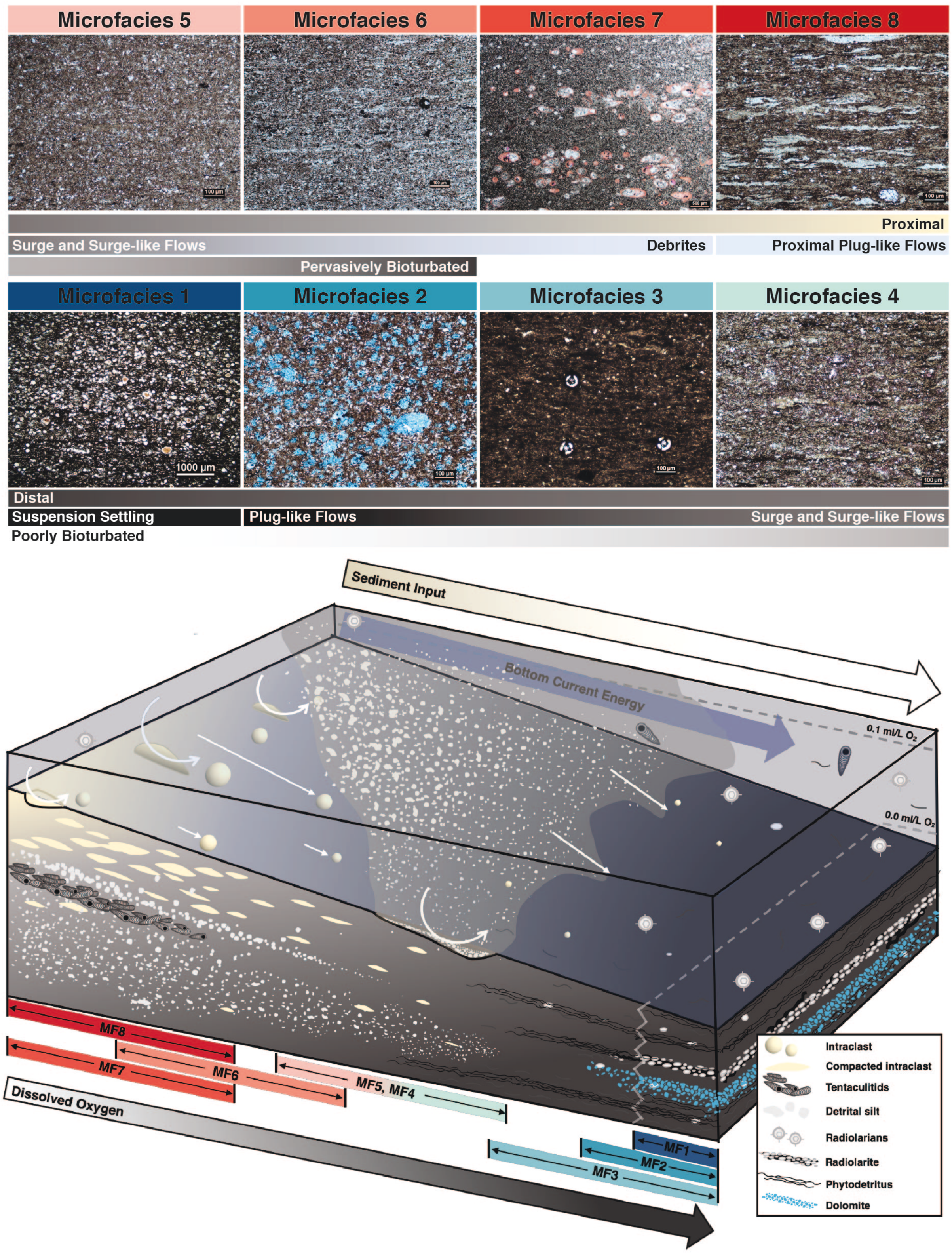
Microfacies 5
Microfacies 6
Microfacies 7
Microfacies 8
Proximal
Surge and Surge-like Flows
Debrites
Proximal Plug-like Flows
Pervasively Bioturbated
Microfacies 1
Microfacies 2
Microfacies 3
Microfacies 4
1000 µm
Distal
Suspension Settling
Plug-like Flows
Surge and Surge-like Flows
Poorly Bioturbated
Sediment Input
Bottom Current Energy
0.1 ml/L O2
0.0 ml/L O2
MF8
MF7
MF6
MF5, MF4
MF1
MF2
MF3
Dissolved Oxygen
Intraclast
Compacted intraclast
Tentaculitids
Detrital silt
Radiolarians
Radiolarite
Phytodetritus
Dolomite

Figure 2.16: Summary of microfacies and schematic depositional model block diagram for the Horn River Group mudstones in the Central Mackenzie Valley. Relative location, bioturbation intensity, and dominant transportation mechanism is identified for each microfacies in the schematic block diagram.

2.6.4 Comparison to Sequence Stratigraphic Interpretations

The microfacies stacking patterns in the N-09 core parallel the transgressive and regressive cycles identified through geochemical analyses by (LaGrange et al., 2019) (Figure 2.17). Transgressive-Regressive Sequences with Maximum Regressive Surfaces as sequence boundaries are used herein because it is not possible to distinguish forced regression from normal regression with the datasets available to us (chemostratigraphic, petrophysical, and sedimentological) and given the nature of the Horn River Group in the study area.

No thin section data falls exactly on interpreted sequence stratigraphic surfaces (maximum surfaces of regression and maximum flooding surfaces), but the vertical microfacies trends reflect the progradation and subsequent microfacies shallowing associated with regressive intervals and deepening accompanying transgressive cycles. Maximum flooding surfaces in the N-09 core are associated with distal detrital-derived microfacies (silt-poor fine mudstones, MF3). Maximum regressive surfaces are associated with intraclastic-rich mudstones (MF8) and fossiliferous mudstones (MF7), as well as occurring in close proximity to silt-rich medium mudstones (MF6); the three most proximal (shallowest) microfacies identified.

Bioturbation intensities (% reworking, blue bars in Figure 2.17) appear highest in regressive cycles, and relatively low in transgressive cycles. However, there is no obvious trends within transgressive or regressive cycles themselves. Ichnofossil diversity also does not appear to have any significant trends associated with T-R cycles (yellow dots, Figure 2.17).

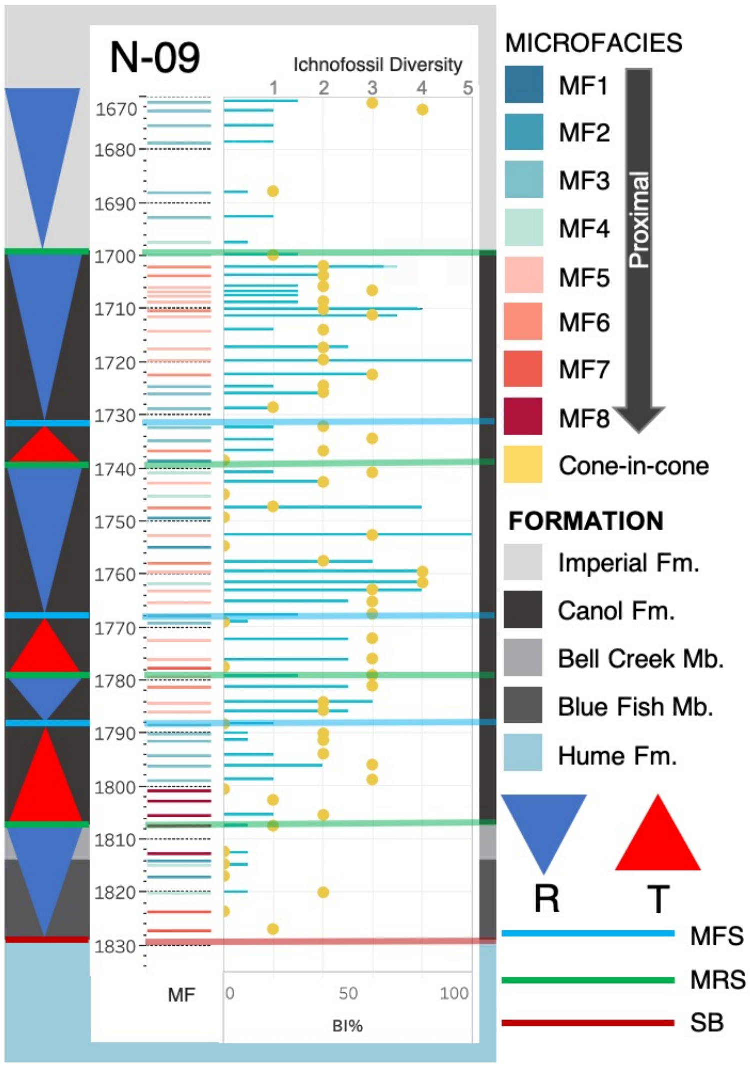

Figure 2.17: Comparison of microfacies (color-coded), bioturbation intensity (blue bars), and ichnofossil diversity (yellow dots) to identified transgressive and regressive cycles for the Husky Little Bear N-09 core. Sequence stratigraphic interpretations can be found in LaGrange et al., 2019. Abbreviations: regression (R), transgression (T), maximum flooding surface (MFS), maximum regressive surface (MRS), and sequence boundary (SB).

2.6.5 Mechanisms of Organic Carbon Preservation

Source rocks, such as the Canol Formation and Bluefish Member of the HRG, are characterized by their elevated preserved total organic carbon content (in these cases TOCs ranging from 1.5% to 9.2%) (Kabanov & Gouwy, 2017). It is generally accepted that the high rates of organic matter preservation in organic-rich mudstones are the result of slow hemipelagic suspension settling paired with persistently anoxic/euxinic bottom waters (*e.g.* Katz, 2005; Ghadeer & Macquaker, 2012). Low sediment accumulation rates prevent clastic dilution of organic matter and poorly oxygenated waters inhibit oxidative decay of settling organic carbon. When combined, these conditions create ideal settings for increased organic matter accumulation and preservation within sediments.

Horn River Group source rocks are compositionally more heterogenous and depositionally more dynamic than previously understood. It therefore stands that the mechanisms of organic-matter preservation within the HRG may also have been more dynamic than organic-matter simply accumulating under poorly oxygenated stagnant bottom waters, with low rates of detrital sediment input. In fact, TOC analyses of HRG microfacies reveals that the highest rates of TOC preservation occur in the most proximal coarsest-grained microfacies having the highest bioturbation intensities, and steadily decline basinward (Figure 2.18 and 14). Although TOC values fluctuate within individual microfacies, there is a clear trend between increasing TOC and increasing proximity to the paleoshoreline. The very same trend was identified by Borcovsky et al. (2017) in the organic-rich mudstone Bakken Formation. The relationship between proximity and TOC in the Bakken Formation was attributed, in part, to episodic sediment deposition acting to enhance organic matter preservation. The interpreted mechanisms behind the TOC trends in the HRG are discussed hereunder.

Sedimentation in the HRG is interpreted to be dominated by episodic storm generated sedimentation, where increased influx of detrital sediment and organic matter leads to increased sediment accumulation and subsequent burial. Many studies have suggested that increased sedimentation is one of the key mechanisms in organic matter preservation, as it shelters organic carbon from oxidants within the water column and pore waters, as well as from bacterial degradation (Egenhoff & Fishman, 2013; Ghadeer & Macquaker, 2012; Coleman, Curtis, & Irwin, 1979; Ibach, 1982; Bohacs et al., 2005). This process may also act to reduce the exposure time of organic matter to oxidants (Coleman et al., 1979). Sedimentation rates up to 5-10 cm/1000 years have been postulated to have the best ability to preserve organic matter, whereas depositional rates >5-10 cm/1000 years have declining TOCs as a result of clastic dilution (Katz, 2005; Betts & Holland, 1991). The sedimentation rate for the proposed shelfal position of the HRG was likely lower, not exceeding 5 cm/1000 years (*e.g.* Lesueur, Jouanneau, Boust, Tastet, & Weber, 2001). This would allow for increased organic matter preservation without clastic dilution (Betts & Holland, 1991). The sediments of the Bell Creek Member have the lowest TOC content, and are thought to have experienced increased depositional rates around 15–23 cm/1000 years (Al-Aasm, Muir, & Morad, 1992). Increased sedimentation rates may have led to clastic dilution and lower TOC values. In addition, the relatively low TOC values for the Bell Creek Member may also be the result of the member being composed dominantly of the intraclast-rich microfacies (MF8). Lower TOC values associated with the intraclast-rich microfacies (MF8) is expected, as significant volumes of the sediment are composed of organic-poor intraclasts (>30%) which would result in a 30% decline in TOC% when compared to other microfacies.

Ichnological analyses reveal that many of the microfacies display highly variable rates of biogenic reworking, ranging from 0 - 100%, by deposit-feeding meiofauna. The presence of such burrowing indicates that bottom waters were not fully anoxic, but rather intensely dysoxic (straddling the anoxic-dysoxic boundary). Micropaleontologic observation showed that the occurrence of benthic microfossils is seemingly low. These, when combined, disprove persistent bottom water anoxia as the sole mechanism for organic matter preservation within these organic rich rocks. Similar conclusions have been reached by Egenhoff and Fishman (2013) and Ghadeer and Macquaker (2012) regarding TOC preservation in other organic rich mudstones.

2.6.6 Microbioturbation Potential as a Paleo-redox Proxy

The availability of high-quality cored data from Hare Indian and Canol formations presents an opportunity to study how trace fossil morphology, abundance, diversity, and other associated characteristics reflect low-oxygen depositional settings, and how these oxygen-related traits can be applied to other fine-grained reservoirs in hopes of estimating extents of depositional oxygenation. Previous attempts at using ichnological characteristics as paleoredox proxies have resulted in the identification of four separate biofacies that are inherently linked to dissolved oxygen content of the bottom waters (aerobic, dysaerobic, anaerobic, and anoxic) (Rhoads & Morse, 1971; Byers, 1977). The quantitative boundaries of available dissolved oxygen (DO2) for each biofacies are as follows: >1.0 mL/L = aerobic (oxic), 0.1 – 1.0 mL/L = dysaerobic (dysoxic), 0.0 - 0.1 mL/L = anerobic (dysoxic), and 0.0

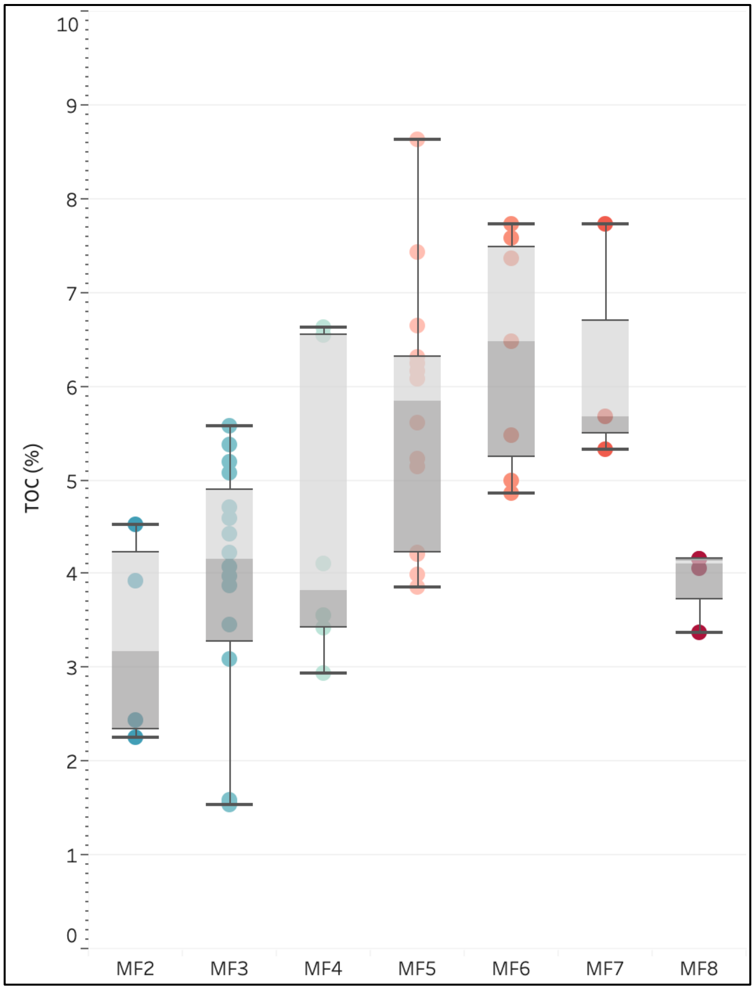

Figure 2.18: Distribution of TOC% within each microfacies (MF). No TOC data available for MF1 (radiolarian-rich fMs).

mL/L anoxic (Rhoads & Morse, 1971; Byers, 1977). The general consensus is that with declining rates of DO2, infaunal organism body size, ichnogenera diversity, depth of burrow penetration, and bioturbation intensity all decline (Bromley, 1996; Gingras et al., 2011; Savrda & Bottjer, 1984; Bromley & Ekdale, 1984; Savrda & Bottjer, 1987; Rhoads & Morse, 1971; Byers, 1977; Rhoads, 1975; Savrda & Bottjer, 1986; Bottjer & Savrda, 1990).These previous studies were focused on macroscopic features (e.g. macrofauna and/or macroscopic burrows), have utilized tiering or burrow cross cutting relationships, depth of burrow penetration, and burrow size to elucidate relative paleo-oxygenation

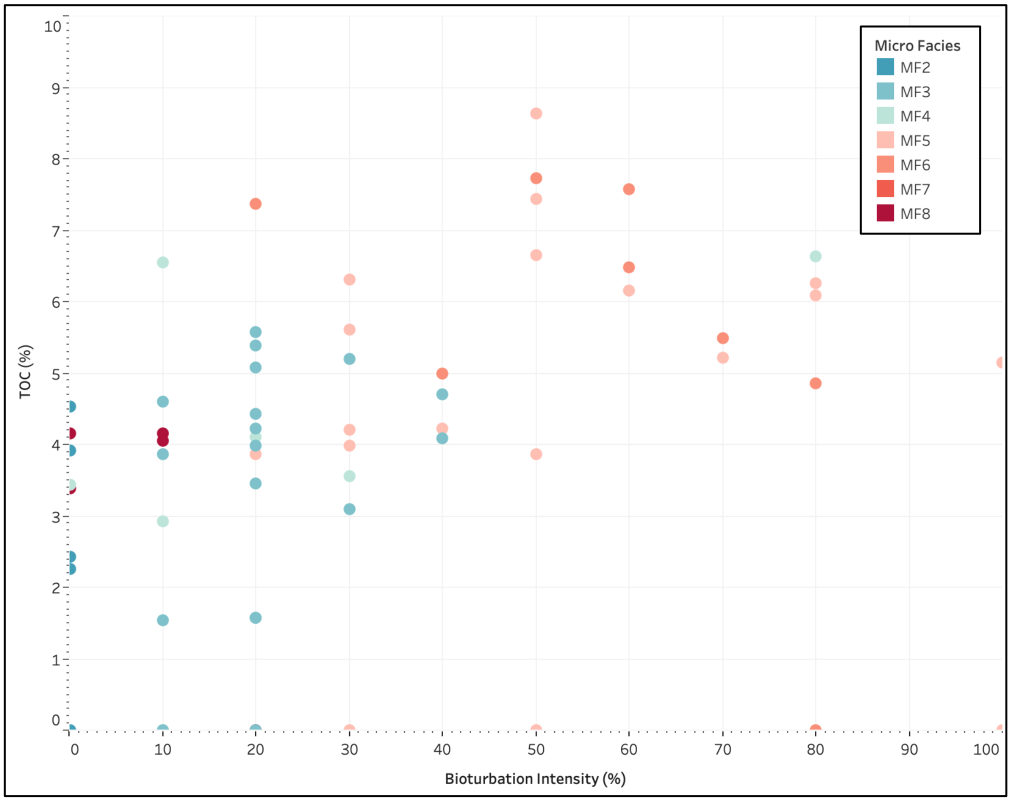

Figure 2.19: TOC% content in relation to bioturbation intensity (BI%) within the sediments.

(Savrda & Bottjer, 1987, 1986; Ekdale et al., 1984). The smallest burrows identified within those studies are millimeters to centimeters in diameter, orders of magnitude larger than the micro-scale burrows identified herein (maximum burrow diameters of 150 μm). The substantial size difference between the HRG burrows and those of previous studies, combined with the lack of cross cutting relationships and the purely morphological classification scheme used in this study makes applying previous ichnological paleoredox proxies difficult.

These previous studies have also focused on identifying relative paleo-oxygenation curves within the broad dysoxic realm (spanning from aerobic to anerobic conditions). In this particular study we are focused on identifying DO2 contents under very poor oxygen regimes, within the lower dysoxic realm. The mudstone intervals of the HRG are well-laminated, pyritic, organic-rich, sparsely fossiliferous sediments that lack any macroscale biogenic or sedimentary features; characteristics that have dubbed them anoxic by conventional interpretation (Muir, 1988; Dixon, 1984; Pyle et al., 2014; Kabanov et al., 2020). As previously mentioned, microscopic bioturbation in the HRG indicates at least some level of available dissolved oxygen in bottom waters and sediment pore waters during most of the mudstone deposition, but the low diversity suite and extremely small burrow sizes indicate such oxygen levels were likely straddling the dysoxic-anoxic transition zone.

The challenge lies in identifying the maximum DO2 concentrations available during deposition. The lower limit of identified living infaunal metazoans in modern day oxygen restricted basins (*e.g.* the Santa Barbra Basin) was originally taken by Rhoads and Morse (1971) to fall at bottom water dissolved oxygen levels of 1.0 mL/L, where concentrations <1.0 mL/L are devoid of endobenthic organisms (Rhoads & Morse, 1971; Byers, 1977). However, several authors (*e.g.* Savrda & Bottjer, 1984; Bottjer & Savrda, 1990) have described benthic meiofauna below the 0.1 mL/L anaerobic-dysaerobic transition zone. As well, the previous oxygenation studies have proposed several lower limit values of DO2 necessary to support benthic carbonate shelled organisms. Rhoads and Morse (1971) and Byers (1977) set this level at 1.0 mL/L, Thompson et al., (1985) set it at 0.3 mL/L, and Savrda et al., (1984) noted small shelly fauna down to the dysaerobic – anerobic transition zone of 0.1 mL/L. Considering these oxygen thresholds were identified for macroscopic biota, the microscopic organisms in this study likely have lower DO2 thresholds. SMall macrofauna and meiofaunal organisms have lower oxygen requirements than larger macrofauna, owing to their small body size (Giere, 1993; Grego, Riedel, Stachowitsch, & De Troch, 2014). The smaller body size leads to greater surface area to volume ratios (SA:V), allowing them to diffuse more oxygen across their membranes, when compared to larger benthos with significantly smaller SA:Vs (Giere, 1993). The lower oxygen requirements for meiofauna and small macrofauna makes them more resilient to survival in dysoxic sediments. However, the lack of any identified in-situ benthic carbonate shelled organisms in the HRG (the identified tentaculitid shells are interpreted to be pelagic) means that by conservative estimate, using the lower limit put forth by Savrda et al., (1984), bottom water oxygen contents within the HRG likely never exceeded 0.1 mL/L. Consequently, the range of bottom water oxygenations during deposition of the HRG mudstones was constrained to the anerobic biofacies (0.0 – 0.1 mL/L).

There is a limited assortment of microfossils identified within HRG intervals (Fig. 5), and their size, abundance, and diversity are extremely low. The four most prominent microfossils include phosphatic conodonts, calcite tentaculitids, siliceous radiolarians, and siliceous agglutinated foraminifera. As previously discussed, living organisms of the first three microfossils listed are considered to be entirely pelagic, and thus may be taken as evidence of (at the very least) a semi-oxygenated overlying water column (*e.g.* Rhoads & Morse, 1971; Byers, 1977; Savrda & Bottjer, 1984; Thompson, Mullins, Newton, & Vercoutere, 1985; Kaiho, 1994; Schieber, 2009). Agglutinated foraminifera, however, are taken as benthic sediment dwelling organisms, and thus, provide further insights into the bottom water chemistry during the deposition of these units (Schieber, 2009). Again, Dashtgard et al. (2015) and Dashtgard and MacEachern (2016) showed that modern-day and ancient unbioturbated shelfal muds, which would by conventional interpretation be deemed anoxic, may actually record only slightly reduced oxygenation (70% DO2 saturation). Hence, the identification of these benthic agglutinated foraminifera provide a further constraint on the paleo-oxygenation window for the HRG sediments. Under conditions of only slightly reduced oxygenation, which can preclude sediment colonization by burrowing metazoan macrofauna, one would expect to find a diverse assemblage of benthic foraminifera (Dashtgard & MacEachern, 2016; Dashtgard, Snedden, & MacEachern, 2015). The low diversity (only siliceous agglutinated benthic foraminifera were identified, using the methodology put forth by Schieber (2009)) and occurrence (occur as rare, isolated specimens, and are identified in a maximum of 26% of thin sections from a single microfacies), strengthens the interpretation that the bottom waters during the deposition of the HRG sediments were severely dysoxic. In fact, benthic foraminifer trends parallel that of the oxygen interpretations made for each microfacies, where identified foraminifers increase in percent abundance from MF1 through MF6 (Fig. 5). No agglutinated foraminifera tests were identified in MF7 and MF8, possibly a consequence of heightened depositional energies, precluding the burrowing of such organisms. Further constraints can be placed on paleo-bottom-water oxygenation using foraminiferal micropaleontologic data, by employing techniques put forth by Kaiho in 1994. Applying the 'dysoxic indicators' (thin walls, no ornamentation, sizes <500 μm) for calcareous foraminifera to the siliceous agglutinated forms identified in the HRG intervals, pore water dissolved oxygen contents can be constrained, again, to a maximum of 0.1-0.3 ml/l.

Looking at bioturbation intensities alone and considering that these sediments represent rapid and episodic storm generated deposition, one might feel that the low degrees of bioturbation reflect the frequency of sediment emplacement rather than an extremely low availability of dissolved oxygen. To combat this notion, one must consider all biogenic attributes together, such as the diminutive body size of the bioturbating organisms, reduction in diversity and bioturbation intensity, and the interpreted trace fossil ethology. Organism diminution is as a rule almost always associated with enhanced chemical stress, be that salinity or oxygenation (Gingras et al., 2011; Rhoads & Morse, 1971); in the case of the HRG mudstones this is oxygenation. Both reduction in diversity and bioturbation intensity are also considered to be good indicators of dysoxic marine conditions (Bromley, 1996; Gingras et al., 2011; Savrda & Bottjer, 1984; Bromley & Ekdale, 1984; Savrda & Bottjer, 1987; Rhoads & Morse, 1971; Byers, 1977; Rhoads, 1975; Savrda & Bottjer, 1986; Bottjer & Savrda, 1990). Ethologically, the absence of fugichnia or other equilibrichnia generally preclude rapid deposition rates as a cause for the paucity of burrowing fauna (Gingras et al., 2011). Also, if the high frequencies of sediment emplacement was the dominant dictator on burrow attributes, one may expect to see a top-down or "lam-scram" style of bed colonization, which again, is not the case with HRG mudstones. Furthermore, considering that the diminutive trace fossils crosscut multiple bed boundaries (*e.g.* Figure 2.13B and C), and being that these episodically deposited units are sub-millimeter thicknesses, it is unlikely that these rapid sedimentation events were able to stop even the most diminutive of burrowing organisms. In addition, evidence for microbioturbation even in the most depositionally energetic and thickest-bedded microfacies (MF6) disregards the notion that high sedimentation rates were dominantly responsible for the low degrees of bioturbation.

Comparison to Geochemical Paleoredox Proxies

Bulk composition (ppm concentrations) and enrichment factors of the redox sensitive trace metals vanadium (V) and molybdenum (Mo) are widely used as geochemical proxies for anoxic and euxinic conditions during deposition of organic rich mudstones, respectively (Tribovillard et al., 2006; Scott & Lyons, 2012; Dahl et al., 2013; Tinnin & Darmaoen, 2016). The processes that result in the enrichment of V within sediments occur primarily under oxygen-depleted conditions, whereas Mo enrichment occurs in bottom waters containing H2S. These trace metals are delivered to the sediments in a reduced state through organic acid complexation, precipitated as oxy-hydroxides, and solid-solution transformation via authigenic sulfides (Algeo & Maynard, 2004).

Contrary to expectation, there is no strong relationship between bioturbation (size diversity index and bioturbation intensity) and redox proxies (Figure 2.20 and 2.21). However, the absence of bioturbation and a paucity of benthic foraminifera equivocally helps to identify sediments deposited in anoxic bottom waters. The lack of correlation between the geochemical proxies and trace fossil indicators may be due to the wealth of factors other than available oxygen or the presence of H2S that act to influence V and Mo concentrations within sediment during deposition (*e.g.* sedimentation rates, position of the redox interface, and the presence of a depleted water column) (Tribovillard et al., 2006; Scott & Lyons, 2012; Morford, Emerson, Breckel, & Kim, 2005). As well, a temporal disconnect between the two data sets may have obscured any expected relationship. Bioturbation represents in situ instantaneous reflections of sediment and pore water chemistry at the time of burrowing, whereas diffusion of elements through pore waters can affect the distributions of elements over time (Scott & Lyons, 2012).

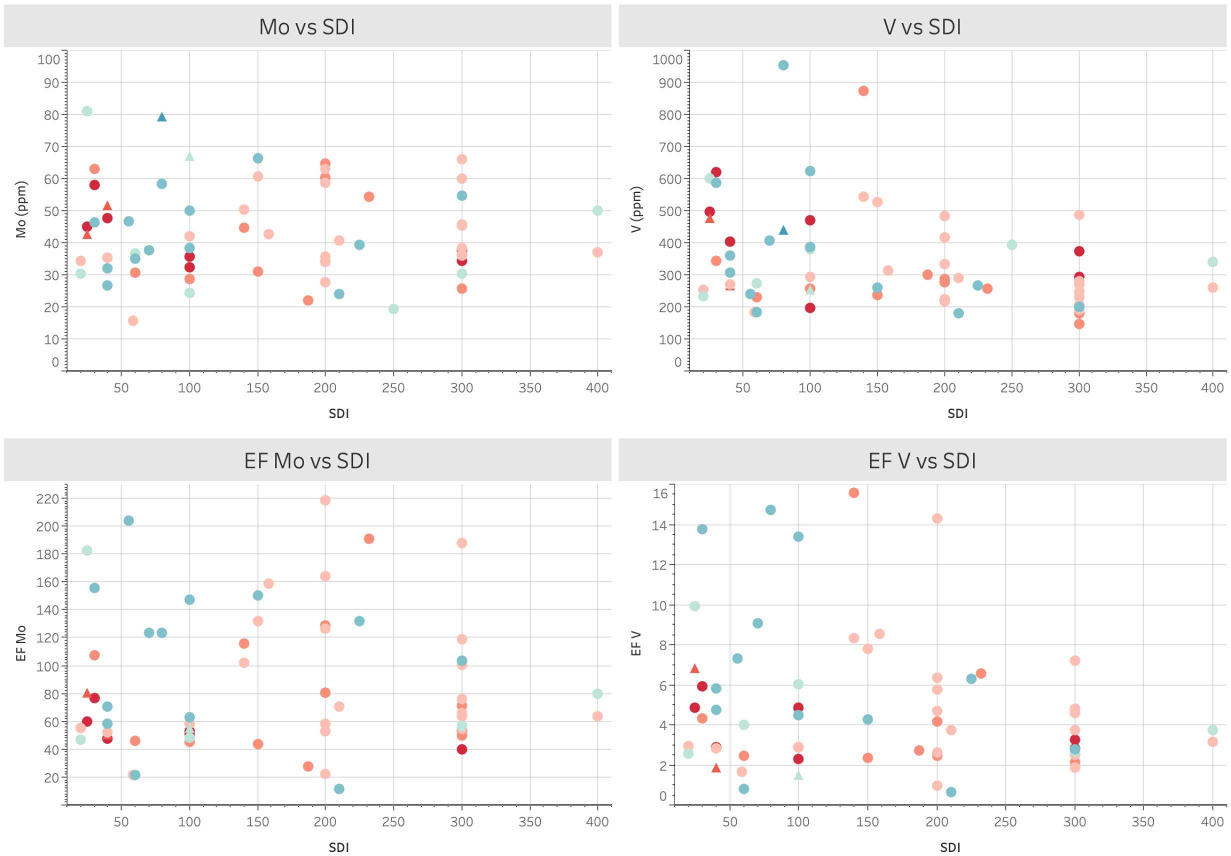

Figure 2.20: Trace fossil size-diversity index (SDI) vs Mo and V enrichment factors (EF) and bulk compositions (ppm).

2.7 Conclusions

The organic-rich mudstone intervals of Middle to Late Devonian Hare Indian and Canol formations contain eight distinct microfacies. These mudstone units, which appear plane parallel laminated in hand sample, represent dynamic sedimentation. Identified microfacies can be broken down into four distinct distinct depositional mechanism associations: 1) pelagic suspension settling, 2) plug-like dominated, 3) combined low density turbidites (surge and surge-like flows), plug-like flows, and debrites, and 4) proximal plug-like flows. Pelagic suspension settling dominated in distal quiet waters out of

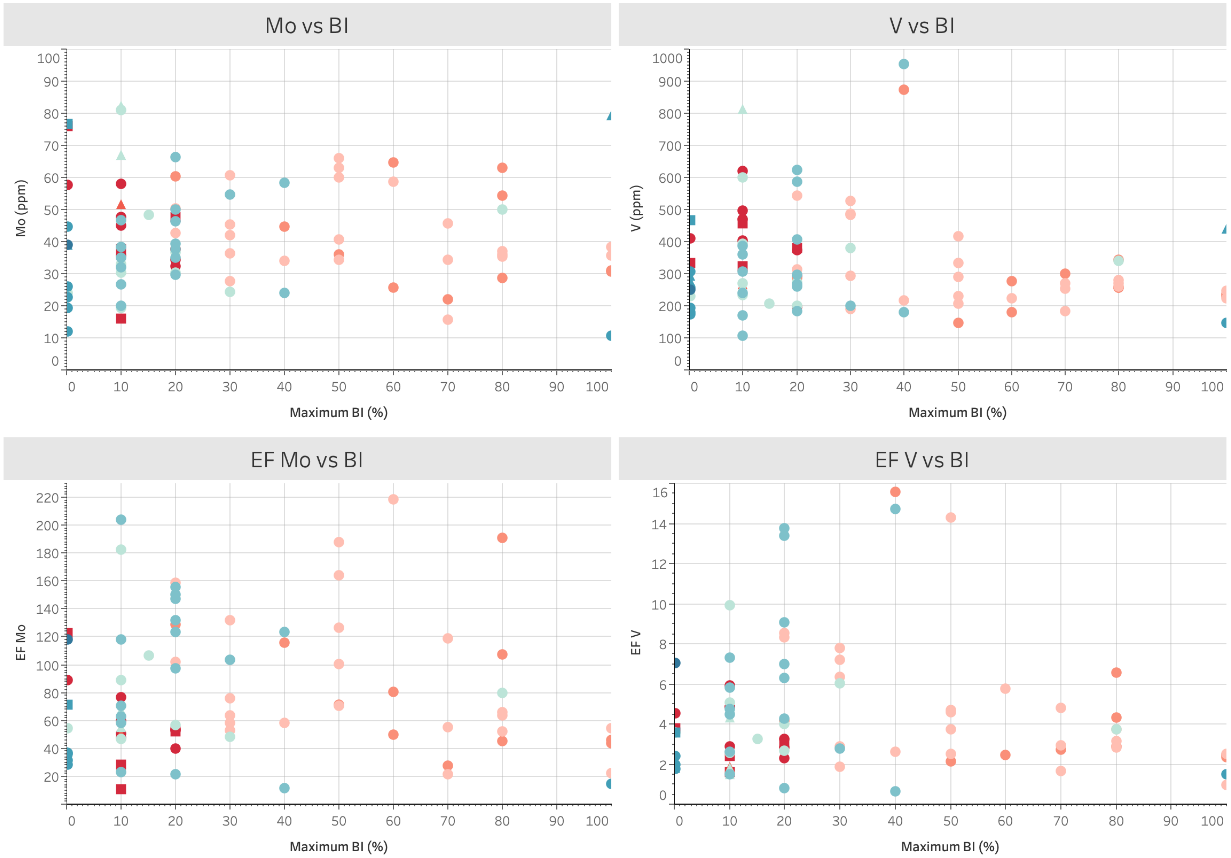

Figure 2.21: Bioturbation intensity (BI) vs Mo and V enrichment factors (EF) and bulk compositions (ppm).

the reach of persistent storm influence. Debrites, plug-like flows, and low density turbidite current processes represent a continuum, where storm influence is the dominant driver in sediment delivery. The distribution of organic matter suggests that persistent anoxia was not the dominant factor in TOC preservation, but rather a combination of heightened sedimentation, rapid burial, and possible elevated rates of primary production. Identified endobenthic microbioturbation throughout the Horn River Group mudstone successions indicates that sediment pore waters were at least periodically partially oxygenated. Petrographic ichnological and sedimentological analysis integrated with molybdenum and vanadium paleoredox proxies indicate that dissolved oxygen content of the sediment pore waters likely did not exceed 0.1 mL/L.

The depositional model, methods of TOC preservation, and paleo-oxygenation interpretations presented in this study are in contrast to previous assumptions of environmental conditions during accumulation of the Horn River Group, and of organic-rich mudstones in general. Discrepancies between the interpretations presented herein and conclusions from past studies highlight the importance of a combined micro-ichnological, sedimentological, and geochemical analysis of fine-grained organic rich deposits lest they be mischaracterized. This may spark the need for petrographic re-evaluation of the depositional mechanisms responsible for or influencing the deposition of other organic rich mudstones successions.

Chapter 3

Conclusions and Summary

This study has shed light on both the physical and chemical conditions at and just below the sediment-water interface during deposition of the organic-rich mudstones of the Horn River Group. Results of this study are in-line with the modern view on depositional controls of marine fine-grained sediments, resulting in a preferred interpretation of a partially oxygenated and energetically dynamic depositional setting.

3.1 Ichnology and Paleo-oxygenation

Petrographic analysis of the organic-rich mudstones in this study have revealed the existence of several credible morphologically distinct microscopic ichnofossil types. Identification of microbioturbation in these mudstones has an appreciable impact on the interpretations of the physico-chemical stresses at play during deposition of these fine-grained sediments. Sediment-penetrating (infaunal) organisms require dissolved oxygen for respiration; therefore, their presence in sediments indicates some level of available dissolved oxygen at the time of burrow construction. The organic-rich mudstones of the Horn River Group have historically been thought to represent deposition under anoxic and/or euxinic bottom waters (Kabanov et al., 2020; Muir, 1988; Tassonyi, 1969). The identification of microbioturbation within these intervals is a direct contradiction to these previous interpretations; and whereby the updated interpretation reflects deposition under at least periodically partially oxygenated (severely dysoxic) bottom waters. Petrographic ichnological and sedimentological analysis integrated with molybdenum and vanadium paleoredox proxies indicate that dissolved oxygen content of the sediment pore waters likely did not exceed 0.1mL/L.

Applying the proposed criteria for the identification of microbioturbation to other "anoxic" organic-rich mudstones may spark similar re-evaluations of depositional oxygenation interpretations.

3.2 Sediment Transport Mechanisms

The organic-rich mudstone intervals of Middle to Late Devonian Hare Indian and Canol Formations contain eight distinct microfacies. These mudstone units, which appear plane parallel laminated in hand sample, represent dynamic sedimentation. Identified microfacies can be broken down into four distinct primary sedimentation mechanisms: 1) pelagic suspension settling, 2) plug-like flow dominated, 3) combined low density turbidites (surge and surge-like flows), plug-like flows, and debrites, and 4) proximal plug-like flows.

Pelagic suspension settling is represented by siliceous radiolarian-rich fine-grained mudstones and is interpreted to have dominated distal quiet waters out of the reach of persistent storm influence. Plug-like flow is represented by homogenous-looking thin (<mm) fine-grained beds, interpreted to form from the distal ends of cohesive sediment-gravity

flows, where grain-grain interaction prevented selective settling of larger grains (Baas et al., 2009; Sumner et al., 2009). These plug-like flows dominated in both proximal and distal settings, with proximal expressions containing abundant intraclasts and distal expressions dominated by dispersed clay with some incorporated detrital silt. Surge and surge-like flows represent low-density-turbidite sediment transportation mechanisms, whereby grain-grain interaction is nil and selective suspension settling of larger grains leads to deposition of thin (<mm) normally graded beds (Mulder & Alexander, 2001). Surge and surge-like flows are present in almost all identified microfacies but dominated the intermediately located fine mudstones. Debrites are represented by mass jumbles of randomly oriented bi-modal coarse-grained allochems (tentaculitids) dispersed within an argillaceous matrix. Debrites were only identified in proximal microfacies. Nonetheless, debrites, plug-like flows, and low density turbidite processes represent a continuum where storm influence is the dominant driver in sediment delivery.

3.3 Organic Matter Preservation

Analysis of total organic carbon content against individual microfacies and bioturbation intensities shows, contrary to expectation, that TOC values increase with both increasing depositional proximity and bioturbation intensity. This relationship suggests that persistent anoxia was not the dominant factor in TOC preservation, but rather a combination of heightened sedimentation, rapid burial, and possible elevated rates of primary production.

3.4 Future Work

3.4.1 Suggested Improvements for Methods

The methods used in this study may be improved by 1) collecting thin section samples at regular intervals, as opposed to only at areas of interest, 2) having all thin sections prepared in the same style (thin sections in this study were of variable thicknesses with some being wedge cut, and some were stained while others were not), and 3) having geochemical analyses performed on the rock samples cut for thin section preparation. Improving the vertical coverage of thin sections and having direct comparisons to geochemical data would allow for a more comprehensive analysis of microfacies changes through core elevations, and how changes may be related to sea level or provenance trends identified through geochemical analysis (e.g. chemostratigraphy).

3.4.2 Potential of Approach

The results of this study have shown that the Hare Indian and Canol Formations have more complex depositional and oxygenation histories than previously understood. The techniques and ideas presented herein may have merit in future analysis of other fine-grained reservoirs, in helping to identify subtle indicators of the physical and chemical conditions present during deposition. However, this study opens up many more questions regarding the validity and importance of petrographic microfacies analysis.

A comprehensive integration of the proposed microfacies depositional settings with sequence stratigraphic interpretations and geochemical trends may help to assess the legitimacy of the proximal to distal microfacies relationships proposed herein. Future work may also entail comparisons of the microfacies identified within this study to those in other organic rich mudstones, to see if such microfacies are common occurrences or if they are localized to the Horn River Group. Neoichnological studies of microbioturbation in fine-grained sediments with variable pore water dissolved oxygen contents may be a valuable way to comprehensively assess the potential of microbioturbation as a paleo-redox proxy in mudstones. Future investigations of microbioturbation within organic rich mudstones may evaluate how microscopic burrows alter the reservoir properties of unconventional reservoirs. Potential studies may attempt answering such question as: 1) can micro burrows act as fluid conduits or migration pathways within fine-grained reservoirs, 2) how (if at all) does microbioturbation affect fracture propagation within reservoirs, and how does this change with varying bioturbation intensities (unbioturbated vs. biogenically homogenized), and 3) does the positive relationship between bioturbation intensity and TOC preservation hold true in other organic-rich mudstone formations? If the microfacies identified within this study are found to be common occurrences in other organic rich mudstones, if their proximal to distal interpretations can be validated by integration with other methods (e.g. sequence stratigraphy and geochemical analysis), and if there is a recurring trend between increasing proximity and increasing TOC, such microfacies analyses may have merit in identifying potential "sweet spots" in other fine-grained reservoirs. Additional future directions in the field mudstone microfacies analysis may include the development of agreed upon microfacies standards and possible petrographic facies models, similar to those for carbonates and coarse-grained clastic deposits.

Overall, petrographic microfacies analysis is of great importance when assessing fine grained deposits. Petrographic analysis sheds light on compositional, textural, and fabric characteristics that are very likely to go unidentified during macro-scale assessment techniques, such as lithofacies analysis and geochemical analysis. Although, there is no debate that the integration of as many data sets as possible will ultimately lead to the most complete interpretations of the depositional history and reservoir properties of organic rich fine-grained rocks.

3.5 Summary

The paleo-oxygenation interpretations, depositional model, and methods of TOC preservation presented in this study are in contrast to previous assumptions of environmental conditions during accumulation of the Horn River Group, and of organic-rich mudstones in general. Discrepancies between the interpretations presented herein and conclusions from past studies highlight the importance of a combined micro-ichnological, sedimentological, and geochemical analysis of fine-grained organic rich deposits lest they be mischaracterized. This may spark the need for petrographic re-evaluation of the depositional mechanisms responsible for or influencing the deposition of other organic rich mudstones successions.

References

Abbott, S. T. (2000, feb). Detached mud prism origin of highstand systems tracts from mid-Pleistocene sequences, Wanganui Basin, New Zealand. *Sedimentology*, *47*(1), 15–29. Retrieved from http://doi.wiley.com/10.1046/j.1365-3091.2000.00275.x doi: 10.1046/j.1365-3091.2000.00275.x

Al-Aasm, I. S., Muir, I. D., & Morad, S. (1992). Diagenetic conditions of fibrous calcite vein formation in black shales: petrographic, chemical and isotopic evidence. *Bulletin of Canadian Petroleum Geology*, *41*(1), 46–56.

Algeo, T. J., & Maynard, J. B. (2004, jun). Trace-element behavior and redox facies in core shales of Upper Pennsylvanian Kansas-type cyclothems. *Chemical Geology*, *206*(3-4), 289–318. Retrieved from https://www.sciencedirect.com/science/article/abs/pii/S0009254103003930 doi: 10.1016/j.chemgeo.2003.12.009

Anderson, R. F., Lehuray, A. P., Fleisher, M. Q., & Murray, J. W. (1989, sep). Uranium deposition in saanich inlet sediments, vancouver island. *Geochimica et Cosmochimica Acta*, *53*(9), 2205–2213. Retrieved from http://www.sciencedirect.com/science/article/pii/001670378990344X doi: 10.1016/0016-7037(89)90344-X

Aplin, A. C., & Macquaker, J. H. (2011). Mudstone diversity: Origin and implications for source, seal, and reservoir properties in petroleum systems. *AAPG Bulletin*, *95*(12), 2031–2059. Retrieved from http://archives.datapages.com/data/bulletns/2011/12dec/BLTN10162/IMAGES/BLTN10162.PDF doi: 10.1306/03281110162

Baas, J. H., Best, J. L., Peakall, J., & Wang, M. (2009, apr). A Phase Diagram for Turbulent, Transitional, and Laminar Clay Suspension Flows. *Journal of Sedimentary Research*, *79*(4), 162–183. doi: 10.2110/jsr.2009.025

Baird, G. C. (1978, jun). Pebbly Phosphorites in Shale: A Key to Recognition of a Widespread Submarine Discontinuity in the Middle Devonian of New York. *SEPM Journal of Sedimentary Research*, *48*(2), 545–555. Retrieved from https://pubs.geoscienceworld.org/jsedres/article/48/2/545-555/97107 doi: 10.1306/212F74CD-2B24-11D7-8648000102C1865D

Bassett, H., & Stout, J. (1967). Devonian of Western Canada. In *International symposium of the devonian system* (pp. 717–752). Calgary: CSPG Special Publications. Retrieved from http://archives.datapages.com/data/cspg{_}sp/data/ASPG-011/011001/717{_}cspgsp110717.htm

Baumgartner, L. K., Reid, R. P., Dupraz, C., Decho, A. W., Buckley, D. H., Spear, J. R., … Visscher, P. T. (2006, mar). Sulfate reducing bacteria in microbial mats: Changing paradigms, new discoveries. *Sedimentary Geology*, *185*(3-4), 131–145. Retrieved from https://www-sciencedirect-com.login.ezproxy.library.ualberta.ca/science/article/pii/S0037073805004252 doi: 10.1016/j.sedgeo.2005.12.008

Berner, R. A., & Raiswell, R. (1983, may). Burial of organic carbon and pyrite sulfur in sediments over phanerozoic time: a new theory. *Geochimica et Cosmochimica Acta*, *47*(5), 855–862. Retrieved from http://www.sciencedirect.com/science/article/pii/0016703783901515 doi: 10.1016/0016-7037(83)90151-5

Betts, J. N., & Holland, H. D. (1991, dec). The oxygen content of ocean bottom waters, the burial efficiency of organic carbon, and the regulation of atmospheric oxygen. *Palaeogeography, Palaeoclimatology, Palaeoecology*, *97*(1-2), 5–18. Retrieved from https://www-sciencedirect-com.login

.ezproxy.library.ualberta.ca/science/article/pii/092181819190123E doi: 10.1016/0031-0182(91)90178-T

Bohacs, K. M., Grabowski, G. J., Carroll, A. R., Mankiewicz, P. J., Miskell-Gerhard, K., Schwalbach, J. R., … Simo, J. (2005). Production, Destruction, and Dilution—The Many Paths to Source-Rock Development. In N. B. Harris (Ed.), *Deposition of organic-carbon-rich sediments: Models* (SEPM (Soci ed., pp. 61–101). Special Publications of SEPM. Retrieved from http://archives.datapages.com.login.ezproxy.library.ualberta.ca/data/sepm{_}sp/SP82/Production{_}Destruction{_}and{_}Dilutionthe.htm?q={%}2BtextStrip{%}3Abohacs+textStrip{%}3Akm+textStrip{%}3Agrabowski+textStrip{%}3Agj+textStrip{%}3Ajr+textStrip{%}3Acarroll+textStrip{%}3Aar+text doi: 10.2110/pec.05.82.0061

Borcovsky, D., Egenhoff, S., Fishman, N. S., Maletz, J., Boehlke, A., & Lowers, H. (2017, oct). Sedimentology, facies architecture, and sequence stratigraphy of a Mississippian black mudstone succession-The upper member of the Bakken Formation, North Dakota, United States. *AAPG Bulletin*, *101*(10), 1625–1673. Retrieved from www.aapg. doi: 10.1306/01111715183

Bottjer, D. J., & Savrda, C. E. (1990). Oxygen Levels from Biofacies and Trace Fossils. In D. E. G. Briggs & P. R. Crowthere (Eds.), *Paleobiology: a synthesis* (pp. 408–410). London: Blackwell Scientific Publications. Retrieved from http://www.palass.org/sites/default/files/media/publications/palaeobiology/palaeobiology{_}section4{_}pp305-414.pdf

Bromley, R. G. (1996). *Trace Fossils: Biology, taphonomy and applications* (2nd ed.). London: Chapman & Hall.

Bromley, R. G., & Ekdale, A. A. (1984). Chondrites : A Trace Fossil Indicator of

Anoxia in Sediments. *Science*, *224*(4651), 872–874.

Byers, C. W. (1977). Biofacies Patterns in Euxinic Basins: a General Model. *The Society of Economic Paleontologists and Mineralogists Special Publication 25*, 5–17.

Coleman, M. L., Curtis, C. D., & Irwin, H. (1979). Burial Rate a Key to Source and Reservoir Potential. *World Oil*, *188*(4), 83 – 92.

Cuomo, M. C., & Bartholomew, P. R. (1991). Pelletal black shale fabrics: Their origin and significance. *Geological Society Special Publication*, *58*, 221–232. doi: 10.1144/GSL.SP.1991.058.01.15

Dahl, T. W., Ruhl, M., Hammarlund, E. U., Canfield, D. E., Rosing, M. T., & Bjerrum, C. J. (2013, dec). Tracing euxinia by molybdenum concentrations in sediments using handheld X-ray fluorescence spectroscopy (HHXRF). *Chemical Geology*, *360-361*, 241–251. Retrieved from `https://www-sciencedirect-com.login.ezproxy.library.ualberta.ca/science/article/pii/S0009254113004786` doi: 10.1016/J.CHEMGEO.2013.10.022

Dashtgard, S. E., & MacEachern, J. A. (2016, may). Unburrowed mudstones may record only slightly lowered oxygen conditions in warm, shallow basins. *Geology*, *44*(5), 371–374. Retrieved from `www.gsapubs.org` doi: 10.1130/G37648.1

Dashtgard, S. E., Snedden, J. W., & MacEachern, J. A. (2015). Unbioturbated sediments on a muddy shelf: Hypoxia or simply reduced oxygen saturation? *Palaeogeography, Palaeoclimatology, Palaeoecology*, *425*, 128–138. Retrieved from `http://dx.doi.org/10.1016/j.palaeo.2015.02.033` doi: 10.1016/j.palaeo.2015.02.033

Dawson, W. C. (2000). Limestone Microfacies and Sequence Stratigraphy : Eagle Ford Group (Cenomanian-Turonian) North-Central Texas

Outcrops. *GCAGS Transactions*, 99–105.

Dixon, O. A. (1984). Sedimentology and Straigraphy of a Middle-Upper Devonian Sequence in the Powell Creek Area, NWT. *Contributions to the Geology of the Northwest Territories*, *1*, 29–38.

Egenhoff, S. O., & Fishman, N. S. (2013). Traces in the dark-sedimentary processes and facies gradients in the upper shale member of the Upper Devonian-Lower Mississippian Bakken Formation, Williston Basin, North Dakota, U.S.A. *Journal of Sedimentary Research*, *83*(9), 803–824. doi: 10.2110/jsr.2013.60

Ekdale, A. A., Muller, L. N., & Novak, M. T. (1984, mar). Quantitative ichnology of modern pelagic deposits in the abyssal Atlantic. *Palaeogeography, Palaeoclimatology, Palaeoecology*, *45*(2), 189–223. Retrieved from `https://www.sciencedirect.com/science/article/pii/0031018284900403` doi: 10.1016/0031-0182(84)90040-3

Faugères, J. C., & Mulder, T. (2011, jan). Contour currents and contourite drifts. In H. Huneke & T. Mulder (Eds.), *Developments in sedimentology* (Vol. 63, pp. 149–214). Amsterdam: Elsevier. Retrieved from `https://www.sciencedirect.com/science/article/pii/B9780444530004000032` doi: 10.1016/B978-0-444-53000-4.00003-2

Fishman, N. S., Egenhoff, S. O., Boehlke, A. R., & Lowers, H. A. (2015). Petrology and diagenetic history of the upper shale member of the late Devonian-early Mississippian Bakken Formation, Williston Basin, North Dakota. *Special Paper of the Geological Society of America*, *515*, 125–151. Retrieved from `https://pubs.geoscienceworld.org/books/book/675/chapter/3807976/` doi: 10.1130/2015.2515(07)

Folk, R. L. (1960, mar). Petrography and Origin of the Tuscarora, Rose Hill, and Keefer Formations, Lower and Middle Silurian of Eastern West

Virginia. *SEPM Journal of Sedimentary Research*, *Vol. 30*(1), 1–58. doi: 10.1306/74d709c5-2b21-11d7-8648000102c1865d

Folk, R. L. (1962, sep). Petrography and Origin of the Silurian Rochester and McKenzie Shales, Morgan County, West Virginia. *SEPM Journal of Sedimentary Research*, *Vol. 32*(3), 539–578. doi: 10.1306/74d70d17-2b21-11d7-8648000102c1865d

Fraser, T. A., Allen, T. L., Lane, L. S., & Reyes, J. C. (2011). Shale gas potential of Devonian shale in north Yukon: Results from a diamond drillhole study in western Richardson Mountains. *Yukon Exploration and Geology 2011*, 45–74. Retrieved from `https://cseg.ca/assets/files/resources/abstracts/2014/158{_}GC2014{_}Petroleum{_}potential{_}of{_}Middle-Upper{_}Devonian{_}Canol{_}Fm.pdf`

Gautier, D. L. (1986, mar). Cretaceous shales from the western interior of North America: sulfur/carbon ratios and sulfur-isotope composition. *Geology*, *14*(3), 225–228. Retrieved from `https://pubs.geoscienceworld.org/geology/article/14/3/225-228/204011` doi: 10.1130/0091-7613(1986)14<225:CSFTWI>2.0.CO;2

Geological Rock Color Chart. (2009). Grand Rapids, MI: Munsell Color. Retrieved from `http://munsellstore.com/files/CIPA00011{%}5C599.pdf`

Ghadeer, S. G., & Macquaker, J. H. (2012, aug). The role of event beds in the preservation of organic carbon in fine-grained sediments: Analyses of the sedimentological processes operating during deposition of the Whitby Mudstone Formation (Toarcian, Lower Jurassic) preserved in northeast England. *Marine and Petroleum Geology*, *35*(1), 309–320. Retrieved from `https://www-sciencedirect-com.login.ezproxy.library.ualberta.ca/science/article/pii/S0264817212000025` doi: 10.1016/j.marpetgeo.2012.01.001

Ghadeer, S. G., & Macquaker, J. H. S. (2011, sep). Sediment transport processes in an ancient mud-dominated succession: a comparison of processes operating in marine offshore settings and anoxic basinal environments. *Journal of the Geological Society*, *168*(5), 1121–1132. Retrieved from http://jgs.lyellcollection.org/cgi/doi/10.1144/0016-76492010-016 doi: 10.1144/0016-76492010-016

Giere, O. (1993). *Meiobenthology: The Microscopic Fauna in Aquatic Sediments*. Berlin, Heidelberg: Springer-Verlag Berlin Heidelberg. doi: 10.1017/CBO9781107415324.004

Giere, O. (2009). *Meiobenthology: The microscopic motile fauna of aquatic sediments*. Berlin: Springer-Verlag Berlin Heidelberg. doi: 10.1007/978-3-540-68661-3

Gingras, M. K., MacEachern, J. A., & Dashtgard, S. E. (2011, jun). Process ichnology and the elucidation of physico-chemical stress. *Sedimentary Geology*, *237*(3-4), 115–134. Retrieved from https://www-sciencedirect-com.login.ezproxy.library.ualberta.ca/science/article/pii/S0037073811000601 doi: 10.1016/j.sedgeo.2011.02.006

Gingras, M. K., Zonneveld, J.-P., & Konhauser, K. O. (2014). Using X-ray Radiography to Observe Fe Distributions in Bioturbated Sediment. In D. Hembree, B. Platt, & J. Smith (Eds.), *Experimental approaches to understanding fossil organisms* (pp. 195–206). Dordrecht: Springer, Dordrecht. doi: 10.1007/978-94-017-8721-5_9

Grego, M., Riedel, B., Stachowitsch, M., & De Troch, M. (2014). Meiofauna winners and losers of coastal hypoxia: Case study harpacticoid copepods. *Biogeosciences*, *11*(2), 281–292. doi: 10.5194/bg-11-281-2014

Harman, R. A. (1964, jan). Distribution of Foraminifera in the Santa Barbara Basin, California. *Micropaleontology*, *10*(1), 81. Retrieved from http://www

.jstor.org/stable/1484628?origin=crossref doi: 10.2307/1484628

Hart, B. S., Macquaker, J. H., & Taylor, K. G. (2013, aug). Mudstone ("shale") depositional and diagenetic processes: Implications for seismic analyses of source-rock reservoirs. *Interpretation*, *1*(1), B7–B26. doi: 10.1190/INT-2013-0003.1

Hickey, J. J., & Henk, B. (2007). Lithofacies summary of the Mississippian Barnett Shale, Mitchell 2 T.P. Sims well, Wise County, Texas. *AAPG Bulletin*, *91*(4), 437–443. doi: 10.1306/12040606053

Ibach, L. E. J. (1982). Relationship between sedimentation rate and total organic carbon content in ancient marine sediments. *American Association of Petroleum Geologists Bulletin*, *66*(2), 170–188. doi: 10.1306/03B59A5D-16D1-11D7-8645000102C1865D

Irwin, H., Curtis, C. D., & Coleman, M. L. (1977). Isotopic evidence for source of diagenetic carbonates formed during burial of organic-rich sediments. *Nature*, *269*(5625), 209–213. doi: 10.1038/269209a0

Jonk, R., Potma, K., Bohacs, K. M., Advocate, D., & Starich, P. (2014). Integrating outcrop and subsurface data to evaluate data-poor shale plays: The Canol Formation, northwest territories, Canada. In *Society of petroleum engineers - unconventional resources technology conference.* Denver, Colorado: Unconventional Resources Technology Conference (URTEC). Retrieved from http://archives.datapages.com/data/urtec/2014/1896700.htm doi: 10.15530/urtec-2014-1896700

Kabanov, P., Fallas, K. M., & Deblonde, C. (2016). Geological and geochemical data from Mackenzie Corridor. Part IV: Formation tops and isopach maps of Horn River Group and basal beds of Imperial Formation, central Mackenzie Plain, NTS map sheets 96C-E. *Geological Survey of Canada, Open File*, *8023*, 1–14. Retrieved from https://

geoscan.nrcan.gc.ca/starweb/geoscan/servlet.starweb?path=geoscan/fulle.web{&}search1=R=297903 doi: 10.4095/297903

Kabanov, P., & Gouwy, S. A. (2017, apr). The Devonian Horn River Group and the basal Imperial Formation of the central Mackenzie Plain, N.W.T., Canada: Multiproxy stratigraphic framework of a black shale basin. *Canadian Journal of Earth Sciences*, *54*(4), 409–429. Retrieved from http://www.nrcresearchpress.com/doi/10.1139/cjes-2016-0096 doi: 10.1139/cjes-2016-0096

Kabanov, P., Gouwy, S. A., Lawrence, P. A., Weleschuk, D. J., & Chan, W. C. (2016). Geological and geochemical data from Mackenzie Corridor. Part III: New data on lithofacies, micropaleontology, lithogeochemistry, and Rock-EvalTM pyrolysis from the Devonian Horn River Group in the Mackenzie Plain and Norman Range, Northwest Territories. *Geological Survey of Canada, Open File*, *7951*, 1–52. Retrieved from http://geoscan.nrcan.gc.ca/starweb/geoscan/servlet.starweb?path=geoscan/fulle.web{&}search1=R=297832https://geoscan.nrcan.gc.ca/starweb/geoscan/servlet.starweb?path=geoscan/fulle.web{&}search1=R=297832 doi: 10.4095/297832

Kabanov, P., Vandenberg, R., Pelchat, P., Cameron, M., Dewing, K. E., & Mort, A. (2020, mar). Lithostratigraphy of Devonian basinal mudrocks in frontier areas of Northwestern Canada augmented with ED-XRF technique. *arktos*, 1–14. Retrieved from http://link.springer.com/10.1007/s41063-020-00074-zhttps://geoscan.nrcan.gc.ca/starweb/geoscan/servlet.starweb?path=geoscan/fulle.web{&}search1=R=313311 doi: 10.1007/s41063-020-00074-z

Kaiho, K. (1994, aug). Benthic foraminiferal dissolved-oxygen index and dissolved-oxygen levels in the modern ocean. *Geology*, *22*(8), 719–722. Retrieved from https://pubs.geoscienceworld.org/gsa/geology/article-pdf/22/8/719/3515317/i0091-7613-22-8-719.pdf doi: 10.1130/0091-7613(1994)022<0719:BFDOIA>2.3.CO;2

Katz, B. J. (2005). Controlling Factors on Source Rock Development—A Review Of Productivity, Preservation, and Sedimentation Rate. In N. Harris (Ed.), *Deposition of organic-carbon-rich sediments: Models, mechanisms, and consequences* (SEPM Speci ed., pp. 7–16). SEPM Special Publication No. 82. Retrieved from http://archives.datapages.com.login.ezproxy.library.ualberta.ca/data/sepm{_}sp/SP82/Controlling{_}Factors{_}on{_}Source{_}Rock{_}Development.htm?q={%}2BtextStrip{%}3Akatz+textStrip{%}3Abj+textStrip{%}3A2005+textStrip{%}3Acontrolling+textStrip{%}3Afactors+textStrip{%}3Asource+textS doi: 10.2110/pec.05.82.0007

Knapp, L. J., McMillan, J. M., & Harris, N. B. (2017). A depositional model for organic-rich Duvernay Formation mudstones. *Sedimentary Geology*, *347*, 160–182. Retrieved from http://dx.doi.org/10.1016/j.sedgeo.2016.11.012 doi: 10.1016/j.sedgeo.2016.11.012

Konitzer, S. F., Davies, S. J., Stephenson, M. H., & Leng, M. J. (2014, mar). Depositional Controls On Mudstone Lithofacies In A Basinal Setting: Implications for the Delivery of Sedimentary Organic Matter. *Journal of Sedimentary Research*, *84*(3), 198–214. Retrieved from https://pubs.geoscienceworld.org/jsedres/article/84/3/198-214/145391 doi: 10.2110/jsr.2014.18

LaGrange, M., Harris, B., Biddle, S., Atienza, N., Fiess, K., & Gingras, M. K. (2019). *Preliminary data for an integrated depositional and sequence stratigraphic framework for the Hare Indian and Canol formations (Horn River Group), Central Mackenzie Valley and Mackenzie Mountains, Northwest Ter-*

ritories - Part II (Tech. Rep.). Northwest Territories Geological Survey.

Lazar, O. R., Bohacs, K. M., Macquaker, J. H., Schieber, J., & Demko, T. M. (2015, mar). Capturing Key Attributes of Fine-Grained Sedimentary Rocks In Outcrops, Cores, and Thin Sections: Nomenclature and Description Guidelines. *Journal of Sedimentary Research*, *85*(3), 230–246. Retrieved from https://pubs.geoscienceworld.org/jsedres/article/85/3/230-246/145457 doi: 10.2110/jsr.2015.11

Lesueur, P., Jouanneau, J. M., Boust, D., Tastet, J. P., & Weber, O. (2001, aug). Sedimentation rates and fluxes in the continental shelf mud fields in the Bay of Biscay (France). *Continental Shelf Research*, *21*(13-14), 1383–1401. Retrieved from https://www-sciencedirect-com.login.ezproxy.library.ualberta.ca/science/article/pii/S0278434301000048 doi: 10.1016/S0278-4343(01)00004-8

Levin, L. (2003). Oxygen minimum zone benthos: adaptation and community response to hypoxia. *Oceanography and Marine Biology: an Annual Review*, *41*, 1–45. Retrieved from http://books.google.com/books?hl=en{&}lr={&}id=64crGFXWn5gC{&}oi=fnd{&}pg=PA1{&}dq=Oxygen+minimum+zone+benthos:+adaptation+and+community+response+to+hypoxia{&}ots=LXJDHtKi3-{&}sig=z7UbcIajtcoUDCFsxJFmjB7igaw

Lobza, V., & Schieber, J. (1999, sep). Biogenic sedimentary structures produced by worms in soupy, soft muds; observations from the Chattanooga Shale (Upper Devonian) and experiments. *Journal of Sedimentary Research*, *69*(5), 1041–1049. Retrieved from https://pubs.geoscienceworld.org/jsedres/article/69/5/1041-1049/99042 doi: 10.2110/jsr.69.1041

Löhr, S. C., & Kennedy, M. J. (2015). Micro-trace fossils reveal pervasive reworking of Pliocene sapropels by low-oxygen-adapted benthic meiofauna. *Nature Communications*, *6*, 1–8. Retrieved from http://www.nature.com.login.ezproxy.library.ualberta.ca/articles/ncomms7589.pdf doi: 10.1038/ncomms7589

Lyle, M. (1983, sep). The brown-green color transition in marine sediments: A marker of the Fe(III)-Fe(II) redox boundary. *Limnology and Oceanography*, *28*(5), 1026–1033. Retrieved from http://doi.wiley.com/10.4319/lo.1983.28.5.1026 doi: 10.4319/lo.1983.28.5.1026

Macquaker, J. H., & Adams, A. (2003, sep). Maximizing Information from Fine-Grained Sedimentary Rocks: An Inclusive Nomenclature for Mudstones. *Journal of Sedimentary Research*, *73*(5), 735–744. Retrieved from https://pubs.geoscienceworld.org/jsedres/article/73/5/735-744/114175 doi: 10.1306/012203730735

Macquaker, J. H., Bentley, S. J., & Bohacs, K. M. (2010, oct). Wave-enhanced sediment-gravity flows and mud dispersal across continental shelves: Reappraising sediment transport processes operating in ancient mudstone successions. *Geology*, *38*(10), 947–950. Retrieved from http://pubs.geoscienceworld.org/geology/article/38/10/947/130135/Waveenhanced-sedimentgravity-flows-and-mud doi: 10.1130/G31093.1

Macquaker, J. H., Keller, M., & Davies, S. J. (2010, nov). Algal Blooms and Marine Snow: Mechanisms That Enhance Preservation of Organic Carbon in Ancient Fine-Grained Sediments. *Journal of Sedimentary Research*, *80*(11), 934–942. Retrieved from https://pubs.geoscienceworld.org/jsedres/article/80/11/934-942/145299 doi: 10.2110/jsr.2010.085

Macquaker, J. H., & Taylor, K. G. (1996). A sequence-stratigraphic interpretation of a mudstone-dominated succession: The Lower Jurassic Cleveland Ironstone Formation, UK. *Journal of the Geological Society*, *153*(5), 759–770. Retrieved from http://jgs.lyellcollection.org/ doi: 10.1144/gsjgs.153.5.0759

Macquaker, J. H., Taylor, K. G., & Gawthorpe, R. L. (2007, apr). High-Resolution Facies Analyses of Mudstones: Implications for Paleoenvironmental and Sequence Stratigraphic Interpretations of Offshore Ancient Mud-Dominated Successions. *Journal of Sedimentary Research*, *77*(4), 324–339. Retrieved from https://pubs.geoscienceworld.org/jsedres/article/77/4/324-339/145138 doi: 10.2110/jsr.2007.029

Macquaker, J. H., Taylor, K. G., Keller, M., & Polya, D. (2014, mar). Compositional controls on early diagenetic pathways in fine-grained sedimentary rocks: Implications for predicting unconventional reservoir attributes of mudstones. *AAPG Bulletin*, *98*(3), 587–603. doi: 10.1306/08201311176

Matz, M. V., Frank, T. M., Marshall, N. J., Widder, E. A., & Johnsen, S. (2008, dec). Giant Deep-Sea Protist Produces Bilaterian-like Traces. *Current Biology*, *18*(23), 1849–1854. doi: 10.1016/j.cub.2008.10.028

Milliken, K. L., & Olson, T. (2017, apr). Silica Diagenesis, Porosity Evolution, and Mechanical Behavior In Siliceous Mudstones, Mowry Shale (Cretaceous), Rocky Mountains, U.S.A. *Journal of Sedimentary Research*, *87*(4), 366–387. doi: 10.2110/jsr.2017.24

Morford, J. L., Emerson, S. R., Breckel, E. J., & Kim, S. H. (2005, nov). Diagenesis of oxyanions (V, U, Re, and Mo) in pore waters and sediments from a continental margin. *Geochimica et Cosmochimica Acta*, *69*(21), 5021–5032. doi: 10.1016/j.gca.2005.05.015

Morrow, D. W. (2018). Devonian of the northern Canadian mainland sedimentary basin: A review. *Bulletin of Canadian Petroleum Geology*, *66*(3), 623–694. Retrieved from https://pubs.geoscienceworld.org/cspg/bcpg/article-pdf/66/3/623/4588427/623.morrow.66.3.pdf

Muir, I. D. (1988). *Devonian Hare Indian and Ramparts Formations, Mackenzie*

Mountains, N.W.T: Basin-Fill, Platform and Reef Development (Unpublished doctoral dissertation). University of Ottawa.

Muir, I. D., Wong, P., & Wendte, J. (1985). Devonian Hare Indian - Ramparts (Kee Scarp) evolution, Mackenzie Mountains and subsurface Norman Wells, N. W. T.: Basin-fill and platform-reef development. *SEPM Rocky Mountain Carbonate Reservoirs*, 311–341.

Mulder, T., & Alexander, J. (2001, apr). The physical character of subaqueous sedimentary density flow and their deposits. *Sedimentology*, *48*(2), 269–299. Retrieved from `http://doi.wiley.com/10.1046/j.1365-3091.2001.00360.x` doi: 10.1046/j.1365-3091.2001.00360.x

Newport, S. M., Jerrett, R. M., Taylor, K. G., Hough, E., & Worden, R. H. (2018, mar). Sedimentology and microfacies of a mud-rich slope succession: In the Carboniferous Bowland Basin, NW England (UK). *Journal of the Geological Society*, *175*(2), 247–262. Retrieved from `http://jgs.lyellcollection.org/lookup/doi/10.1144/jgs2017-036` doi: 10.1144/jgs2017-036

Norris, D. K., & Yorath, C. J. (1981). The North American Plate from the Arctic Archipelago to the Romanzof Mountains. In A. Narin, M. Churkin, & F. Francis (Eds.), *The arctic ocean* (pp. 37–103). Boston, MA: Springer US. Retrieved from `http://link.springer.com/10.1007/978-1-4757-1248-3{_}3` doi: 10.1007/978-1-4757-1248-3_3

Pike, J., Bernhard, J. M., Moreton, S. G., & Butler, I. B. (2001). Microbioirrigation of marine sediments in dysoxic environments: Implications for early sediment fabric formation and diagenetic processes. *Geology*, *29*(10), 923–926. Retrieved from `https://gsw.silverchair-cdn.com/gsw/Content{_}public/Journal/geology/29/10/10.1130{_}0091-7613(2001)029{_}0923{_}MOMSID{_}2.0.CO;2/3/i0091-7613-29-10-923.pdf?Expires=1524546539{&}Signature=`

kjThR{~}xdtbkfE3DO9vd2vcVgl8ROJ89pdTtbYKB{~}lWmWAfvRO{~}Vfxz-O2ddYq584SH98q7RZbDPYqj doi: 10.1130/0091-7613(2001)029<0923:MOMSID>2.0.CO;2

Plint, A. G., Macquaker, J. H., & Varban, B. L. (2012, oct). Bedload Transport of Mud Across A Wide, Storm-Influenced Ramp: Cenomanian-Turonian Kaskapau Formation, Western Canada Foreland Basin. *Journal of Sedimentary Research*, *82*(11), 801–822. Retrieved from https://pubs.geoscienceworld.org/jsedres/article/82/11/801-822/330458 doi: 10.2110/jsr.2012.64

Prior, D. B., Suhayda, J. N., Lu, N. Z., Bornhold, B. D., Keller, G. H., Wiseman, W. J., … Yang, Z. S. (1989). Storm wave reactivation of a submarine landslide. *Nature*, *341*(6237), 47–50. doi: 10.1038/341047a0

Pugh, D. C. (1983). *Pre-mesozoic Geology in the Subsurface of Peel River Map Area, Yukon Territory and District of Mackenzie*. Ottawa: Geologic Survey of Canada.

Pyle, L. J., & Gal, L. P. (2016, mar). Reference Section for the Horn River Group and Definition of the Bell Creek Member, Hare Indian Formation in central Northwest Territories. *Bulletin of Canadian Petroleum Geology*, *64*(1), 67–98. Retrieved from https://pubs.geoscienceworld.org/bcpg/article/64/1/67-98/242742 doi: 10.2113/gscpgbull.64.1.67

Pyle, L. J., Gal, L. P., & Fiess, K. M. (2014). *Devonian Horn River Group: A Reference Section, Lithogeochemical Characterization, Correlation of Measured Sections and Wells, NWT Open File 2014-06* (Tech. Rep.).

Racki, G., & Cordey, F. (2000, nov). Radiolarian palaeoecology and radiolarites: Is the present the key to the past? *Earth Science Reviews*, *52*(1-3), 83–120. Retrieved from https://www-sciencedirect-com.login.ezproxy.library.ualberta.ca/science/article/pii/S0012825200000246 doi:

10.1016/S0012-8252(00)00024-6

Raiswell, R. (1971, dec). The Growth of Cambrian and Liassic Concretions. *Sedimentology*, *17*(3-4), 147–171. Retrieved from http://doi.wiley.com/10.1111/j.1365-3091.1971.tb01773.x doi: 10.1111/j.1365-3091.1971.tb01773.x

Rhoads, D. C. (1975). The Paleoecological and Environmental Significance Of Trace Fossils. In R. Frey (Ed.), *The study of trace fossils* (pp. 147–160). Berlin, Heidelberg: Springer Berlin Heidelberg. Retrieved from http://www.springerlink.com/index/10.1007/978-3-642-65923-2{_}9 doi: 10.1007/978-3-642-65923-2_9

Rhoads, D. C., & Morse, J. W. (1971, oct). Evolutionary and Ecologic Significance of Oxygen-Deficient Marine Basins. *Lethaia*, *4*(4), 413–428. Retrieved from http://doi.wiley.com/10.1111/j.1502-3931.1971.tb01864.x doi: 10.1111/j.1502-3931.1971.tb01864.x

Savrda, C. E. (2007). Trace Fossils and Marine Benthic Oxygenation. In W. I. Miller (Ed.), *Trace fossils: Concepts, problems, prospects* (pp. 149–158). Amsterdam: Elsevier. Retrieved from http://linkinghub.elsevier.com/retrieve/pii/B9780444529497501352 doi: 10.1016/B978-044452949-7/50135-2

Savrda, C. E., & Bottjer, D. J. (1984). Development of a Comprehensive Oxygen-Deficient Marine Biofacies Model: Evidence from Santa Monica, San Pedro, and Santa Barbara Basins, California Continental Borderland. *AAPG Bulletin*, *68*(9), 1179–1192. Retrieved from http://archives.datapages.com.login.ezproxy.library.ualberta.ca/data/bulletns/1984-85/data/pg/0068/0009/1150/1179.htm?q={%}2BtitleStrip{%}3Adevelopment+titleStrip{%}3Acomprehensive+titleStrip{%}3A{%}22oxygen+deficient{%}22+titleStrip{%}3Amarine+titleStrip{%}3Abiofacies+M doi: 10.1306/ad4616f1-16f7-11d7-8645000102c1865d

Savrda, C. E., & Bottjer, D. J. (1986). Trace-fossil model for reconstruction of paleo-oxygenetation in bottom waters.pdf. *Geology*, *14*(1), 3–6. doi: 10.1130/0091-7613(1986)âĂŃ14<3:TMFROP>âĂŃ2.0.CO;2

Savrda, C. E., & Bottjer, D. J. (1987). Trace fossils as indicators of bottom-water redox conditions in ancient marine environments. In D. J. Bottjer (Ed.), *New concepts in the use of biogenic sedimentary structures for paleoenvironmental interpretation* (pp. 3–26). Retrieved from `http://archives.datapages.com/data/pac{_}sepm/067/067001/pdfs/3.pdf`

Schieber, J. (1986, aug). The possible role of benthic microbial mats during the formation of carbonaceous shales in shallow Mid-Proterozoic basins. *Sedimentology*, *33*(4), 521–536. Retrieved from `http://doi.wiley.com/10.1111/j.1365-3091.1986.tb00758.x` doi: 10.1111/j.1365-3091.1986.tb00758.x

Schieber, J. (1989, apr). Facies and origin of shales from the mid-Proterozoic Newland Formation, Belt Basin, Montana, USA. *Sedimentology*, *36*(2), 203–219. Retrieved from `http://doi.wiley.com/10.1111/j.1365-3091.1989.tb00603.x` doi: 10.1111/j.1365-3091.1989.tb00603.x

Schieber, J. (1994, nov). Evidence for high-energy events and shallow-water deposition in the Chattanooga Shale, Devonian, central Tennessee, USA. *Sedimentary Geology*, *93*(3-4), 193–208. Retrieved from `https://www.sciencedirect.com/science/article/pii/0037073894900051?via{%}3Dihub` doi: 10.1016/0037-0738(94)90005-1

Schieber, J. (1998). Sedimentary Features Indicating Erosion , Condensation , and Hiatuses in the Chattanooga Shale of Central Tennessee : Relevance for Sedimentary and Stratigraphic Evolution. In J. Schieber, W. Zimmerle, & P. Sethi (Eds.), *Shales and mudstones: Basin studies, sedimentology and paleontology* (Vol. 1, pp. 187–215).

Stuttgart. Retrieved from https://pdfs.semanticscholar.org/dfea/a296ad5814dcf87ddb2658937ef8e4f8347c.pdfhttp://cat.inist.fr/?aModele=afficheN{&}cpsidt=1809617

Schieber, J. (1999, feb). Microbial Mats in Terrigenous Clastics: The Challenge of Identification in the Rock Record. *PALAIOS*, *14*(1), 3–12. Retrieved from https://pubs.geoscienceworld.org/palaios/article/14/1/3-12/99703 doi: 10.2307/3515357

Schieber, J. (2001, oct). A role for organic petrology in integrated studies of mudrocks: Examples from Devonian black shales of the Eastern US. *International Journal of Coal Geology*, *47*(3-4), 171–187. doi: 10.1016/S0166-5162(01)00041-6

Schieber, J. (2002, feb). The Role of an Organic Slime Matrix in the Formation of Pyritized Burrow Trails and Pyrite Concretions. *PALAIOS*, *17*(1), 104–109. Retrieved from https://pubs.geoscienceworld.org/palaios/article/17/1/104-109/99834 doi: 10.1669/0883-1351(2002)017<0104:troaos>2.0.co;2

Schieber, J. (2003). Simple Gifts and Buried Treasures—Implications of Finding Bioturbation and Erosion Surfaces in Black Shales. *The Sedimentary Record*, *1*(2), 4–8. Retrieved from https://www.sepm.org/CM{_}Files/SedimentaryRecord/Articles/1{_}2{_}article.pdf doi: 10.2110/sedred.2003.2.4

Schieber, J. (2007). Microbial Mats on Muddy Substrates – Examples of Possible Sedimentary. In J. Schieber et al. (Eds.), *Atlas of microbial mat features preserved within the clastic rock record* (pp. 117–134). London: Elsevier. Retrieved from http://www.indiana.edu/{~}sepm04/PDF/JS-B22-Matbook-Chapter5.pdf

Schieber, J. (2009, jan). Discovery of agglutinated benthic foraminifera in Devonian black shales and their relevance for the redox state of ancient seas. *Palaeogeography, Palaeoclimatology, Palaeoecology*, *271*(3-4), 292–300. Retrieved from https://www-sciencedirect-com.login.ezproxy.library.ualberta.ca/science/article/pii/S0031018208005993 doi: 10.1016/j.palaeo.2008.10.027

Schieber, J. (2011). Shifting paradigms in shale sedimentology; the implications of recent flume studies for interpreting shale fabrics and depositional environments. *CSPG CSEG CWLS Conference, 2011*, 4. Retrieved from http://login.ezproxy.library.ualberta.ca/login?url=http://search.ebscohost.com/login.aspx?direct=true{&}db=guh{&}AN=628467-43{&}site=ehost-live{&}scope=site{%}5Cnhttp://cseg.ca/resources/abstracts/2011-conference-abstracts-m-to-z

Schieber, J. (2014). Traces In the Dark-Sedimentary Processes and Facies Gradients In the Upper Devonian-Lower Mississippian Upper Shale Member of the Bakken Formation, Williston Basin, North Dakota, U.S.A.-Discussion. *Journal of Sedimentary Research*, *84*(10), 837–838. Retrieved from http://dx.doi.org/10.2110/jsr.2014.73 doi: 10.2110/jsr.2014.73

Schieber, J., Bose, P., Eriksson, P., Banerjee, S., Sarkar, S., Altermann, W., & Catuneau, O. (2007). *Atlas of microbial mat features preserved within the siliciclastic rock record.* Elsevier. doi: 10.1017/CBO9781107415324.004

Schieber, J., Southard, J. B., & Schimmelmann, A. (2010, jan). Lenticular Shale Fabrics Resulting from Intermittent Erosion of Water-Rich Muds–Interpreting the Rock Record in the Light of Recent Flume Experiments. *Journal of Sedimentary Research*, *80*(1), 119–128. Retrieved from https://pubs.geoscienceworld.org/jsedres/article/80/1/119-128/145277 doi: 10.2110/jsr.2010.005

Schieber, J., Southard, J. B., & Thaisen, K. (2007, dec). Accretion of mudstone beds from migrating floccule ripples. *Science*, *318*(5857), 1760–1763. Retrieved from http://www.ncbi.nlm.nih.gov/pubmed/18079398 doi: 10.1126/science.1147001

Schieber, J., & Zimmerle, W. (1998). The history and promise of shale research. In J. Schieber & W. Zimmerle (Eds.), *Shales and mudstones: Vol. 1: Basin studies, sedimentology and paleontology* (Vol. 1, pp. 1–10). Stuttgart: Schweizerbart'sche Verlagsbuchhandlung.

Scott, C., & Lyons, T. W. (2012, sep). Contrasting molybdenum cycling and isotopic properties in euxinic versus non-euxinic sediments and sedimentary rocks: Refining the paleoproxies. *Chemical Geology*, *324-325*, 19–27. Retrieved from https://www-sciencedirect-com.login.ezproxy.library.ualberta.ca/science/article/pii/S0009254112002318 doi: 10.1016/j.chemgeo.2012.05.012

Snowdon, L. R., Brooks, P. W., Williams, G. K., & Goodarzi, F. (1987, jan). Correlation of the Canol Formation source rock with oil from Norman Wells. *Organic Geochemistry*, *11*(6), 529–548. Retrieved from http://www.sciencedirect.com/science/article/pii/0146638087900088 doi: 10.1016/0146-6380(87)90008-8

Soyinka, O. A., & Slatt, R. M. (2008, jan). Identification and micro-stratigraphy of hyperpycnites and turbidites in Cretaceous Lewis Shale, Wyoming. *Sedimentology*, *55*(5), 1117–1133. Retrieved from http://doi.wiley.com/10.1111/j.1365-3091.2007.00938.x doi: 10.1111/j.1365-3091.2007.00938.x

Sumner, E. J., Talling, P. J., & Amy, L. A. (2009, nov). Deposits of flows transitional between turbidity current and debris flow. *Geology*, *37*(11), 991–994. doi: 10.1130/G30059A.1

Tassonyi, E. J. (1969). Subsurface Geology, Lower Mackenzie River and

Anderson RIver Area, District if Mackenzie. *Department of Energy, Mines and Resources*, *25*, 1689–1699. doi: 10.1017/CBO9781107415324.004

Taylor, A. M., & Goldring, R. (1993). Description and analysis of bioturbation and ichnofabric. *Journal - Geological Society (London)*, *150*(1), 141–148. Retrieved from http://jgs.lyellcollection.org.login.ezproxy.library.ualberta.ca/content/jgs/150/1/141.full.pdf doi: 10.1144/gsjgs.150.1.0141

Taylor, K. G., & Macquaker, J. H. (2011, apr). Iron minerals in marine sediments record chemical environments. *Elements*, *7*(2), 113–118. doi: 10.2113/gselements.7.2.113

Taylor, S. R., & McLennan, S. M. (1985). *The continental crust: Its composition and evolution*. Palo Alto: Blackwell Publishing Ltd.

Thompson, J. B., Mullins, H. T., Newton, C. R., & Vercoutere, T. L. (1985, apr). Alternative biofacies model for dysaerobic communities. *Lethaia*, *18*(2), 167–179. Retrieved from http://doi.wiley.com/10.1111/j.1502-3931.1985.tb00695.x doi: 10.1111/j.1502-3931.1985.tb00695.x

Thomsen, E., & Vorren, T. O. (1984, aug). Pyritization of tubes and burrows from Late Pleistocene continental shelf sediments off North Norway. *Sedimentology*, *31*(4), 481–492. Retrieved from http://doi.wiley.com/10.1111/j.1365-3091.1984.tb01814.x doi: 10.1111/j.1365-3091.1984.tb01814.x

Tinnin, B. M., & Darmaoen, S. T. (2016). Chemostratigraphic variability of the eagle ford shale, South Texas: Insights into paleoredox and sedimentary facies changes. In B. J. (Ed.), *The eagleford shale, aapg memoir* (Vol. 110, pp. 259–283). AAPG Special Volumes. Retrieved from http://archives.datapages.com.login.ezproxy.library.ualberta.ca/data/specpubs/memoir110/data/259{_}aapg-sp1990259.htm?q={%}2BtextStrip{%}3Achapter+7{%}3Achemostratigraphic+textStrip{%}3Avariability+textStrip{%}3Aeagle+

textStrip{%}3Aford+textStrip{%}3Ashale+textStrip{%}3Aso doi: 10.1306/13541965M1103664

Tribovillard, N., Algeo, T. J., Lyons, T. W., & Riboulleau, A. (2006, aug). Trace metals as paleoredox and paleoproductivity proxies: An update. *Chemical Geology*, *232*(1-2), 12–32. Retrieved from https://www-sciencedirect-com.login.ezproxy.library.ualberta.ca/science/article/pii/S000925410600132X doi: 10.1016/j.chemgeo.2006.02.012

Tyson, R. V. (1986). *Palynofacies and sedimentology of some Late Jurassic sediments from the British Isles and northern North Sea* (PhD Thesis, The Open University). Retrieved from http://oro.open.ac.uk/56911/

Ulmer-Scholle, D. S., Scholle, P. A., Schieber, J., & Raine, R. J. (2014). Mudrocks: Siltstones, Mudstones, Claystones and Shales. In *Memoir 109: A color guide to the petrography of sandstones, siltstones, shales and associated rocks* (pp. 181–212). Retrieved from http://archives.datapages.com/data/specpubs/memoir109/data/pdfs/181.pdf doi: 10.1306/13521911m1093637

Uyeno, T. T. (1979). Devonian conodont biostratigraphy of Powell Creek and adjacent areas, western District of Mackenzie. *Western and Arctic Canadian Biostratigraphy.*, *18*, 233–257.

Wignall, P. B. (1989, mar). Sedimentary dynamics of the Kimmeridge Clay: tempests and earthquakes. *Journal - Geological Society (London)*, *146*(2), 273–284. Retrieved from http://jgs.lyellcollection.org/lookup/doi/10.1144/gsjgs.146.2.0273 doi: 10.1144/gsjgs.146.2.0273

Wignall, P. B. (1991). Dysaerobic Trace Fossils and Ichnofabrics in the Upper Jurassic Kimmeridge Clay of Southern England. *PALAIOS*, *6*(3), 264–270. Retrieved from http://palaios.sepmonline.org/cgi/doi/10.2307/3514906 doi: 10.2307/3514906

Williams, G. K. (1983). What does the term ' Horn River Formation' mean? A review. *Bulletin of Canadian Petroleum Geology*, *31*(2), 117–122. Retrieved from http://archives.datapages.com.login.ezproxy.library.ualberta.ca/data/cspg/data/031/031002/pdfs/0117.pdf

Yawar, Z., & Schieber, J. (2017). On the origin of silt laminae in laminated shales. *Sedimentary Geology*, *360*, 22–34. Retrieved from http://dx.doi.org/10.1016/j.sedgeo.2017.09.001 doi: 10.1016/j.sedgeo.2017.09.001

Yeun Ahn, S., & Babcock, L. E. (2012). Microorganism-mediated preservation of Planolites, a common trace fossil from the Harkless Formation, Cambrian of Nevada, USA. *Sedimentary Geology*, *263-264*(1), 30–35. doi: 10.1016/j.sedgeo.2011.08.003

Appendix A

Digital Microfacies Logs

Husky Little Bear N-09 Core, Petrographic, and XRF Data

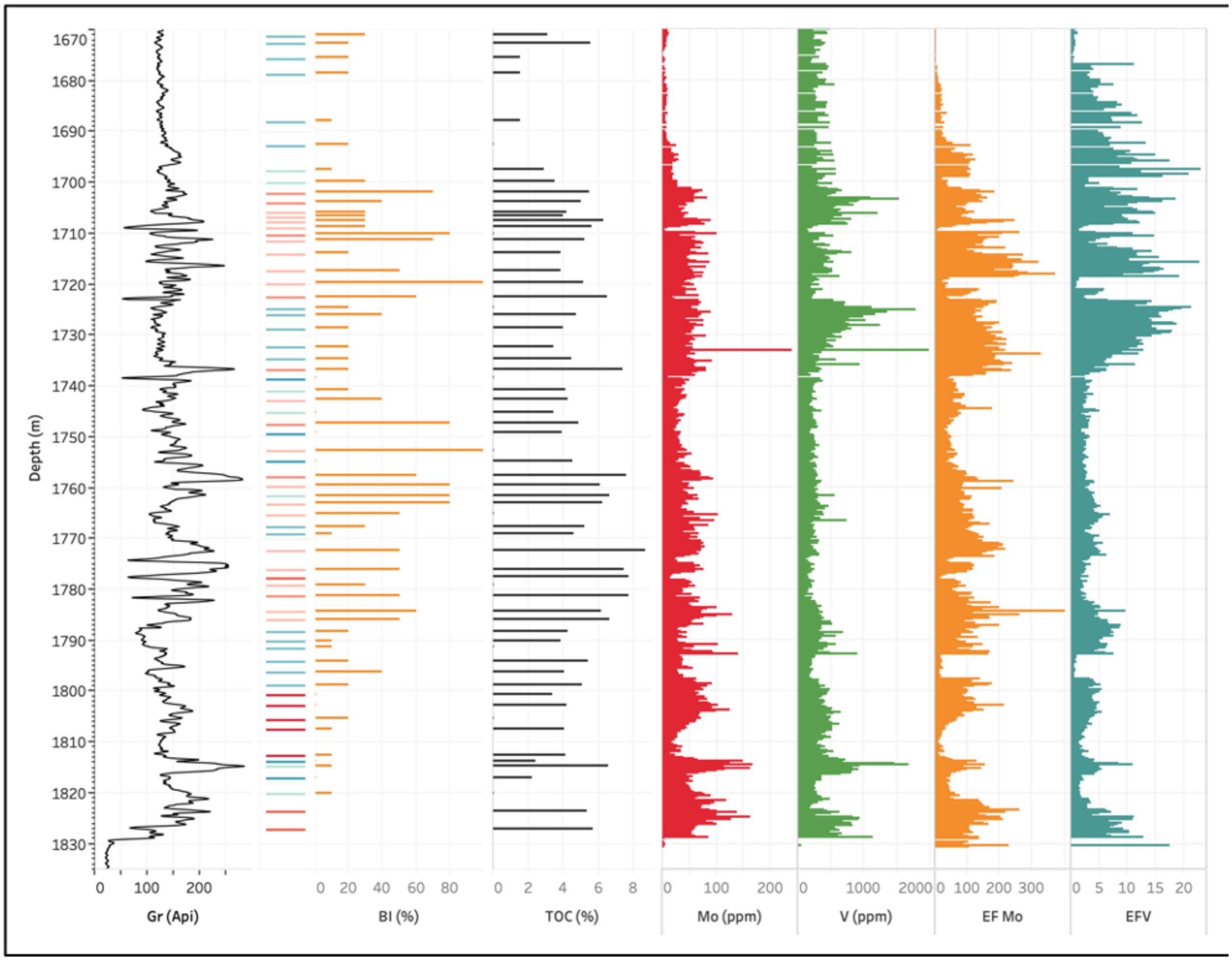

Figure A1: Digital log of microfacies and bioturbation data plotted along side Gamma ray, TOC, and geochemical paleoredox proxies for the N-09 core.

Husky Little Bear H-64 Petrographic and XRF Data

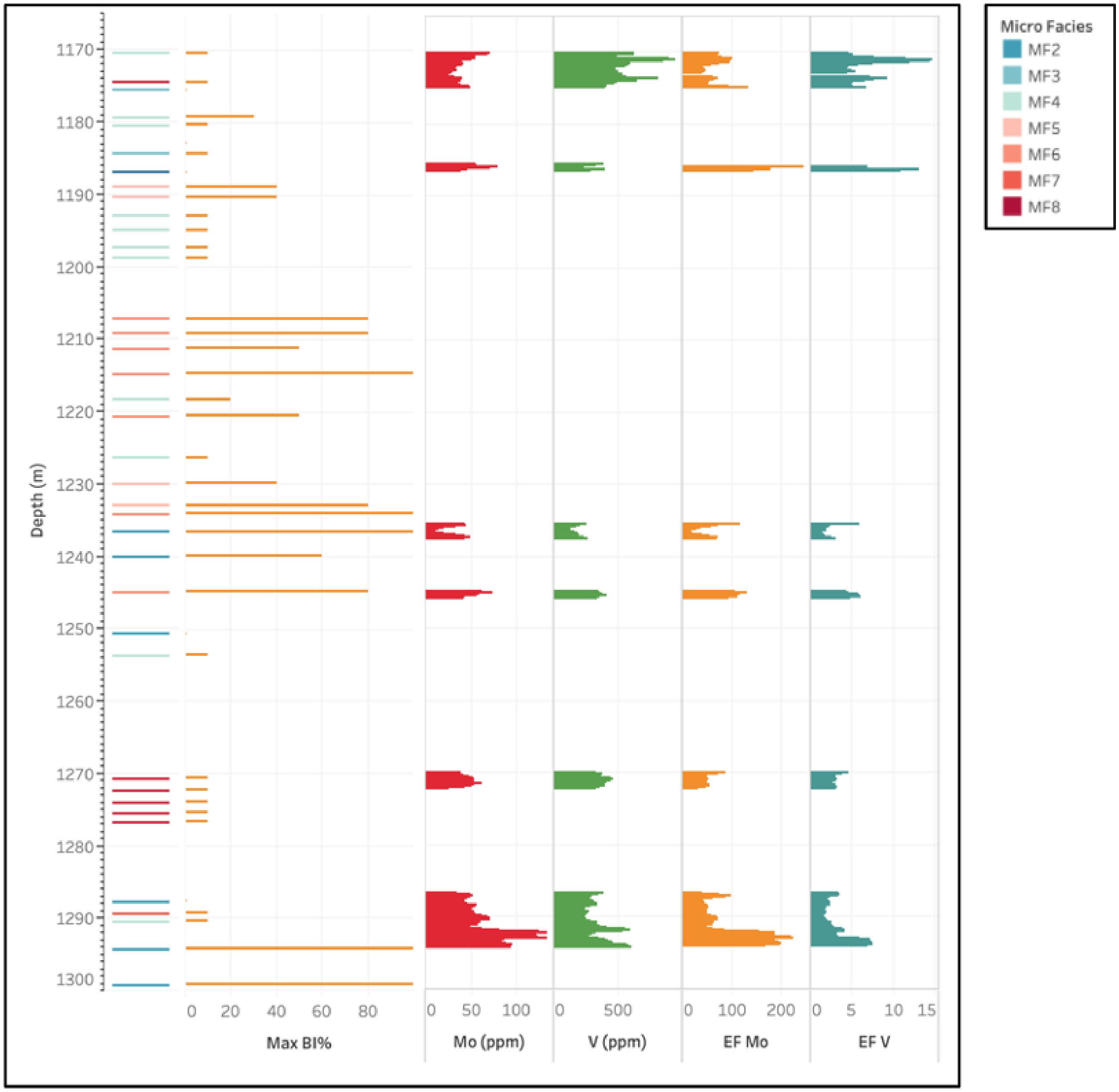

Figure A3: Digital log of microfacies and bioturbation data plotted along side geochemical paleoredox proxies for the H-64 core.

MGM Shell East Mackay I-78 Core, Petrographic, and XRF Data

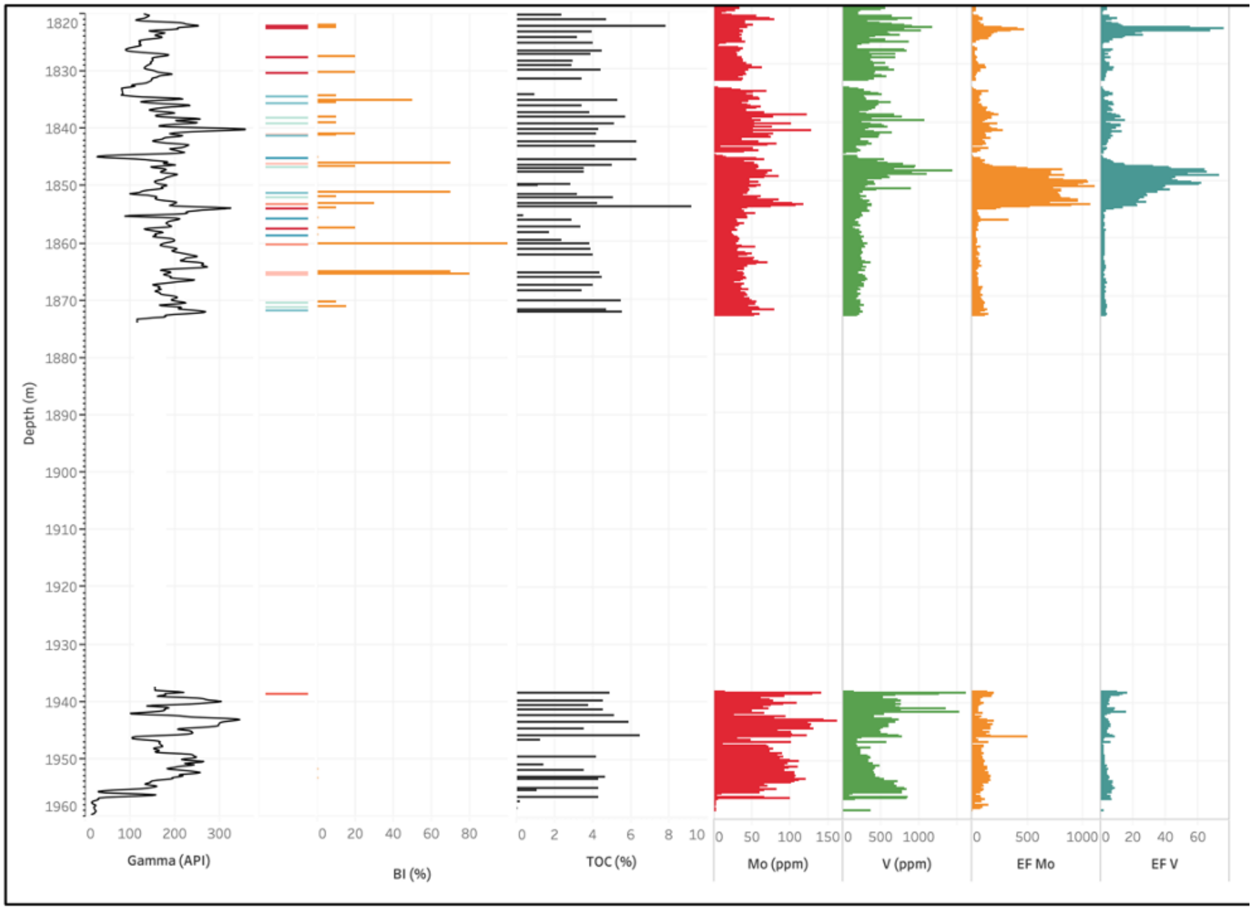

Figure A2: Digital log of microfacies and bioturbation data plotted alongside Gamma ray, TOC, and geochemical paleoredox proxies for the I-78 core.

ConocoPhillips Mirror Lake N-20 Petrographic Data

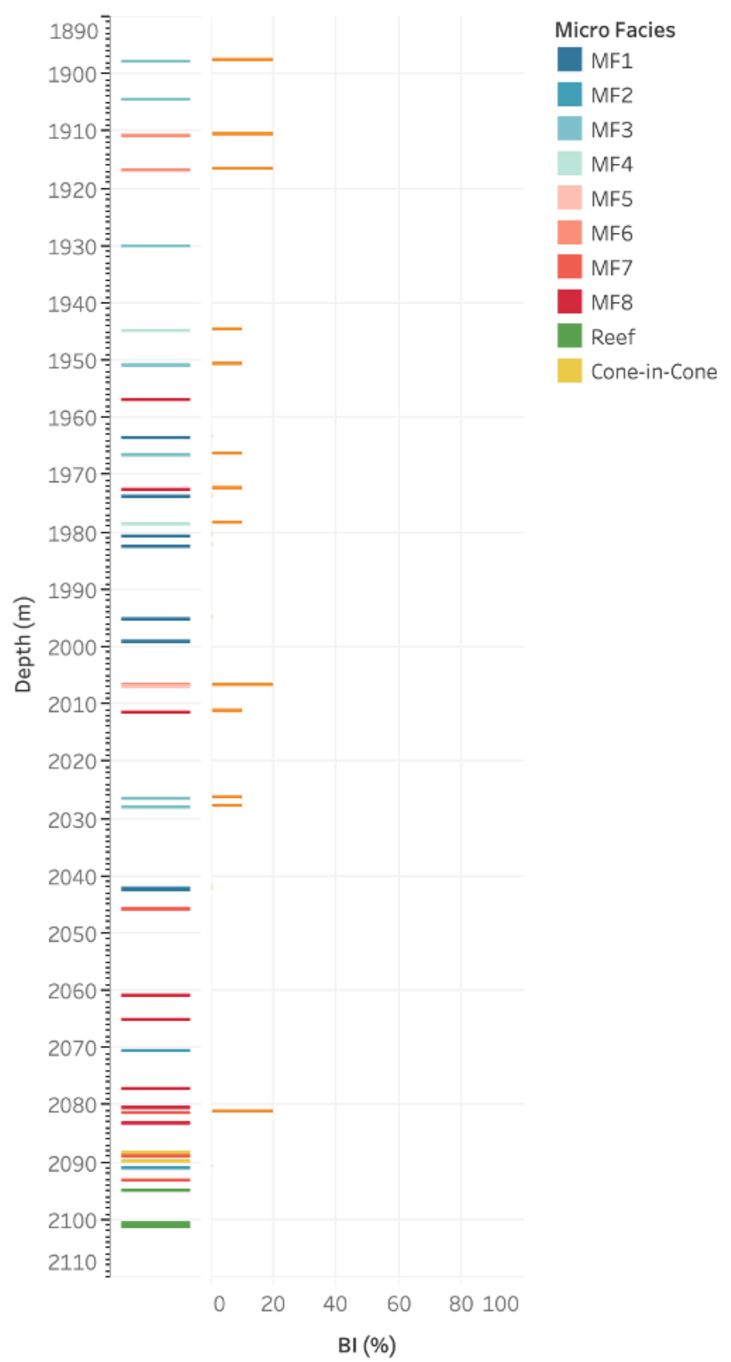

Figure A4: Digital log of microfacies and bioturbation data for the N-20 core.

Appendix B

Thin Section Descriptions

	# of Thin Sections	Notes
Husky Little Bear N-09	65	Most thin sections are wedge cut (variable thickness)
Husky Little Bear H-64	39	
MGM Shell East Mackay I-78	31	
ConocoPhillips Mirror Lake N-20	46	Thin sections are thick cut and appear quite dark – makes identification of structures difficult
ConocoPhillips Loon Creek O-06	45	Thin sections are thick cut and appear quite dark – makes identification of structures difficult

	Term	Abbreviation
	Thin Section	TS
	Microfacies	MF
Ichnology	Sinuous Tunnels	ST
	Tubular Unlined Tunnels	TUL
	Tubular Lined Tunnels	TL
Sedimentology	Organic Matter	OM
	Elongate Organic Matter/Detritus	EOM/EOD
	Intraclast	IC
Staining	Alizarin Red	AZR
	Potassium Ferricyanide	PF

Husky Little Bear N-09

rmation	Depth (m)	TOC	MicroFacies	BI % Range	Max BI%	Trace Size Max (µm)	Diversity #	Most Abundant Trace	Sedimentary and Ichnological Characteristics	Fossil Fragments	Staining	Calcite/Dolomite abundance-Mode:Max (microns)	Pyrite Abundance	Pyrite Type	Sand:Silt:Clay
	1670.87	**3.09**	**MF3**	0 - 30	30	100	3	ST	No evidence of scour or erosion surfaces. Two possible homogenized turbidity current depostis. Tubular unlined traces - consist of darker homogenized clay without silt grains. Sinuous trails are darker and referentially pyritized.	rare conodonts	PF	dolomite: common to abundant (varies at different elevations)- 10:100	abundant	Occurs as individule framboids sproadically throughout the matrix, as well as concentrated along some horizontal laminae	1:25:75
	1672.46	**5.57**	**MF3**	0-20	20	100	4	ST	No evidence of bedding contacts (e.g. no scour or erosion surfaces). Sinuous trails are preferntially pyritized by individule vertically aligned pyrite framboids	rare conodonts	PF	Dolomite: common throughout 10:220	abundant	framboidal pyrite throughout, no heavily pyritized laminae. Some fraboids are large clusters (100um)	0:5:95
	1675.34	**1.58**	**MF3**	0-20	20		1	ST	Intrabasinal microbial mat rip-ups and lots of OM. Possible thin distal turbidite beds. Lack of lithological contrast makes identifying traces extremely difficult. Vertically/sinuously aligned individule pyrite framboids could possibly indicate sinuous trails.	rare conodonts	PF	common throughout 50:100	abundant	framboidal pyrite throughout, heavily pyritized laminae occur frequently throughout the section.	0:0:100
mperial	**1678.51**	**1.57**	**MF3**	0-20?	20		1	ST	Rafted silt and rip microbial clasts. almost rhymitic alterations of organic-rich and organic poor laminae. No solid evidence of scour surfaces. One homogenized bed that could possibly represent rapid deposited sediment - no clay caps or laminated laminae like in wave erosion. "Wavy" lmainated texture similar to that seen in schiebers paper. Possible sinuous trails, only way to identify them is by vertical aligened small pyrite framboids. Can't estimate trace sizes due to lack of identifyible structures.	conodonts	PF	abundant throughout 30:50	abundant	no heavily pyritized laminae. Just individule framboids abundant and random throughout. Possible pyritization of dolomite nodules? Large framboids throughtou matrix	0:<5:>95
	1687.87	**1.54**	**MF3**	0-10	10		1	ST	Wavy discontinuous laminae. Possible scour surfaces or thin ripple laminae. Sinuous trails are only distinguishable by vertically aligned framboids and interuptions through laminae.		PF	abundant throughout 30:50	abundant	no havily pyritized laminae but ramdom abundant individule framboids throughout. Large abundant framboids. Large framboids are prevasive.	0:<5:>95
	1692.58	**0**	**MF3**	0-20?	20		2		Possible microbial mat near then top of the thin section. Agglomerated silt grains (rafted silt or agglutinated forams?), sporadic intraclasts. Vertical interuptions in OM possibly attributed to sinuous vertical traces. Trails are boardered by individule pyrite framboids		PF	abundant throughout 20:90	abundant	no havily pyritized laminae but ramdom abundant individule framboids throughout.	0:<5:>95
	1697.31	**2.93**	**MF4**	0-10	10	50	5	ST	Intraclast-rich laminae throughout. No evidence of scour surfaces or other storm assocaited beds. One bed contains silt-rich intraclasts. Pyritized sinuous vertical traces throughout.	calcite and dolomite angular shell fragments	PF	common - abundant 10:100	abundant	no havily pyritized laminae, but occurs as abundant random individule framboids throughout.	0:5:95
	1699.77	**3.55**	**MF4**	10-30%	30	100	1	ST	No evidence of scour surfaces. Possible silt lag (or compressed ripple laminae) along one otherwise poorly defined horizio. Euhedral pryrite near the base of the TS. Silt content flucuates with elevation - possible coarsening up/down laminae? Faint wavy discontinous bedding. Pyritic sinuous trails throughout. Trails crosscut intraclasts and thin silt lags. U-shaped scratches on thin section could be mistaken for burrows.	possible partially dissolved radiolarians	PF	abundant	abundant	euhedral and framboidal. No heavily pyritized laminae, just ramdom abundant individule pyrite framboids throughout. Fraboids are large!	0:5:95
	1701.91	**5.48**	**MF6**	40-70	70	93.63	2	ST	Silt rich very dark TS. Silt appears relatively evenly distributed throughout, concentrated along silt lags. Large diameter sinuous vertcal traces can be seen at the 2x magnification. Small vertical sinuous trails present. Possible concentraically lined tunnels.	possible radiolarians	None	common 5:200	abundant	no heavily pyritized laminae. Occurs as abudant random individule framboids that are pervasive throughout the matrix.	0:40:60
	1703.64	**5**	**MF6**	20-40	40	70	2	ST	Preferentially pyrtiized horizions occur somewhat regularily throughout elevations. No indication of scour surfaces or ripple laminae. Silt grains are sporadic throughout matrix. Diagenetic silica cementation of agglomerated silt (possible silt raft or agglutinated foram). Sinuous trails are pervasive throughout and commonly show vertically aligned framboids. Round hz burrow x-sections (liely uncompressed due to high slit content?).	partially dissolved radiolarians	None	common 5:175	abundant	minorly pyritized laminae thoughout, but most pyrite occurs as ramdom individule framboids. Large framboids can be seen in more heavily pyritized horizions	0:30:70
	1705.7	**4.21**	**MF5**	5 to 30	30	100	2	ST	No indication of wave erosion/scour surfaces or graded beding. Anglular silica/quartz fragments with apparent OM linings sporadic througout - may represent partially dissolved achritarchs. Undulating silt-rich bed at base of TS. Stacked fining up beds with abundant intraclasts at base, grading into clay rich tops and capped by preferentially pyritized horizons. Abundant sinuous trails - identified by warped laminae and aligned pyrite framboids.	radiolarians	None	common - abundant 10:100	abundant	pyrite framboids abundant throughout, both large ant small. Heavily pyritized laminae also occur commonly throughout. Rare (?) Euhedral pyrite thoughout (100um).	0:10:90
	1706.58	**3.99**	**MF5**	5 - 30	30	100	3		Planar distal turbidite bed. Alternating intraclast-rich and intraclast-poor beds. Stacked fining up beds with intraclast-rich bases and framboidally pyritized tops. Abundant sinous trails throughout.	radiolarians	None	10:150	abundant	Large euhedral and framboidal (up to 100um thick). preferentially pyritized lam common (concentraed framboidal pyrite along certain bedding planes)	0:5:95
	1707.49	**6.31**	**MF5**	10 to 30	30	50	3		Preferentially pyritized horizons. No indication of scour/erosion surfaces or graded bedding. Wavy-discontinous bedding. Burrow structures are hard to identify (dominantly sinuous trails).	possible agglutinated forams	None	rare - sporadic :5	abundant	abundant as individual framboids, heavily priteized laminae and large clusters. Bulk of pyrite in section is small individual framboids. Euhedral pyrite occurs sporadically throughout.	0:5:95
	1708.56	**5.61**	**MF5**	10 to 30	30	50	2	ST	Preferentially pyrtiized horizons at somewhat regularily spaced intervals throughout the TS. Silt appears evenly distributed throughout with no indications of wave or scour surfaces. Faint wavy-discontinous bedding. Large ST visible at 2x scale. Small ST can be seen throughout and are often framboidally pyrtiized.	conodonts	None	10:	abundant	heavily pyritized laminae, individual and clustered framboids throughout. Preferentially pyritized horizons. Large euhedral pyrite can been seen througout (but rare) 200um diam.	0:10:90

	1710.08	**0**	**MF6**	60-80	80	116	2	ST	Microbial mat rip-up clasts throughout. Silt-rich beds with pyritized horizions are spaced at irregulat intervals with varying degrees of pyrtization. No evidence of erosion or scour surfaces. Silt distribution seems even and random - with no sign of graded bedding. Beds are indistinct and intraclasts have been throughouly reworked. Biogenically homogenized texture. Sinuous trails are pervasive. Less common large horizontal TUL trails.	radiolarians	none	abundant 10:75	abundant	weird cresent-shaped pyritized strucutres throughout - possibly pyritized fossil frag? Pyrite consists of mainly individule framboids with common clustered framboids.	0:40:60
	1711.23	**5.22**	**MF5**	20-70	70	100	3	ST	Preferentially pyrtitized horiozons at somewhat regular spaced intervals. Wavy discontinous bedding throughout. Possible fining up bed with somewhat more abundant intraclasts at base, clear bed boundry to lighter coloured finer grained bed capped by pyritized horizion. Sand-sized cryatalline quartz grains with dark inclusions (pyrite?). No evidence of erosion/scour surfaces. ST can be seen throughout at 10x. Burrowed intraclasts occur throughout. deformed pellet indicating biogenic reowrking. Inclined intraclasts indicate possible biogenic reworking.	radiolarians	PF	common 10:100	abundant	heavily pyritized laminae. Individule framboids and clusters throughout.	0:15:85
	1713.88	**3.86**	**MF5**	0 to 20	20	70	2	ST	Overall wavy-discontinuous bedding. Planar discontinuous pyritized laminae with euhedral pyrite. No evidence of scour surfaces, ripples or graded beds. Silt is randomly disperesed througout. Sand-sized calcite nodules throughout. Burrows are difficult to distinguish due to lack of lithologic contrast. Weakly laminated texture may be attributed to high degrees of reworking. Evidence for some TUL burrows.		none	common 10:150	abundant	discontinuous heavily pyritized laminae throughout. Occurs as individual framboids throughotu the matrix and clusters.	0:<2:98
	1717.17	**3.86**	**MF5**	20 to 50?	50	100	2	ST	Discontinuous planar pyritized horizions. Quartz silt aggregates (agglutinated foraminifera or rafted silt?). One distal turbidite bed near center of TS. ST traces cross cut intraclasts. Possible tubular tunnels in xpl where internal fill extinction differs from the surrounding matrix.	possible agglutinated forams	PF	10 common :150	abundant	individule and clusteres framboids throughout matrix. Discontinuous heavily pyritized laminae throughout. Pyritized OM stringers throughout.	0:7-10:90-93
	1719.63	**5.14**	**MF5**	50-100?	100	100	2	ST	TS is wealky laminated to massive appearing, with bedding orrientation denoted by intraclast orrientation. No evidence of scour/erosion or ripples other than one microbial matt rip-up fragment. Carbonate nodules (sand-sized) are present throughout section. A microbial mat (dark/black carbonaceous horizontal feature) near center of TS. Difficult to identify individual traces due to inffered pervasive reworking and lack of lithologic contrast (overall biogenically homogenized texture).	radiolarians, possible agglutinated forams	PF and ARS	10:175	abundant	no heavily pyritized laminae. Occurs as abudant random individule framboids and less common large framboid clusters	0:5-10:90-95
	1722.36	**6.48**	**MF6**	20-60	60	100	3	ST	Possible discontinuous intraclastic lag. No other obvious bed bounding surfaces. Even and sporadic distribution of silt throughout TS. Sinuous trails are the easiest-to-spot traces due to silt grains shafted along their edges. TUL burrows present. Some completley biogenically homogenized beds.	radiolarians	none	20:50	abundant throughout	frabboids and framboidal clusters (up to 300um). No heavily pyritized laminae	0:40:60
	1724.5	**0**	**MF3**	0-20	20	50	2	ST	Irreggular light-pink stained bands horizontally across TS - possibly representing calcite rich (micritic) areas, or concenrations of pink epoxy? Wavy-discontinuous bedding. No obvious bed boundries and no erosion, scour, or ripple indications. TS is dark (thick cut) making identification of structures difficult.	conodonts	ARS?	20:200	individual framboids abundant throughout. Euhedral pyrite clustered in possible pelagic fecal pellets. Rare heavily pyritized laminae, not continuous throughout section.	framboids, euhedral (7:30). No heavily pyritized lam - but rare lenticular discontinuous lam. Framboidal is much more abundant than euhedral.	0:20:80
	1725.83	**4.7**	**MF3**	0-40	40	40	2	ST	Microbial-mat-encased radiolarite bed at base. Weakly laminated sediment texture with no evidence of bed planes, sour/erosion surfaces, or ripple laminae. No silt or intraclast lags present. No good evidence of bedding in general. Traces can be poorly defined and hard to identify. ST traces present throughout. At some elevations elongate OM is intact and continuous whereas at others is it fragmented- possibly indicating biogenic reworking and consumption?	possible tasmanites, conodonts, agglutinated forams	none	15:150	framboids - abundant Euhedral - locally common	frabmboids - individule and clusters. Framboidal pyrite altering fecal pellets. Large clusters can be clustered along some hz laminae, but are not as abundant as in some of the heavily pyritized laminae present in other sections. Euhedral pyrite (7:30). lenticular euhedrally pyritized areas	0:30:70
	1728.62	**3.98**	**MF3**	0-20	20	30	1		Wavy-discontinuous bedding with abundant elongate OM.	conodonts	none	15:200	framboids - abundant	framboids - abundant individual and clustered framboids throughout. No heavily pyritized laminae.	0:10:90
	1732.16	**3.46**	**MF3**	0-20	20	35	2	ST	Wavy-discontinuous bedding. Sand sized carbonate nodules throughout. Weakly bedded with bedding defined by alternating EOM and intraclast content. No erosion/scour or ripple indicators. Discontinuous lenticular preferentially pyritized lam. ST traces are common in top half of TS.	conodonts	PF	10:150	abundant	pyrite occurs as individule framboids and larger clusters. No preferential pyritization of some laminae	0;15:85
	1734.54	**4.43**	**MF3**	0-20	20	75	3	ST	Bedding is difficult to identify. intraclasts are sporadic but common. No evidence of erosion/scour or ripple forms. Crenulated horizontal OM accumulation, possible stylolitte or thin microbial mat (25 microns thick)? ST traces occur throughout, often easily identified by vertically sinously aligned quartz grains. TUL traces show lighter coloured, sinuous, homogenized infills. TL traces recongnized by homgenized silt-free infill with dark outlines.	agglutinated foaminiferea	none	common - 10:150	abundant	heavily pyritized but no preferential laminat pyritiztion - likey consistant with the lack of obvious bedding. Pyrite occurs as random framboids throughout. Small areas of clustered euhedral pyrite.	0:20:80
	1736.63	**7.37**	**MF6**	0-20	20	100	2	ST	Thick continuous microbial mat (dark carbonaceous bed) running through center of TS. Bedding character is difficult to identify, and bedding orrientation is denoted by the orrientation of intraclasts. No evidence of scour, erosion, or graded beds. Pyrite framboids are abundant throughout. ST traces are preferentially pryitized with detrital quartz along their margins - making them easily identified.	conodonts, possible agglutinated forams	none	ave. 10 - no large crystals	abundant	heavly pyritized laminae (up to 200um thick). Pyrite occurs as individule and clustered framboids throughout the matrix.	0:40:60
	1738.45	0	**MF2**	-	0			-	Cannot identify any primary sedimentary structures due to pervasive dolomitization. Clay between dolomite crystals is dark - possibly lots of organics. Fossil fragments concentrated within specific beds. Biotubation structures cannot be determined due to pervasive dolomitization	tentaculitids throughout.	ARS	-	-	-	-
	1740.78	4.1	**MF4**	0-20?	20	100	3	ST	Clustered pyrite framboids and discontinuous pyritized laminae. Thin discontinuous intraclastic lags with clasts stacked a maximum of 3 high. TUL traces have homoegenized clay infill, with diameters up to 100um. Possible concentrically lined traces with diameters of 75um. ST traces are denoted by pyrite framboids along the burrow margins. Individual traces are generally easily identified due to lack of pervasive bioturbation.	calcitic fossil fragments - likely tentaculitids. Possible agglutinated forams	PF	abundant 10:150	abundant	no heavily pryitized lam, but preferentially pritized areas (clustered framboids). Possibly euhedralpyrite - hard to tell.	0:15:85
	1742.61	4.23	**MF5**	10-40?	40	100	2	ST	No evidence of scour or erosion surfaces. Silt is evenly distributed throughout, no graded bedding. Intraclastic lags only 2-3 intraclasts thick. Possiblt microbial mat rip-up clast with detrital quartz silt encompassed in mat. ST traces throughout the TS. The abundance of silt in the matrix makes identifying these traces easy.	conodonts	PF	abundant 10:100	abundant	no heavily pyritized laminae in this section. Pyrite occurs mainly as individule framboids throughout the matrix. Framboids sometimes occur clustered together.	0:30:70
	1745.06	3.43	**MF4**	-	0			-	Heavily calcified section with dolomite fossil fragments. Clay intraclasts can be seen, but are altered by post depostional calcite. Some bedds show more pyrite farmboids than others. Cant identify any traces due to pervasive calcification	possible agglutinated forams	ARS	abundant - calcite makes up up-to 70% of section	abundant	occurs as individule or clustered framboids. No heavily pyritized laminae, but some laminae show discontinuous lenticular preferential pyrtization.	0:10:90
	1747.35	4.86	**MF6**	60-80	80	100	1	ST, TL, TUL,	Dark thick-cut TS. Discontinuous heavily pyritized laminae. Framboidally pyritized horizions and large euhedral pyrite features. Extremely rare sand-sized grains. ST traces are generally preferentially pyritized, and are easily identified due to aligned silt along boundries. Tubular unlined tunnels are also obvious due to shafting of silt. Tubular lined tunnels are lined w/ clay or silt.	possible agglutinated forams, conodonts are rare	PF	common 10:300	abundant	heavily pyritized laminae are common (framboidal). Individule and clustered framboids common/abundant throughout matrix.	0:20:80
Canol	**1749.21**	3.92	**MF2**	-	0			-	Primary sedimentary structures have been masked by heavily dolomitized character. Overall the matrix is homogenous-looking with absent intraclasts. Bedding orrientation is denoted by the preferential orrientation of elongate micaceous grains. Cant identify any traces due to pervasive dolomitization.	conodonts	PF	abundant, ave crystal size of 50	abundant	individule and clustered framboids throughout matrix.	0:5:95

1752.53	0	**MF5**	60-80	100	100	3	ST	Rare intraclasts in a silt-rich matrix. Thin silt lags throughout. Bedding is hard to identify - best identified by silt lags. Relatively large pyrite framboids thought. ST traces are abundant. TUL traces are small with a horizontal internal organization, and a general absence of silt grains. TUL are lighter coloured and more homogenized than surrounding matrix (10um -25 diam) - but are rare. TL traces often boardered by quartz silt (50um trace diameters), and are aslo rare. Possible that other traces are masked by ST reworking. Relatively short EOM could be a possible indication of heavy biogenic reworking. Vertical disruptions in silt lags represents biogenic reworking.	possible agglutinated foram	PF	ave crystal size of 10um	abundant	individual and clustered framboids. OM appears pyritized. Strands of hz linearly orriented framboids	0:20:80
1754.68	4.53	**MF2**	-	0			-	Primary sedimentary strucutres have been masked by the pervasive dolomitization. Rare clay-rich intraclasts. Elongate organic matter is short. Cant identify any traces due to pervasive dolomitization. Possible TUL traces?	conodont	PF	abundant ave crystal size of 50um	common	individual framboids throughout matrix - no clusters or heavily pyritized lam.	
1757.59	7.58	**MF6**	40-60	60	100	2	ST, TUL, TL	Homogenous-looking and silt-rich. Silt-beaing intraclasts are sporadic throughout and relatively small, and clay intraclasts are small. Silt is evenly distributed throughout - no silt lags. No evidence of erosion or scour or graded bedding. Mica silt is common. Some TUL traces can be traced latterally within beds as puncuated cross sections of traces. EOM is relatively short - possibly indicating commuition by burrowing orgznisms.	conodont	PF	common ave diam. 10um	common	sporadic discontinuous clustered pyrite in certain lam.	0:25:75
1759.49	6.08	**MF5**	60-80	80	100	4	ST	Homogenous-looking with abundant micas. Possible faint intraclastic lag and intraclasts are short/small. ST traces are pervasive throughout. EOM is short and sediments appear rbiogenically homogenized.		PF	average: 5um largest (rare): 100um	common	framboids throughout matrix. No heavily pyritized laminae, small clusters of framboids.	0:10:90
1761.5	6.63	**MF4**	50-80	80	100	4	ST	Generally homogenized with rare intraclasts. No evidence of scour/erosion or graded bedding. ST traces easily identified due to high abundance of quartz silt shafted along boarders.	conodont. Unidentified carbonate fossil fragment.	none - possible PF (small blue stained instances)	common - abundant 10:150	common	occurs as individule or clustered framboids. No heavily pyritized laminae. Some pyrite occurs as large circular pyrtie (20um)	0:20:80
1762.95	6.25	**MF5**	60-80	80	100	3	ST	Bedding is faint. No evidence of scour, erosion or graded bedding. Small calcite fossil fragments present. Sand sized post depositional carbonate throught. ST traces are pervasive throughout. Tubular unlined traces look similar to ST traces but are larger and mainly horizontal (20um in diameter).		none	common - abundant 25:100	common	individual framboids throughout the matrix, often occur as framboid clusters. Some laminae occur more heavily pyritized or preferentially pyritized.	0:15:85
1765.07	0	**MF5**	30-50	50	70	3	ST	No evidence of scour/erosion. Thin clay intraclastic lag. Silt evenly distributed throughout matrix - no graded bedding. Sand-sized carbonate nodules. Small clay rich intraclasts appear partially reworked. Large ST traces are sporadic throughout, with diameters up to 50um. Most ST are 15-20um diam. Tubular unlined traces have both darker and lighter clay fill (30um in diameter).	agglutinated foram	none	common - abundant 20:250	common	framboids are prevalent throughout the matrix as indivules and cluster framboids.	0:15:85
1767.52	5.19	**MF3**	0-30	30	100	3	ST	One-grain-thick discontinuous silt lags. Diagenetically calcified matrix. Small clay intraclasts appear reworked. Overally wavy-discontinuous bedding. TUL traces are subtle and short, not laterally continuous, and generally devoid of silt and have lighter coloured homogenized infill. ST traces sre often darker dur to incorperaetd pyrite, and boardered by quartz silt.	Phosphatic lenticular fossil fragment	ARS	common	common	framboids throughout matrix. No heavily pyritized laminae, small clusters of framboids.	0:10:90
1768.93	4.59	**MF3**	0-10	10			-	Bedding is faint and wavy-discontinuous. No evidence of scour/erosion orgraded bedding. Silt is evenly distributed throught. Thick microbial mat feature with intraclasts incorperated into the carbonaceous material. intraclasts are rare or too small to see. ARS stain appears to concentrate in strands and punctuated horizontal trail - possibly indicating calcite alteration of burrows. Withou the staining these "trails" would be difficult to identify.	possible agglutinated foram	ARS	common	common	individual and clustered framboids throughout. No heavily pyritized lam.	0:10:90
1772.19	8.63	**MF5**	20-50	50	100	3	ST	Overall very dark thin section (thick cut). Unlaminated to weakly laminated character. Small silt-bearing intraclasts. ST traces throughout (20um in diametter). TL traces are present (diameters of 100um).	abundant small agglutinated foraminifera.	none	common 7:50	common - abundant	individual and clustered framboids throughout matrix. Rounded clusters are more common than in other sections. No heavily pyritized lam.	0:20:80
1775.97	7.43	**MF5**	20-50	50	100	3	ST	Silt rich and homogenous-looking. No evidence of wave/scour/ or erosion surfaces. No intaclastic or silt lags. Detrital silts are evenly distributed throughout the matrix. Difficult to identify individual traces. Overall character appears to be biogenicall homogenized.	abundant small agglutinated formaninfera.	none	common ave 10	common	common individule and clustered framboids thoughout matrix. No heavily pyritized lam.	0:20:80
1777.48	7.73	**MF7**	-				-	Rhombically dolomitized section with medium silt sized rhombs. Microcrystaline carbonate is also present throught the TS. Large tentaculitid fragments generally clustered along specific bed boundries (possible lags?). Tentaculitids have diagenetic intragranular dolomite fill. Tentaculitids are generally intact - possably owing to early diagenetic dolomitization of interiors thus preventing fracture upon compaction; or short transport distances. Cant distinguish and biogenic features due to pervasive calcification/dolomitization	Tentaculitids - calcite with dolomitic centers and sometimes pyritized. Diameters range from 100um(ave) - 350um (max)	ARS	abundant/pervasive	less common	framboidal pyrite throughout matrix, less common than in other sections.	-
1779.04	0	**MF5**	0-30	30	100	3	ST	Overall unlaminated dark organic rich character with no evidence of wave scour/erosion, turbidites, or silt/intraclastic lags or graded bedding. Small intraclasts throughout - generally concentrated along specific bedding planes. Large detrital micas - some inclined. Traces are hard to identify due to thickness of the thin section (dark section). Small tubular unlined traces. TL traces present, average diameters of 100um.	abundant small agglutinated formaninfera.	ARS	common ave 10	common	individual and clustered framboids throughout matrix. No heavily pyritized laminae.	0:30:70
1781.14	7.73	**MF6**	20-50	50	100	3	ST	Thin section is dark due to being thick cut. Overall unlaminated texture. Silt rich intralcasts are sommon throughout. Possible discontinuous thin silt lag. Large dark vertical sinuous trace that appears to taper in diameter downwards. Appears unlined, with lesser silt infill than in surrounding matrix. Presence of some TL traces. Darkness of section makes identifying individual traces difficult.	Calcite fossil fragments throughout, genreally concentrated along certain lam.	ARS	common ave 10	common	some (rare) large pyrite nodules (up to 600um). Other than that pyrite seems to occur as individual and clustered framboids throughout the matrix.	0:30:70
1784.14	6.16	**MF5**	30-60	60	100	2	ST	Weakly bedded character. Thin intraclastic lags. Possible graded beds with decreaseing silt content upwards. Weakly laminated texture could be result of biogenic disruption of sedimentary structures. ST traces are pervasive throuhgout the matrix, and are obvious due to aligned quartz along the margins. TUL traces, max diams of 100um throughout - less common than ST. Intraclastic lags are disrupted by vertical burrowing.		none	less common	common	individual and clustered framboids throughout matrix. Some laminae have more pyritization, but generally not heavily pyritized.	0:20:80

	1791.31	0	**MF3**	0-10	10	20	2		Weakly bedded character with calcite mud (miciritic matrix - stained pink). Discontinuous pyritized beds throughout with high EOD concentrations. No evidence of wave/scour or graded bedding. Intraclasts are sporadic throughout. Heavily dolomitized clay matrix. Possible microbial mat rp clast? TUL traces are difficult to differentiate from deformed silt poor pellets - usually short, devoid of organics, and unstained and light beige in colour. Traces are not very prevalent.	dolomitic and calcite spines, shell fragments. Possible organic coated achritarch.	ARS	abundant, majority are silt sized grains	abundant	some lam contain more pyrite than others. Individual pyrite framboids and clusters throughout. Framboids are larger than other sections	0:5:95
	1793.98	5.38	**MF3**	0-20	20	30	2	ST	Common clay and silt-bearing intraclasts. Weakly bedded texture with thin horizontal beds. No evidence of wave scour or eorsion. No graded bedding. Different beds distinguished by variable OM and intraclast abundance. Some discontinuous wavy bedding at higher magnifications. Small ST traces cross cutting TUL traces (15-30um). ST traces are sometimes preferentailly filled with framboidal pyrite.	Fully pyritized fossil fragment (150um). Large phosphatic fragment (300um long)	none	common, ave grain size 10um	abundant	large framboids throughout matrix, as well as pyrite replanment of possible fossil fragments, and small framboids within some fecal pellts. Some OM stringers appear pyritized as well.	0:5:95
	1796.05	4.08	**MF3**	20-40	40	70	3	ST	Possibly post-depositional calcite beds below microbial mat lamiane. Varying degrees of diagenetic pyritization and calcification. No evidence of wave scour/erosion or graded bedding. Apparent phosphatic nodules. Medium silt sized rhombic dolomite makes up up to 10% of matirx in some areas. Multilined traces TL (70um in diameter), but rare. ST traces are often darker than surrunding matrix. Can be easily identified when cross- cutting through intraclasts, but can be obscue in the matrix. EOM/microbial mat lamiane appear unreworked.		ARS	abundant	abundant	pryite framboids thoughout matrix, with larger framboids throughout calcite beds. Euhedral appearing pyrite also present in calcite beds.	0:5:95
	1798.67	5.07	**MF3**	0-20	20	50	3	ST	Wavy discontinuous bedding. Intraclastic lag. Apparent change in bedding angle upwards through section. Possible large fugichnia trace - 50um in diameter. ST traces thoughout matrix.	pyritized radiolarians	ARS	common	abundant	framboids throughout matrix. Some possible pyritized fossil fragments.	0:5:95
	1800.5	3.38	**MF8**	-	0			-	Alternating intraclast-rich and intraclast-poor beds. Overall thin section is diagenetiadly dolomitized (mainly rhombic). Pyrite is also abundant throughout. Possible microbial mat rip up clasts. Detrital quartz silt is absent. Possible fining up bed with intraclast lag at base. Detrital micas are rare. Possible ST traces, but hard to tell due to pervasive dolomitization. Lack of silt or lithologic contrast makes it difficult to identify individual traces.	Pyritized fossil fragments (unidentified)	PF	abundant	abundant	individule framboids throughout matrix, as well as pyrite replacing some dolomite crystals. Dolomite is often more heavily concentrated in silt-poor pellets, other pellets devoid of dolomite.	0:2:98
	1802.62	4.16	**MF8**	n/a	0		1	ST	Intraclastic-rich thin section. Beds are denoted on the basis of varying intraclast abundance, organic adundance and pyrite abundance. Dolomitization is variable and decreases upwards through the TS. No evidence of wave scour or erosion. No lags. Difficult to acuratley identify traces due to pervasive dolomitization and lack of lithologic contrast.	phosphatic fragment (conodont?)	PF	abundant	abundant	individual framboids throughout matrix, as well as alteration of some dolomite crystals	0:2:98
Bell Creek Member	**1805.38**	0	**MF8**	0-20	20		2		Dolomitization is less prevalant than in other TS of this facies. Planar preferentially pyritized laminae throughout - typically are discontinuous across thin section. No evidence of wave scour or erosion. No graded bedding. TUL traces are redish in colour with homogenized fill.	phosphatic fragment (conodont?)	PF	sporadic-common	abundant	heavily pyritized laminae, large framboids	0:5:95
	1807.35	4.05	**MF8**	0-10	10		1		Beds are denoted on the basis of varying intradast abundance, size, and organic content. Possible stacked gradded beds with intraclast rich bases and day rich tops. Possible turbidite bed (appears more homogenated and well defined when compared to other beds). Well bedded thin section. ST traces are the only visible traces in this section. Possible pyritized burrow fills of some horizontal burrows.	conodont	PF	common 10:40	abundant	framboidal pyrite abundant throughot matrix.	0:2:98
	1812.42	4.15	**MF8**	0-10	10				Rare (30um large) euhedral quartz grains. No evidence of erosive events, turbidites or graded beds. Completley euhedrally pyrtized intraclasts at base of section. Appears entirely unreworked - intraclasts are intact along with the EOM. Possible issolated pyritized hz burrow fills?	conodont	PF	common 10:	abundant	intensly pyritized fecal pellets as well as large pyrite framboids	0:2:98
	1813.76	2.43	**MF2**	n/a	0			-	Completley diagenetically altered by ferroan rhombic dolomite. Dark remnant matrix character owing to high organinc content.	-	PF				
	1814.67	6.54	**MF4**	0-10	10				TS is dark due to high organic content. Heavily dolomitized by rhombic ferroan dolomite. Dolomitization decreases upwards. Clay intraclasts are common-to-abundant throughout. Diagenetic dolomitization occurred post compaction resulting in crushed tentaculitid tests. Uninterupted intraclasts and EOD indicate low degrees of reworking. Lack of lithologic contrast and pervasive dolomitization in some areas obsqures possible traces.	long/thin calcite fossil fragment (1800 um long). Fragment is partially pyritized. Likely tentaculitid	PF, ARS	abundant dolomite	abundant	framboids dissentinated throguhout matrix. Calcite tentaculitid shells are preferentially partially pyritized.	0:2:98
	1816.92	2.26	**MF2**	n/a	0				TS is almost completed dolomitized (by ferroan dolomite). Partial early dolomitization of tentaculitid test interiors prevented the collapse of tests. Remnant matrix is dark and likely heavily organic rich. Remnant day intraclasts can be seen in some areas. Cant identify any traces due to pervasive dolomitization.	Completley pyritized fragments (unidentified)	PF, ARS	abundant-completley dolomitized section		clustered framboids throughout the matrix and pyritized fossil frag.	0:5:95
Bluefish Member	**1820**	0	**MF4**	0-10	10	50	2		Tentacultiitds throughout - generally sporadic, occasionally concentrated along bedding planes. No pre-compaction early diagenetic dolomitization. Test are partially pyritized. Sporadic ferroan microcrystallline dolomite throughout.	pyritized tentaculitids	PF, ARS	abundand dolomite	abundnat	occurs as individual and clustered framboids throghout matrix, as well as preferntal pyritization of some cacite fossil frags	0:5:95
	1823.52	5.33	**MF7**						Calcite tentaculitid fragments abundant throughout. No early diagenetic dolomitization of interiors resulting in crushed test. Variable test size between beds. Diagenetic kaolinite filling uncompacted test interiors. Clay intraclasts throughout. Diagenetic rhombic dolomite present in small quantities.	abundant tentaculitid fragments - calcite - sometimes partially pyritized	1/2 ARS. PF		abundant	clustered and individual framboids throughotu matrix, as well as partialy pyritized organincs and tentaculitid frag	0:5:95
	1826.95	5.67	**MF7**			25	1		Discontinuous preferentially pyritized laminae. Both calcite and dolomite fossil fragments. Tentaculitid fragments throughout - not concentrated along bedding planes (sporadic throughout). Matrix appears reworked and partially homogenized. Abundant parallel detrital micas. Possible biogenic reworking leading to somewhat homogenized matrix character.		ARS				0:50:50

Husky Little Bear H-64

Formation	Depth (m)	MicroFacies	BI % Range	Max BI%	Trace Size Max (µm)	Max Size Trace Type	Diversity #	Most Abundant Trace	Sedimentological and Ichnological Characteristics	Fossil Fragments	Staining	Calcite/Dolomite abundance-Mode:Max	Pyrite Abundance	Pyrite Type	Sand:Silt:Clay
Canol	**1170.26**	**MF4**	0-10	10	50		3		Large (1750um) mega quartz clast. Microbial rp clast. Discontinuous pyritized horizions. TUL traces are small (20um diam), lack silt grains, have more homogenized fill, and are more redish in colour than surrounding matrix.	common phosphatic fragments - likely conodonts (150um) throughout, as well as unidentified calcite fossil fragments	PF	dolomite inclusion (blue stained) in megaquartz amalgamation	abundant	Framboidal pyrite thoughout matrix (indivule and clustered framboids). Large pyritized calcite fossil fragments. Preferntially pyritized horizons throuhgout	0:20:80
	1174.25	**MF8**	0-10	10	50	TUL	2	ST	Low density turbidite beds ang stacked graded beds. Small unlined and unorganized traces through silt-poor pellets. Horizontal sinuous dissruptions through some pellets (30um diam) sometimes with apparent internal organization and homogenization. Large diam SD traces (up to 50um). Prefterntially pyritized SD traces are common throughout matrix	possible radiolarians or tasmanities	PF	common silt-sized calcite grains. Larger (50um) dolomite crystals	abundant	Framboids dispersed throughout matrix. pyritized horizons throughout, often not latterally coninuous. Clusters of framboids forming thoughout the matrix, usually in close proximity to pyritized horizons. Pyrite alteration/small nodules forming (200um)	0:5:95
	1175.5	**MF3**	0	0	50	TUL	3	ST	Rounded sand-sized (100um) microcrystalline quartz grains throughout matrix. Larger anglular mega quartz crystals less common throughout- some large angular quartz are assocaited with phosphatic fragments. Angular quartz crystals commonly have dark inclusions - pyrite or OM? Large inclined fracture running through thin section - appears to be pre-thin section prep. Fracture is filled with OM. Silt aggregates throughout. Overall crenulated appearance to the thin section. ST traces are present. Possible hz tubular unlined traces throughout matrix (50 um diam) - darker fill than surrounding matrix. Small ST x-section are present clustered together (loccaly common). Lack of lithologic contrast makes identification of traces difficult.	unidentified angular phosphatic fragment (100um x 200um).	none		abundant	Discontinuous pyritized horizions throught thinsection. Framboidal pyrite dissemtinated throughout the matrix.	0:<2:98
	1179.17	**MF4**	0-30%	30	20	ST	2	ST	Pyrite replacing what appears to be lenticular fragments of microcrystalline quartz. Angular quartz grains rare throughout matrix (75 um long). Large organized fill lighter coloured trace (VUM), 30um wide. ST traces throughout - darker than surrounding matrix and vertically cross cut bedding (10um diams).	phosphate (possible conodont) fragments rare throughout section.	none	common throughout the matrix	abundant	Pyritized horizons present throughout the thin section - made up of concentrated framboids. Pyrite clusters also common throughout matrix - possibly preferential pyritization of fecal pellets? Preferentially pyritized fossil fragments throughout.	0:<5:>95
	1180.27	**MF4**	0-10	10		ST	1	ST	Discontinuous pyritized horizions throughout. Microbial mat rip-up clasts throughout. Cherty nodules and phosphatic fragments. Alteranting dark brown and light brown beds. ST traces are best seen at 2x magnification - appear darker than surrounding matrix. Small (30um diam) multilined trace. Possible larger TUL trace (100um diam).	unidentified phosphatic fragments (likey conodonts)	none	common silt-sized calcite grains.	abundant	Discontinuous pyritized hoizions, some more pyritized than others. Preferntially heavily pyritized zones - maybe higher OM content?	0:5:95
	1182.67	**MF6**	0	0	-	-		-	Alternating beds of MF 3 and MF6, MF6 more common. No traces can be identified		-	-	Pervasive	Large euhedral crystals in the pyrite altered bed (50:200). Disseminated abundant framboids thoughout pellet rich beds.	0:50:50
	1184.24	**MF3**	0-10	10	50	TUL	3	TUL	OM rich, silt poor. Large rip up clasts (microbial mat encased radiolarite). Apparent Hz tubular traces. Consist of homogenized clean (lighter coloured) clay with internal organization parallel to bedding (clay particles appear linerally organized - fecal pellets generally random clay orrientation?). Possible tubular lined taces (70um diams). ST traces are hard to identify or absent from this elevation.	possible tasmanites cysts. Appear to be concentrated within certain laminae/horizions. Rare phosphatic fragments.	none	sand-sized C/D - rare/locally common. Silt-sized -uncommon throughout matrix	abundant	Some well rounded pyrite nodules - spherical character may indicate infilling of cyst tests. Small framboidal pyrite disseminated throughout matrix.	0:2:98
	1186.69	**MF1**	0	0	-	-		-	Composed of Radiolarian tests and clay. No traces can be identified	Forams	none	-	-	Framboids disseminated thoughout matrix.	-
	1188.76	**MF5**	20-40	40	20	TUL	2	ST	Pyritized small microbial rip up clasts. Phosphatic fossil fragments. TUL traces can be hard to distinguish from silt-poor intraclasts - in xpl you can see that the clays have an internal organization parallel to bedding. TUL are not laterally continuous (traceable along bedding planes...). ST traces can be identified when they cut through some silty areas - where silt grains get shafted towrads edges of trace (15um diam). disturbed silt rafts and intraclasts.	possible radiolarians or tasmanities	none	common - 5um-10um	abundant	Pyritized horizons concentrated into thin bands. Framboidal pyrite disseminated throughout matrix.	0:15:85
	1190.25	**MF5**	20-40	40	30	ST)	2	ST	ST traces can have larger widths than typical in other thin sections (>30um) - quartz silt is shafted to edges making them somewhat easy to identify. Traces are darker than surrounding matrix. Some TUL traces that are lighter than surrounding matrix and very similar to silt-poor intraclasts.		none	sporadic/bearing		Preferentially pyritized horizions throughout (50-120um thick) - consist of concentrated framboids.	0:20:80
	1192.74	**MF4**	0-10	10		TUL	2	ST	Carbinate nodules formaing throughout. Phosphatic fragments throughout. Microbially encased radiolarite. Carbonate nodules. Overall crenulated appearance. Trace infills appear homogenized and lighter in colour. Some TUL are long (laterally continuous and traceable along beddin g planes). TUL traces present (125um diam). ST traces throughout section.		none	common silt sized grains throughotu matrix. Nodules are common	abundant	Framboidal pyrite disseminated throughout matrix. No preferentially pyritized horizions.	0:20:80
	1194.73	**MF4**	0-10	10	50	TUL	2	TUL	Carbonate nodules throughout. Elongate organic matter is abundant throughout, indication of microbial mat? TUL traces throughout. Small 15 diam max traces through pellets (hz) - uually lighter more homognized fill than surrounding matrix - sometime preferentially pyritized. Possible small tubular hz lined traces. Small circular unlined x-sections throuhout - fill is darker than surrounding matrix and silt grains are absent from fill. Possible hz unlined longitudinal calcite filled trace. Small lithilogically simliars (jut organization of matrix) into strands (similar to SD) - best seen when they cross cute pellets or larger lighter coloured TUL traces - once they reenter the matrix they get lost. darker unlined circles throughout (50um diams) - possible diagentetic alteration of burrows/organism secretions? concentreated OM (appear similar to degrading OM flecks).	small elongate phosphatic fragment.	none	nodules - ave 120um. Silt sized calcite grains sporadic throughout matrix.	abundant	Some horizions slightly more pyritized than others. Disseminated framboids throughout matrix. Possible small pyrite nodules forming.	0:10:90
	1197.14	**MF4**	0-10	10	20	TUL	2	TUL	Variable OM concentration throguhout the thin section elevation. Large angular quartz grains with dark rims and inclusions (possibly infilling of fossil tests?). Carbonate (both dolomite and calcite) and silica nodules throghout. Small rare silt rafts. Thick graded beds with silt and OM rich bases and clay tops. Possible phritite lag. Possible OM stylolite or microbial mat along bottom of thin sectiton. No definitively identifyable traces - om stringers and laminae are all intacted. Possible x-section of TUL, could also be x-section of silt poor pellet. No vertical alignemnt of silt grains owing to SD traces, but also would expect to see disruptions in OM stringers with SD present. some silt-poor lighter coloured pellets at odd oblique orrientatons to bedding - possible burrows? pellets that are possible traces would be TUL traces.	conodonts	PF and AZR	nodules (largest 200um)	abundant	Preferentially pyrtized horizions. Framboids disseminated throughout matrix.	0:10:90
	1198.7	**MF4**	0-10	10	20	TUL	3	ST	Microbial mat at base. OM filled microfractures. Large angular silica growths. Possible fugichnia or vertical trace through pellet. Small dark circular traces through intraclasts, and small light tubular traces through dark matrix (15um). ST traces - most obviously seen when cross cutting intraclasts.	possible tasmanities	PF	nodules are comon throughout, as well as silt sized grains	abundant	Preferntially pyritized horizions throughout.	0:10:90
	1207.08	**MF6**	60-80	80	100	ST	2	ST	Light beige color - low OM content? Silica filled microfractures. No evidence of scour or graded bedding. Some intraclastic lags. Large homogenized fill traces that have a higher concentration of framboids throughout them - large ST traces? Diameters of up to 100um. Some horizons more heavily reworked than others. Possible rare vertical lined traces.	phosphatic fragments (likely conodonts)	PF (1/2 stained)	common-abundant silt sized grains, and common nodules throughout (100 um ave)	abundant	Pyrite throught matrix - framboids up to 20um in diameter. Euhedral pyrite (ave 20um) condensed within some horizons.	0:10-15:85-90
	1209.07	**MF6**	50-80%	80	100	TUL	2	ST	Fractures running throughout section - wide separtation filled with calcite while microfactures are filled with OM. Thin silt lags. ST traces throughout. ST traces easiy identifed on basis of sinuous alignments of shafted quartz silt and pyritie framboids. Possible tubular lined traces	phosphatic fragments (likely conodonts)	PF, AR	common silt-sized calcite grains throughout. Common carbonate nodules forming (150um)	abundant	Framboids disseminated throughout matrix, some concentrated in large clusters.	0:5:95
	1211.18	**MF6**	possibly 50% but unreliable due to diagenetic carbonate	50	50	ST	2	ST	Large calcite filled fractures. Quartz filled inclined to hz uniform diameter strucutres - burrows? - formed beofre carbonate? Organic rich dark section. Tubular unlined traces denoted by silt rims. ST traces obvious due to silt shafting to margins and subseuent sinuous alignment.	phosphatic fragments (likely conodonts)	PF/AZR	common carbonate nodules (100um), abundant silt-sized grains	abundant	Preferntailly pyritized horizon (only one - discontinuous). Disseminated framboids throughout matrix.	0:5:95

	1214.64	**MF6**	80-100%	100	75	TUL	2	ST	Elongate OM is pyritized. Dolomitized by silt sized microcrystaline dolomite. ST traces throughout section. Possibly 100% reworked as no apparent bedding remains. Tubular unlined traces visible in x-section by shafting of grains to boarders (75um). Small homgenized-fill hz burrows throughout (lighter red-ish colour when compared to surrounding matrix) - less well defined shapes than the intraclasts, can be traced hz along planes. Small tubular lined traces (20um diam).	phosphatic fragment	PF			Framboids disseminated through matrix.	0:15:85
	1218.15	**MF4**	-	20	-	-		-	Brecciated thin section.		PF	common silt sized grains	abundant	Framboids disseminated throughout matrix.	0:10:90
	1220.51	**MF6**	20-50%?	50	50	TUL	2	ST	Rare silt-rich intraclasts. Microbial mat present. Small hz TUL traces - lined with pyrite framboids. Possible inclined (45 degrees) meniscate backfilled trace - 150um diameter.		PF and AZR	common - silt sized	abundant	Framboids disseminated throghout matrix. Preferntially pyritized clusters of framboids.	0:10:90
	1226.26	**MF4**	0-10	10	150	TL	3	ST	Silt aggregates throughout. Preferentially pyritized ST traces. TUL traces with framboidally pyritized linings. Some TUL have a lighter-coloured lining, possible carbonate alteration? (150um diam).		PF	common		Pyrite framboids dissementated throughout matrix.	0:5:95
	1229.84	**MF5**	20-40?	40	100	TL	1	ST	Some large diameter ST traces (diams ave 30-40). Rare well defined TUL hz traces (possibly lined?) with diameters up to 100um.		PF	silt sized carbonate is common		Framboids disseminated throughout matrix. Pyrite replacement of fossil fragments is locally common.	0:10:90
	1232.84	**MF5**	80-100%	80	100		2	ST	Bedding plane views of small diameter sinuous horizontal traces 10-15um diam. Horizontal silt-rich TUL. Large (100um) diameter possible hz backfilled traces present. Most traces have lighter coloured homogenized infills.	possible pyritized tentaculitids	ARZ	common	abundant	Disseminated framboids throughout matrix as well as replacment of some fossil fragments.	0:10-15:85-90
	1234.05	**MF6**	80-100%	100	100	TL	3	ST	At 2x magnification large ST traces can be seen. At 10x magnification ST traces are obvious, and pervasive throughout the thin section. Possible TL traces - circular rings of quartz silt, but larger traces have been over printed by smaller ST making them more obsqure. Lighter coloured homogenized infilled TUL traces	pyritized conodont		common	abundant	Framboids disseminated throughout matrix.	0:10:90
	1236.5	**MF2**	80	100					Aggragated quartz silt and large intraclasts present. Possible calcite filled burrows? Seem to be laterally traceable and have circular x-sections (60um across). Some possible TUL traces? No real ichnological analyses can be done to do pervasiveness of dolomitization	abundant unidentified calcite fossil fragments - crushed		abundant	abundant	Abundant pyrite dissesminated throughout matrix.	0:5:95
	1239.84	**MF2**	40-60	60	75	ST or TL	1	ST	ST traces throughout thin section. Some apparent traces that have vertical to horizontal j-shaped morphologies and a faint meniscate backfill (20 um in diameter). TUL trace (one identified - 50um diam).	crushed calcite fossil fragments	AZR	common	common - abundant	Dissemenated framboids throughout matrix.	0:15:85
	1244.78	**MF6**	40-80	80	30	ST	1	ST	ST traces throughout. Possible vertical backfilled trace (50um) diameter.		PF	silt sized calcite (unstained) commn throguhout matrix	abundant	Framboids disseminated throughout matrix.	0:5:95
	1250.52	**MF2**		0	-	-		-	-	-	-	-	-	-	-
	1253.52	**MF4**	10	10	20	ST	1	ST	Wavy-bedded appearance. Intraclastic lag. ST traces throughout. Possible TL.	calcite fragments (rare)	AZR	common	common - abundant	Framboids dissementated throughout matrix, some large framboids (up to 75um). Pyrite nodule (100um diam).	0:<2:>98
	1270.55	**MF8**	0-10%	10	20	TUL	2	ST, TUL	Possible small scale current ripple. One scour surface. Possible normally graded bedding. Intraclasts show evidence of burrowing.		PF	abundant	abundant	Framboids dissemenated throughout matrix. No heavily pyritized horizions. Pyrite nodule forming (100um diam).	0:<2:>98
	1272.26	**MF8**	0-10%	10	25	ST	1	ST	ST traces throughout.	large phosphatic fragment	PF	abundant	abundant	Large framboids disseminated throughout the matrix.	0:<2:>98
Bell Creek	**1273.9**	**MF8**	0-10%	10	25		1	ST	No evidence of sed strucutres. ST traces throughout.		PF	abundant	abundant	Large framboids disseminated throughout the matrix. Pyritization of organominerallic aggregates. Discontinuous heavily framboidally pyritized horizions throughout.	
	1275.38	**MF8**	0-10%	10	25		3		Soft sediment deformation structures/microfaults. Possible ST traces throughout. Hard to tell due to pervasiveness of dolomitization.		PF	abundant	ABUNDANT	Large framboids disseminated throughout matrix.	0:<2:>98
	1276.57	**MF8**	0-10%	10	25		1	ST	Small scale ripple surface and normally graded beds. Possible small (<10um diam) preferentially framboidally pyritized ST traces sporadic throghout. TUL traces - easiest seen when cross cutting silt-poor intraclasts - usually have a darker infill and ovate/rounded x-section.	pyritized fragment of some sort - pyritized spiculitic fragments throghout	PF	abundant	abundant	Abundant large framboids dissemeinated throughout matrix.	0:<2:>98
	1287.59	**MF2**	-	0	-	-		-	Preferentially pyritized horizions throughout. Hard to distingish any primary sed feactures. Accuratley identifying traces in bottom half of section is impossible due to pervasiveness of dolomitization	fossil fragment horizions where calcite and pyritized fossil fragments are concentrated within certain beds	PF	abundnat	abundant	Framboids dissemeinated throughotu matrix. Pyritization of calcite fossil fragments. Preferentail pyritization of some horizions.	0:<2:>98
	1289.26	**MF7**	0-10%	10	20	ST	2		ST traces throughout. TUL traces are rare and seem to be concentrated within individual beds. Absence of lithologic contrast/prefence of silt grains makes identifying trace difficult.	crushed calcite fossil fragments throughout. Often preferntially pyritized.	AZR, PF	common	abundant	Pyrite framboids disseminated throuhout matrix. Pyritization of calcite fossil fragments as well as preferentially more heavily pyritied beds.	0:<2:>98
Bluefish	**1290.33**	**MF4**	0-10%	10			1		Rare TUL traces with homogenized infill and poorly defined boundries. Pyritization and dolomitization makes it hard to identify deformation vs reworking.	pyritized fragments of elongate planar parallel calcite fragments (almost look like bobby pins) range in size from 300um - 2500um. Ovate phosphatic fragments.	AZR, PF	common	abundant	Framboids disseminated throughout the matrix. Pyritized elongate fossil fragments. Large (1100um) euhedral pyrite crystal. Preferentially pyritized horizions throughout.	0:<2:>98
	1294.23	**MF2**	80-100%	100	40	TUL	2	ST	Absence of obvious bedding may indicate a high degree of biogenic reworking. Possible lighter coloured homogenized filled vertical branching traces - or thinsection defets? Havent seen this type of structure in other thin sections... TUL traces with lighter coloured homogenized clay fill (40um diam). ST traces throguhout.	common crushed calcite fossil fragments throughout.	AZR	common	abundant	Framboids disseminated throughout matrix. Pyritized calcite fossil fragments.	0:5:95
	1299.11	**MF2**	80-100%	100			2	ST	Visible ST traces. Possible hz lighter coloured discontinuous bands with poorly defined boundries may be TUL traces?	calcite (pyritized) tentaculitid fossil fragments abundant throguhout.	AZR	common	abundant	Pyritization of calcite tentactulitid fragments. Framboids disseminated throughout matrix. Thin preferntially pyritized horizions.	0:2:98

MGM Shell East Mackay I-78

ormation	Depth (m)	TOC	MicroFacies	BI % Range	SDI	Trace Size Max (µm)	Max Size Trace Type	Diversity #	Most Abundant Trace	Sedimentological and Ichnological Characteristics	Fossil Fragments	Staining	Calcite/Dolomite Habit	Calcite/Dolomite abundance-Mode:Max	Pyrite Abundance	Pyrite Type	Sand:Silt:Clay
	1822		**MF8**	0-10%	30	15	ST	2	ST	Bedding plane thin section. No obvious strucutres in the intraclastic rich sediments. Possible large diameter TUL traces with homogenized fill and difuse boarders.			silt-sized calcite/dolomite throughout matrix - sporadic	sporadic-common	common	clustered framboids throughout as well as individual framboids diseminated throughout. Euhedrally pyritized silt-bearing intraclasts.	0:20:80
	1822.4		**MF8**	0%	25	25		1		Microfractures throughout the thin section with bitumen fill. Some bedding planes are obvious, indicating possible evidence of wave erosion or non sedimentation. One preferntially dolomitized layer. Normally graded intraclast beds. No traces identified.	phosphatic ovate/lenticular fragments throughout (conodonts?) - rare - seem to be concentrated allong certain horizions. Pyritized spherical/circular tests with silica centers (67.96um)	PF	sporadic silt-sized dolomite (stained) grains throughout the matrix.	sporadic - common	common	pyrite framboids dissementated throughout the matrix. Some relatively large framboid clusters (50um diam). Poorly pyritized horizions (have a slightly higher proportion of concentrated framboids).	<1:20:80
	1827.4		**MF8**	0-20%	300	75	TUL	4	ST	Rafted silt aggregates are present. Faint wavy bedding. Discontinuous pyrtie laminae throught. ST traces throughout, much less prevalant than in other sections from other cores. ST traces can be best seen when the cross-cut intraclasts (due to increased lithologic contrast). Possible light clay filled homogenized infill tubular TUL traces (75um). Possible small fugichnia throughouh intraclast-rich bed.	rare phosphatic fragments - some very large (250um)	PF	silt-sized dolomite throughotu matrix. Dolomite nodues sporadic throughout (100um). Phosphatic nodules altering to dolomite.	sporadic	common	preferntailly framboidally pyritized horizions throughout section, thin pyritized layers when compared to someo other sections (30um thick).	0:5:95
	1830.1	**4.43**	**MF8**	0-20%	300	100	ST	3	ST	Possible normally graded beds from intraclast rich beds to clay dominated beds. TUL traces with homogenized and preferentially pyritized infill. ST traces through some intraclasts but not abundant.	single conodont fragment and one possible acritarch test.	PF	dolomite nodules forming. Common silt-sized dolomite grains	common	common	pyrite framboids throughout matrix.	0:2:98
	1834.25		**MF3**	0-10	0					Heavily dolomitized base with declining amounts of dolomite upwards. Euhedral pyrite disseminated throughout. Intraclasts throughout.							
	1835			10-50%	122.46	61.23	TUL	2	ST	Bedding plane thin section. Difficult to distinguish traces due to lack of lithologic and colour contrast. ST traces are slighty darker than surrounding sediment - possible preferential pyritization? Massive appearance is the result of high degrees of biogenic reworking. Larger ST or TUL traces through some intraclasts.	pyritized honey comb strucutres - seem to be incorperated into clay pellets? Pyritized cruciform fossil frags. Possible pyritized tentaculitid fragments.	none	calcite or dolomite nodules common throughout		common	framboids disseminated throughout matrix. Some small clusteres of relatively large diameter framboids.	0:5:95
	1835.4	**5.3**	**MF3**	0-10%	100	50		2	ST	Some siliceous alteration. Small TUL traces throughout but poorly defined. Some heavily bioturbated beds throughout.	Lenticular phosphatic fragments are rare (conodonts?). Possible pyritized achritarchs.	PF	dolomite nodules are common to abundant throughout	common	common	framboids disseminated thought the matrix. Relatively large framboids when compared to other sections.	0:7:93
	1838		**MF4**	0-10%	0			1	ST	Bedding plane thin section. Possible large ST traces. Lack of silt makes distinguishing smaller ST traces difficult as their fill is very similar to the surrounding matrix.	phosphate fossil fragmnrts of some kind (conodont?). Pyritized small spiculitic and honeycomb-like structures throughout the matrix. Recyrtalized achritarchs or radiolarians (silica).		dolomite/carbonate nodules forming throughout.	common	abundant	framboids disseminated throughout the matrix. Some areas show heavy clustered pyritization of tentaculitids or other spicules and framboids.	0:<2:98
	1838.9		**MF4**	0-10%	25	25		1		ST traces present at some elevation. No apparent traces through intraclasts.	recrytalized radilarians (silica)	PF	calcite nodules common throughout (unstained). Some appear organically rimmed	common	abundant	rare preferentially pyritized elevations that are not laterally continuous across section.	0:5:95
	1841		**MF5**	5-20%	158.31	52.77	TUL	3		Bedding plane thin section. Small lined TUL traces. Lack of lithologicc contrast makes it hard to identify traces. Many intraclasts appear to be reworked.	Pyritized unidentified fossil fragments including honeycomb structure and lenticular fossil. Pyritized curciform fragments are common.	none	OM rimmed carbonate sand-sized nodules. Silt-sized carbonate sporadically disseminated troughout matrix.				

Canol	**1841.17**	**4.2**	**MF3**	0-10%	55.66	27.83	TUL	2	ST	TUL traces with homozenized infill and poorly defined trace boundries. ST traces are rare and hard to discern due to lack of lithologic contrast.	Pyritized circular fossil fragments (Achritarchs? Radiolarians?).	none	silt-size carbonate grains and larger carbonate nodules throughout section	sporadic	common	framboids disseminated throughout the matrix. Pyritized fossil fragment are rare. No preferentially pyritized horizions	0<2:>98
	1845.1		**MF2**		0					All bioturbation and sedimentary structures obsqured by pervasive dolomitization.							
	1846		**MF5**	20-70%	58.58	29.29	TUL	2	ST	Bedding plane thin section. ST burrows throughout. Often darker owing to preferentially framboidal pyritization. Large TUL x-section.	phosphatic fragments. Unidentified elongate and cruciform carbonate fossils. Possible carbonate recrystalized radiolarians?	none	silt-sized carbonate grains sporadic throughout the matrix.	common	common	framboids disseminated throughout the matrix. Sometimes clustered into more heavily pyritized zones.	0:10:90
	1846.6	**5**	**MF4**	0-20%	60	30	TUL	2		ST traces can been seen in some beds.	small phosphatic fragments - rare	none	silt-sized carbonate grains are rare-sporadic throught matrix	rare	common-abundant	large pyrite alteration (1cm diameter). Discontinuous preferntailly framboidally pyritized horizions throughout section.	1:9:90
	1851		**MF3**	20-70%	40	20	TUL	2	ST	Bedding plane thin section. Large ST or TUL traces throguh pellets. Possilble backfiled traces.	Pyritized spiculitic and honeycomb-like fossil fragments. Round/spherical carbonate fragments - recrytalized radiolarians or acritarchs?	none	silt-sized calcite/dolomtie sporadically throughout he matrix.	common	common	framboids disseminated throughout the matrix. Some areas more heavily pyritized than others.	0:2:98
	1851.9		**MF4**	0-10	30	30	TUL	1		Traces and sedimentary structures are difficult to identify.	rare phosphatic conodonts	none	rare carbonate nodules throguhout, and rare silt-sized carbonate grains	rare	sporadic - common	pyrite framboids throughout matrix. Some large clustered framboids (100um). Pyrite is relatively less abundant when compared to other sections.	0:3-7:93-97
	1853		**MF6**	0-30%	20	20	ST	1	ST	Bedding plane thin section. ST burrows throughout section.	common conodont fragments. Pyritized radiolarians.	none	silt-sized calcite/dolomite grains sporadic throughout matrix.	rare	common	framboids disseminated throughout the matrix. Some areas appear to be more heavily pyritized than others. Pyritized fossil fragments throughout.	0:10:90
	1853.83	**9.195**	**MF8**	0-10	40	20	ST	2	ST	Possible ST traces throughout, with pyritized trails. Silt grains aligned along ST boundries. Some elevations unburrowed (0%), some more reworked (20%).	rare phosphatic fragments - conodonts?	none	silt-sized carbonate grains are absent.	rare	abundant	Discontinuous prefernetially framboidally pyritized horizion throughout section. Large pyrite alteration/nodules forming (879.66um diameter)	0:20:80
	1855.5		**MF2**		0					Sedimentary structures and bioturbation have been obsqured by pervasive dolomitization.							
	1857.41	**3.33**	**MF8**	0-20%	100	50	TUL	2	ST	Silt rafts. Possible ST traces throughout with framboidally pyritized trails and shafted silt grains to boundries. TUL traces with homogenized fill.	conodonts?	PF	silt-to-sand sized dolomite nodules throughout matrix	common	abundant	relatively large framboids dissemeinated throughout matrix, and occasionally concentrated in lenticular bands.	0:7-10:90-93
	1858.54		**MF2**		0					Silica alteration (re-crystalized silt rafts and laminae). Conodont fossils are concentrated within specific beds. Pyritized ST burrows can be seen.	conodonts	unstaine d	heavily dolomiteized section	abundant	abundant		
	1860		**MF6**	70-100	150	50	ST	3	ST	Bedding plane thin section. Homogenous-appearing matrix (likely due to pervasive dolomitization). ST traces are preferentially pyritized.	recrystallized radiolarians or acritarchs? Pyritized cruciform fragments and honeycomb strucutres.	none	abundant silt-sized carbonate grains throughout matrix (make up about 15% of the matrix). Possible carbonate nodules or carbonate fossil fragments.	abundant	abundant	framboidal pyrite thoughout the matrix. Preferentially pyritized zones are common.	0:25:75
	1860.16	**3.88**	**MF6**	80-100	60	30	ST	2		Biogenically homogeneized section. ST traces with framboidally pyritized trails. Aligned quartz grains along trace boundries.	conodonts?	PF	silt sized dolomite grains throughout matrix	common	abundant	framboids throughout matrix. Preferntially pyritized horizions throughout.	0:15:85

	1865		**MF5**	30-70	20	20	ST	1	ST	Bedding plane thin section. Small carbonate nodules may be re-crystallized fossil fragments. Thin section is biogenically homogenized. Pyritized sinuous horizontal traces are abundant.	Tentaculitids, pyritized cruciform fragments and honeycomb-like fragments are common/abundant. Possible conodonts.	none	possible carbonate nodules or spherical fossil tests? Abundant carbonate (calcite/dolomite?) silt-sized grains throughout matrix (makes up about 5% - 10% of overall matrix).	common	abundant	abundant framboids disseminated throughout the matrix.	0:5:95
	1865.34	**4.36**	**MF5**	50-80	40	20	ST	2	ST	Biogenically homogenized. Not many identifyable traces identified. possible ST traces with pyritized trails. TUL with homogenized fill. Intactness of elongate organic detritus further indicates low degrees of reworking.	pyritized and calcified radiolarians or acritarchs	PF	large pyritized calcite frags. Silt-to-sand sized dolomite grains throughout matrix.	common	abundant	large framboids and framboid clusters throughout thin section. Some elongate OM appears pyritized.	0:5:95
	1870.27	**5.47**	**MF4**	0-10	20	20		1		Traces are uncommon. Possible TUL traces with homogenized fill.		PF	dolomite nodules forming throughout.	common	common	framboids thoughout the matrix.	0:10:90
	1871		**MF4**	15-Oct	0	20				Bedding plane thin section. Framboidally pyritized ST traces					common	framboids and euhedral pyrite throughout	0:10:90
	1871.59		**MF3**		0					no discernable traces		PF	abundant silt-sized calcite throughout matrix (making uo 5% of section).	common	common - abundant	framboids throughout matrix as well as clustered framboids. Some elongae organic detritus is pyritized.	0:5:95
Blue Fish	**1938.4**	**4.89**	**MF7**		0					variable thickness beds composed of tentaculitids (both intact and fragmentded shells present)	tentaculitids	AZR	calcite tentaculitid fragments as well as thick bands of calcite alteration associated with fossilifrous beds and calcite alteration within less-fossilierous interbedded fine grained sediments	abundant		euhedral pyrite present in calcified fossiliferous beds	0:<5:>95
	1951.79	**3.52**	**Cone-in-Cone**		0					cone-in-cone alteration. No sedimentary strucutres remaining.		AZR	calcite tentaculitid fragments and cone-in-cone structures.	abundant	sporadic	small custers of framboids thoughout calcite and clay-rich laminae	0:<2:>98
	1953.3		**Cone-in-Cone**		0					cone-in-cone alteration. No sedimentary strucutres remaining.		AZR					

ConocoPhillips Mirror Lake N-20

Formation	Depth (m)	MicroFacies	BI % Range	Trace Size Mode (µm)	Trace Size Max (µm)	Max Size Trace Type	Diversity Index	Sedimentological and Ichnological Characteristics	Fossil Fragments	Sand:Silt:Clay
Imperial	**1897.6**	**MF3**	20	400	1000	TUL	1	lack of lithologic contrast makes it difficult to identify burrows. Large lenticular silty features - OM poor in OM rich matrix, poss burrows. Partially pyrtized ST burrow margins.	radiolarians	0:2:98
Imperial	**1904.15**	**MF3**						bioclastic calcite fossil fragment lag (likely tentaculitids). Partially dolomitized matrix.	possible tentaculitids	0:2:98
Imperial	**1910.44**	**MF6**			50	SD	1	graded bedding/silt lags common throughout. Carbonate bed at top.	possible tentaculitids	0:10:90
Imperial	**1916.47**	**MF6**		50	200	SD	1	gradded bedding, silt lags, poss ripple forsets. Discontinuous silt lags attributed to biogenic reworking.		2:48:50
Imperial	**1929.92**	**MF3**								
Imperial	**1929.95**							possible volcanic ash bed. Large euhedral unidentified dark mineral. Red clay matrix.	radiolarians, conodonts, tentaculitids	0:2:98
Imperial	**1933.06**							possible volcanic ash bed. Large euhedral unidentified dark mineral. Red clay matrix.		
Imperial	**1944.5**	**MF4**	0-10	20	50		1		radiolarians, conodonts	0:5:95
Imperial	**1950.44**	**MF3**						Microcrystaline dolomite alteration of argillaceous matrix.	radiolarians, conodonts	0:2:98
Imperial	**1956.63**	**MF8**						Dolomitized matrix (microcrystaline) with relatively large lenticular carbonate nodules.		0:2:98
Imperial	**1963.32**	**MF1**						alternating radiolaties with dolomitized beds. No identified bioturbation or sedimentary structures.		
Imperial	**1966.16**	**MF3**						argillaceous beds intercalated with dolomitized beds. Radiolarians are common throughout.	radiolarians	0:2:98
Imperial	**1972.35**	**MF8**						alternating radiolarite beds and intraclst-bearing beds. Possible low angle ripple forsets in intraclast bearing beds.		
Imperial	**1973.5**	**MF1**						heavily dolomtized - no remaning sed features.	radiolarians	0:15:85
Canol	**1978.32**	**MF4**	0-10					possible silt rafts thoughout. Some surge-like normally graded beds (silt rich bases and clay rich tops).	radiolarians, conodonts, possible agglutinated forams or silt rafts	
Canol	**1980.38**	**MF1**	0-10					Discontinuous preferentially pyritized horizions. Some radiolarite beds show microstylolized contacts or thin crenulated microbial mat features.	radiolarians, agglutinated forams	0:5:95
Canol	**1982.12**	**MF1**	0-10							
Canol	**1995.02**	**MF1**	0-10					Alternating radiolarites (MF1) and radiolarite rich beds (MF3). Contacts appear microstylolized or bound by thin crenulated microbial mats.		
Canol	**1998.78**	**MF1**								
Canol	**2006.19**	**MF6**						highi proportion of detrtial silt.		
Canol	**2006.78**	**MF5**	0-20		20	SD	1	Normally graded beds with intraclast rich bases and clay rich tops. Intraclast rich beds are unbioturbated while argillaceous beds show some bioturbation (20%).	radiolarians	0:5:95
	2007.7									
	2011.14								radiolarians	
	2011.14	**MF8**	0-10							
	2026.17	**MF3**	0-10					Variable thickness dolomite beds (MF2) intercalleted with argillaceous MF3 beds.		

Hare Indian	**2027.67**	**MF3**	0-10			Microcrystalline dolomite beds towards the top of the thin section (MF2). ST traces are visible.		
	2041.97	**MF1**				radiolarite deposits. Some elevations have been partially dolomitized.		
	2042.05	**MF1**						
	2045.44	**MF7**					tentaculitids	
	2060.64	**MF8**						
	2064.73	**MF8**						
	2068.7							
	2070.25	**MF2**				heavily dolomitized thin section		
	2076.9	**MF8**						
	2080.05	**MF8**					conodonts	0:20:80
	2080.93	**MF7**	0-20	100	large SD	varibale thickness winnowed tentacultid shell lags.	conodonts, tentaculitids	0:20:80
	2082.92	**MF8**						
	2087.85	**Cone-in-Cone**				Cone-in-cone beds		
	2088.68	**MF7**					tentaculitids	
	2089.63	**Cone-in-Cone**				cone-in-cone beds		
	2090.78	**MF2**						
	2092.83	**MF7**					tentaculitids	
	2092.95	**MF7**					tentaculitids	
Hume	**2094.55**	**Reef**						
	2100.21	**Reef**						
	2101.09	**Reef**						

ConocoPhillips Loon Creek O-06

Formation	Depth (m)	MicroFacies	BI % Range	Trace Size Mode (µm)	Trace Size Max (µm)	Max Size Trace Type	Diversity #	Sedimentary and Ichnological Characteristics	Fossil Fragments	Sand:Silt:Clay
	1659.88	**MF3**	10	20	50	ST	1	No identified sedimentary features. ST traces are the only visible ones. Possible tubular burrow x-sections		0:2:98
Imperial	**1666.95**	**MF3**						No sedimentary features identified - thin sectio is very dark and many defects. Abundant elongate OM and diagenetic carbonate. Thin section has too many defects to accuratley determine traces.		0:2:98
	1687	**MF2**		20	35	ST	1	dolomtized lenticular features - IC, fecal pellets?	Radiolarians, conodonts	
	1687.49	**MF1**						Radiolarite beds		
	1694.49	**MF3**								
	1694.51	**MF1**						radiolarite beds		
	1695.24	**MF3**								
	1695.27	**MF1**						radiolarite beds		
	1698.74	**MF3**								
	1698.76	**MF1**						radiolarite beds		
	1707.91	**MF4**								
	1707.93	**MF1**						radiolarite beds		
	1720.08	**MF6**	30	25	50	ST	1	common carbonate silt lags. Carbonate silt is angular. Sand sized grains are carbonate, while silt is both carbonate and quartz.		10:50:40
	1720.37	**MF7**						abundant large tentaculitids. Winnowed fossil lags with inclined fragments = not suspension settling - remobilization/reworking instead		
	1728.36	**MF4**								
Canol	**1731.22**	**MF3**						pyritized partially dissolved rads		
	1732.26	**MF1**	0-10	20	50	ST	1			
	1743.43	**MF4**								
	1744.27	**MF4**								
	1749.29	**MF2**								

	1755.5	**MF4**	argillaceous thin section. Some intercalated carbonate beds with a graded appearance - possible detrtial carbonate?	
	1757.44	**MF6**	Detrtial carboante silt throughout - entire mudstone beds of carbonate silt. Possible indicator of close proximity to reef. Carbonate agglutinated forams and calcite fragments (fossil) - tentacultitids or sponge spicules?	tentaculitids, acritarchs?, agglutinated forams
	1758	**MF7**		tentaculitids
	1767.17	**MF4**		
	1761.1	**MF1**	radiolarite beds. Some beds have been replaced by carbonate.	
	1782.64	**MF4**	Preferentially pyritized detrtial carbonate silt bed.	
Hare Indian	**1787.1**	**MF7**	fragmented bioclastic bed with apparent eroded and transported diagenetic carbonate clasts.	
Hare Indian	**1787.8**	**MF7**		tentaculitids
Hare Indian	**1791.71**	**MF8**	intraclast rich thin section. Bedding contacts are not obvious.	
Hare Indian	**1796.27**	**MF7**		tentaculitids
Hare Indian	**1800.06**	**MF2**	heavily dolomitized thin section. No sedimentary strucutres or traces can be identified.	
Hare Indian	**1801.34**	**MF7**		tentaculitids
Hare Indian	**1803.28**	**MF7**		tentaculitids
Hare Indian	**1803.54**	**Cone-in-Cone**	Cone-in-cone alteration. No other identifyable structures.	
Hare Indian	**1806.03**	**MF7**		tentaculitids
Hare Indian	**1806.28**	**MF7**		tentaculitids
Hare Indian	**1806.63**	**MF7**		tentaculitids
Hume	**1807.78**	**Reef**		
Hume	**1809.3**	**Reef**		
Hume	**1810.38**	**reef**		
Hume	**1813.05**	**reef**		
Hume	**1827.7**	**reef**		
Hume	**1829.74**	**reef**		
Hume	**1836.77**	**reef**		
Hume	**1839.46**	**reef**		

Appendix C

Petrographic Atlas - Sedimentological and Ichnological Features Present in the Horn River Group

Bioturbation

Micro-burrows

Claystones and mudstones that appear unbioturbated at the macroscopic level can (in the case of the Horn River Group) show evidence of microscopic bioturbation (diameter burrows <1mm).

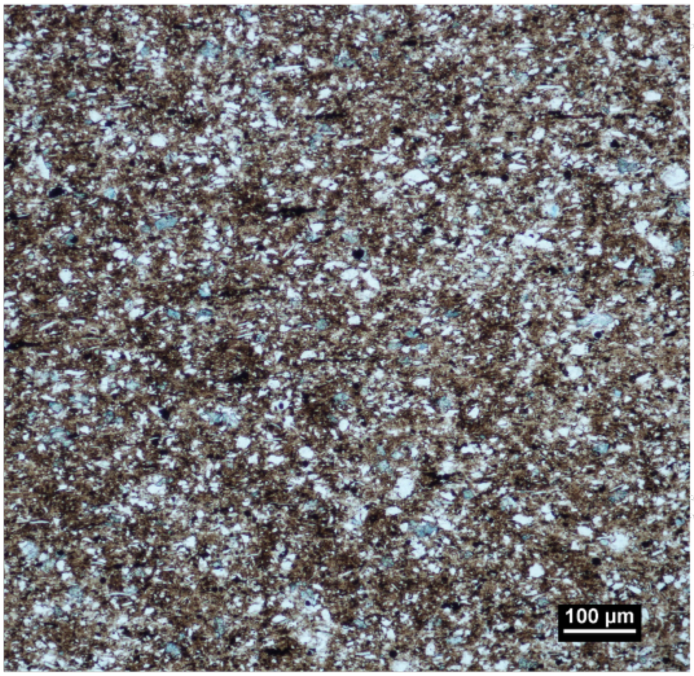

H-64 1214.64 m, Photomicrograph of an intensely micro-burrowed mudstone (BI% = >70). Traces are dominated by sinuous tunnels..

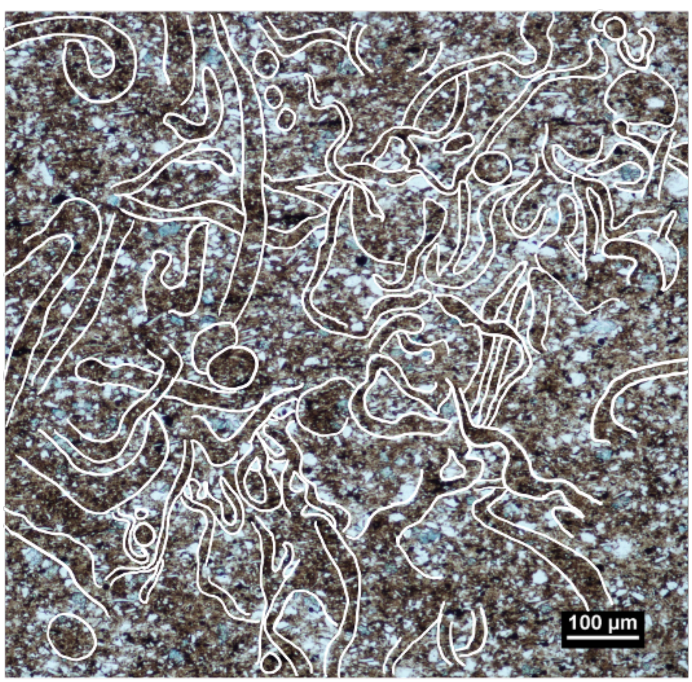

Outlined burrows from upper photo.

Ichnofossil Types

TRACE TYPE	CHARACTERISTICS
Inclined-to-Vertical Unlined Meniscate-Backfilled Trace	• Inclined to vertical traces with straight walls and faint organized internal backfill • No apparent trace lining • In sediments with higher proportion of sand-sized grains, the grains are shafted towards the outer edges of the traces • Often can be seen cross cutting horizontal laminae • Modal size: 20µm, maximum size: 60µm

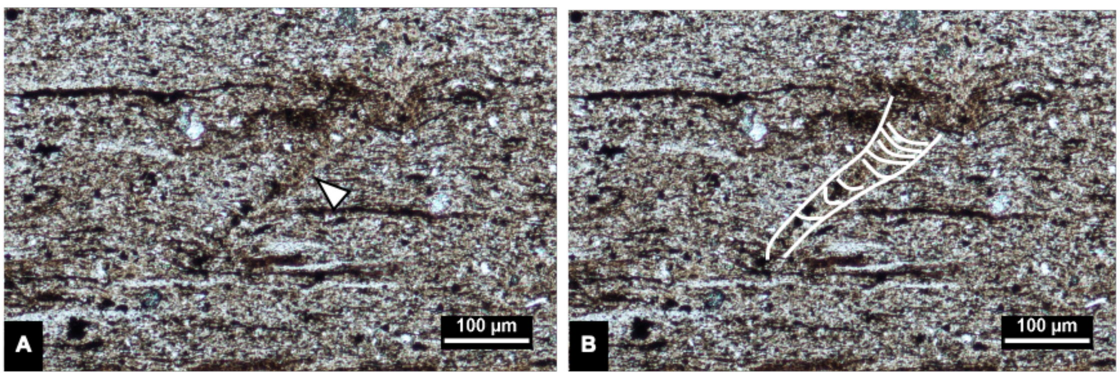

(A) inclined-to-vertical unlined meniscate backfilled trace (white arrow) (N-09 1692.58 m). **(B)** Tracing of the burrow in (A).

TRACE TYPE	CHARACTERISTICS
fugichnia	• Occur in thin lenticular fine-grained lighter-coloured laminae • Horizontal laminations disrupted and pulled downwards • No organized fill or burrow linings • Modal size: 50µm, Maximum size: 100µm

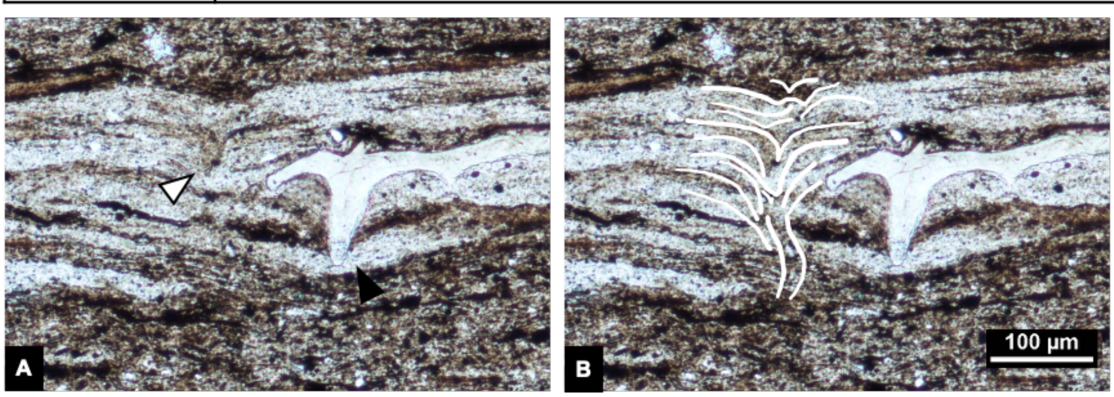

(A) Fugichnia (white arrow) next to a conodont fragment (right) (N-09 1692.58 m). **(B)** Tracing of fugichnia in (A).

TRACE TYPE	CHARACTERISTICS
Tubular Lined Tunnels	• Lined with thin dark layer of clay or compressed organic matter originating from the host sediment • Linings can be preferentially pyritized • Multi-linings are common • Burrows are actively filled • Tunnel fill is either uniform silt-sized grains OR homogenized clay, possibly reflecting cuts through different portions of active meniscate backfill • Modal size: 75µm, maximum size: 100µm

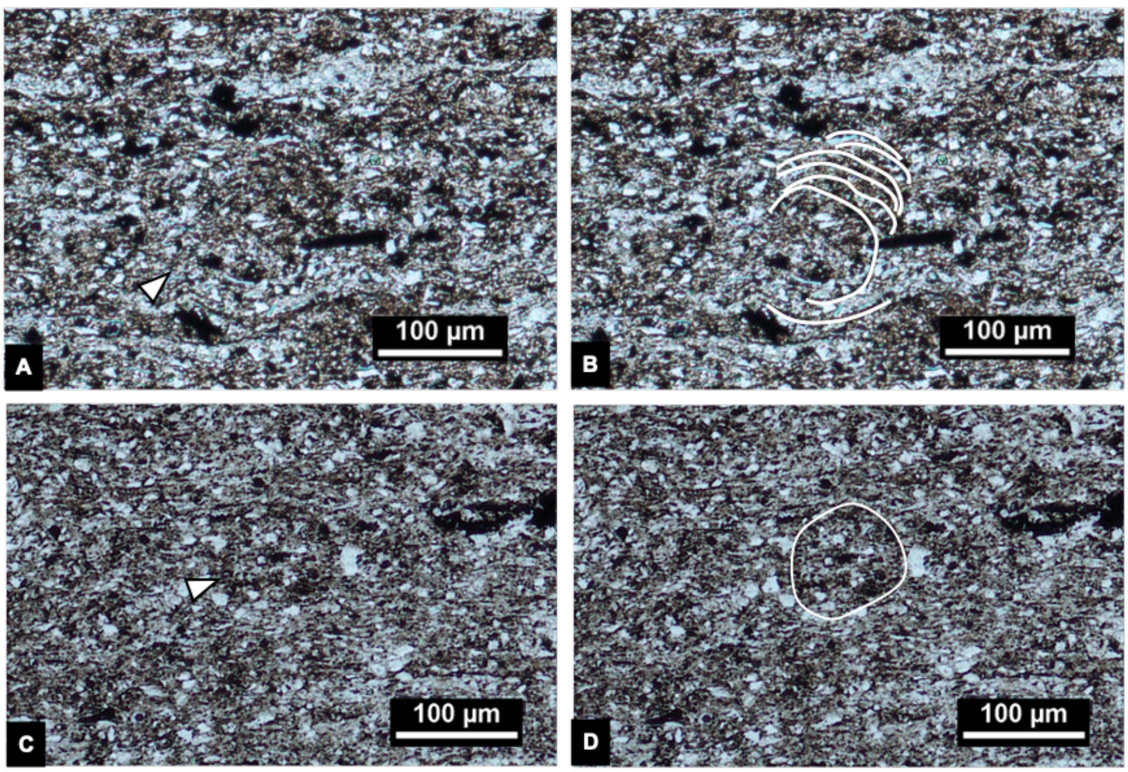

(A) Cross section of a concentrically lined horizontal tunnel (white arrow) (N-09 1703.54 m). **(B)** Tracing of the concentric linings in (A). **(C)** Cross section of a tubular lined burrow (white arrow) (N-09 1703.54 m). **(D)** Tracing of burrow in (C).

TRACE TYPE	CHARACTERISTICS
Tubular Unlined Tunnels	• Fill differs from surrounding matrix in composition and colour, more homogenized and finer-grained • Can be either lighter or darker coloured than surrounding matrix • Larger grains shafted to outer edges of traces • Modal size: 50µm, maximum size: 120µm

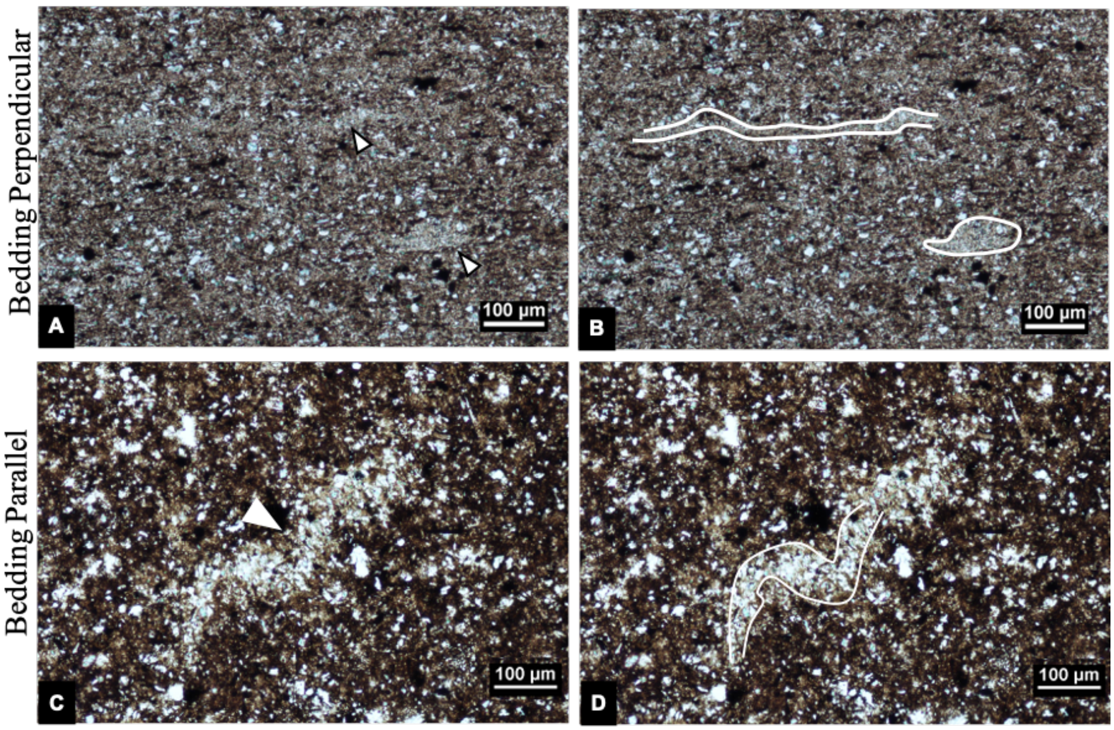

(A) Longitudinal slice (top arrow) and cross section (bottom arrow) through two unlined tunnel burrows (N-09 1670.87 m). **(B)** Tracings of burrow in (A). **(C)** Longitudinal cut through a tubular unlined tunnel (Bedding plane view) (H-64 1232.84 m). **(D)** Tracing of burrow in (C).

TRACE TYPE	CHARACTERISTICS
Sinuous Tunnels	• Uniform-diameter unbranching traces • Most easily spotted in areas with higher silt-sized grains, where the grains become vertically aligned along trace margins • Often appear darker than surrounding sediment, and commonly contain fine-grained framboidal pyrite • Modal size: 20µm, maximum size: 50µm

(Next Page) Photomicrographs of sinuous trails within HRG mudstones. **(A)** Well-defined sinuous trail (white arrow) with clear clay fill. **(B)** Outline of the sinuous trace in (A). **(C)** Several sinuous trails within a silt-bearing claystone. **(D)** Outline of traces in (C). **(E)** sinuous trails along a bedding plane in a silt-bearing claystone. Arrow points to an obvious relatively straight trail. **(F)** outline of the traces in (E). **(G)** Sinuous trail (arrow) cross cutting an intraclast (lighter coloured diffuse structure) along a bedding plane. **(H)** outline of traces in (G).

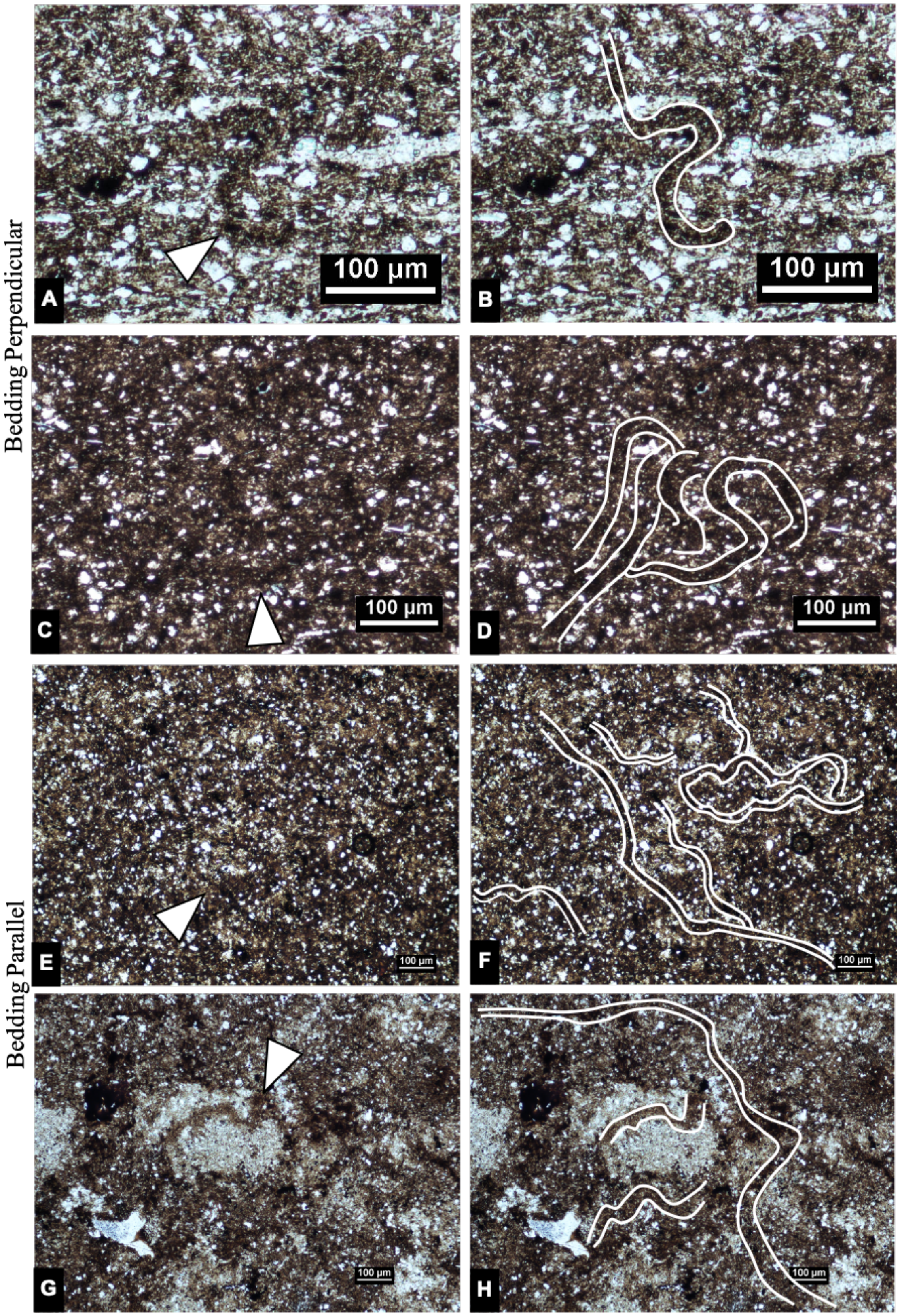
Bedding Perpendicular
Bedding Parallel
A
100 µm
B
100 µm
C
100 µm
D
100 µm
E
100 µm
F
100 µm
G
100 µm
H
100 µm

Components

There are three components that make up fine-grained sedimentary rocks: detrital, biogenic and diagenetic. A fourth component type are the "composite grains", which consist of two or more of the three dominant components.

Detrital

Clay Lithograins

Amalgamation of clay platelets through either flocculation in suspension or re-suspension of previously deposited semi-consolidated clay.

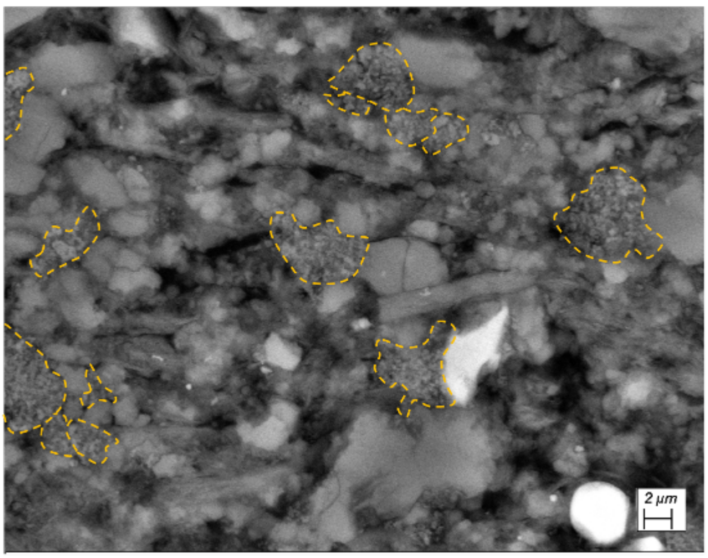

I-78 1827.40 m, SEM BSE photograph of a mudstone with detrital clay lithograins (dashed yellow outlines), detrital silt-sized quartz (intermediate interference colours (n), smooth appearance), organic matter (black), and pyrite (bright n).

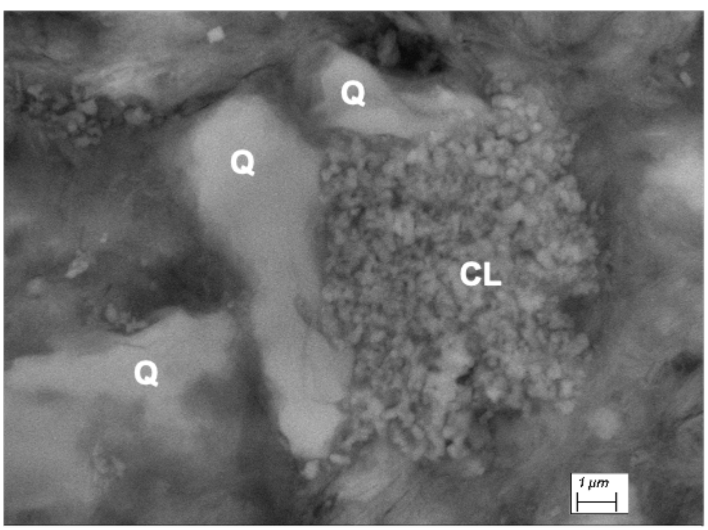

I-78 1827.40 m, Close-up SEM BSE photograph of a clay lithograins (CL) surrounded by detrital quartz silt grains (Q).

Biogenic

Biogenic components in the HRG are dominantly represented as body fossils of micro-organisms.

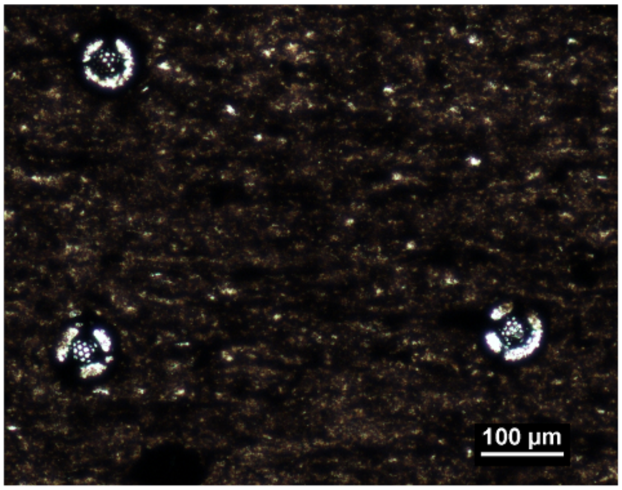

Radiolarians

Siliceous zooplankton. Indicate the presence of an overlying oxygenated water column.

N-09 1966.16 m, Canol Formation, elevation view thin section.

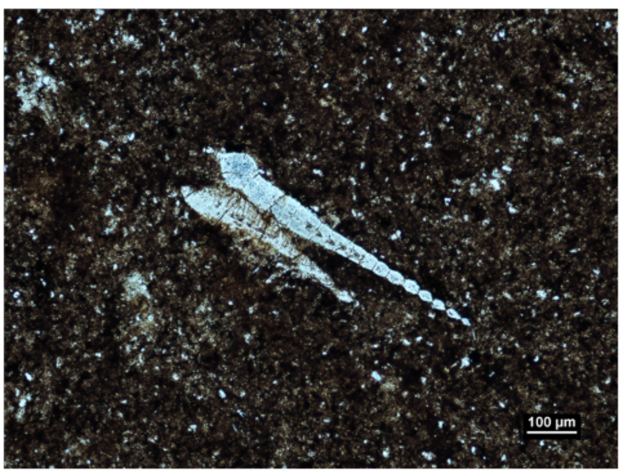

Tentaculitids

Conical pelagic calcite-shelled organisms, especially common in Devonian mudstones (Filipiak and Jarzynka, 2009). Tentaculitids are present throughout the entire HRG elevation, but are especially concentrated in the Bluefish Member. Indicate the presence of an overlying oxygenated water column.

I-78 1838.00m, Bell Creek Member, bedding plane thin section.

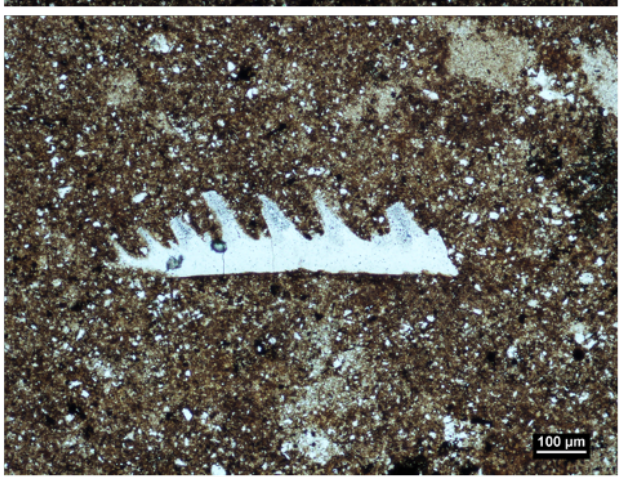

Conodonts

Phosphatic microfossils common in the Canol Fm. Indicate an overlying oxygenated water column.

I-78 1858.00m, Canol Formation, bedding plane thin section.

Microbial Mats

Variable thickness carbonaceous beds and fragments with varying amounts of detrital grains (incorporated clay and silt). The presence of microbial mats indicates a quiet energy depositional setting (no erosive bottom currents) and low amounts of clastic dilution.

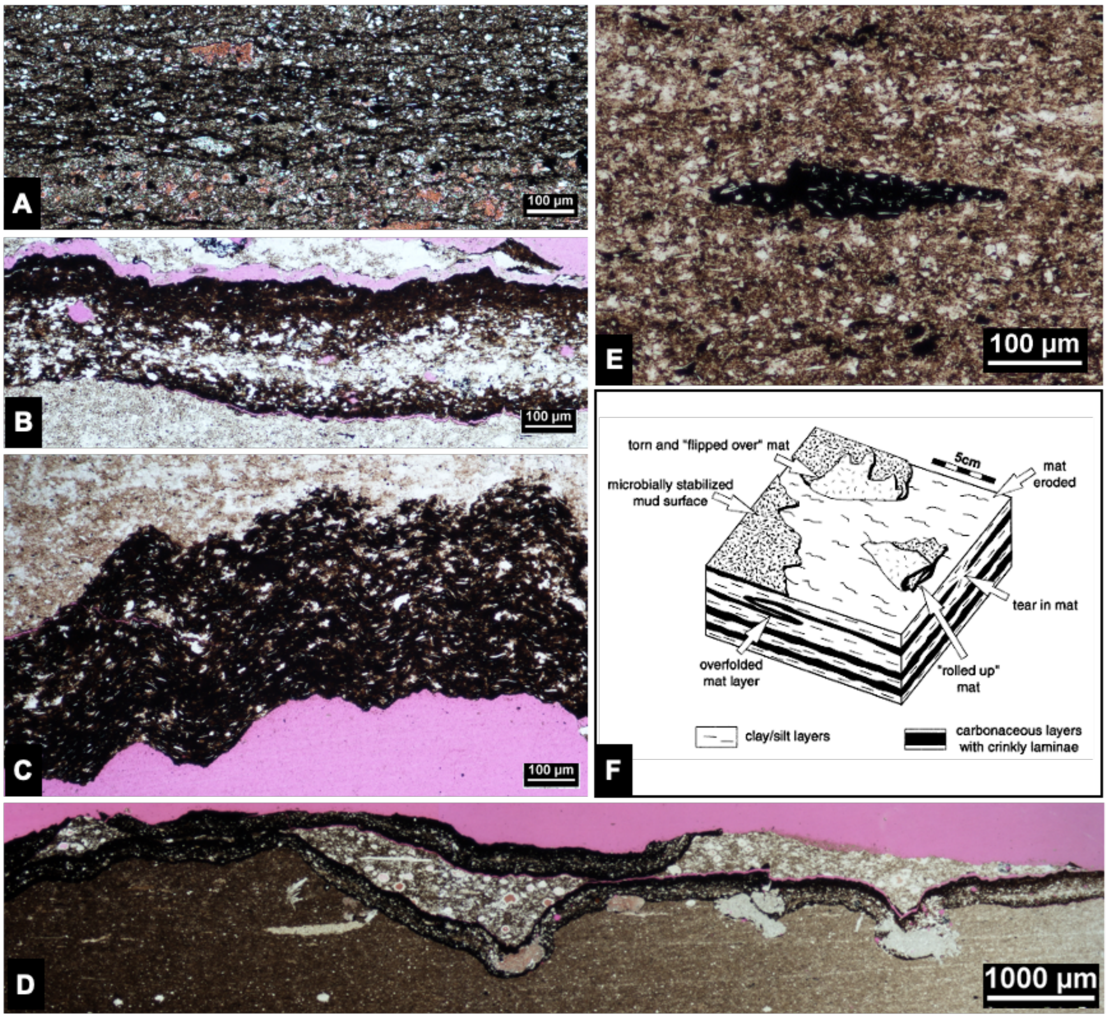

A) Wispy accumulation of elongate organic matter. Represents possible sediment rich microbial mat (N-09 1796.05 m). **B)** Carbonaceous laminae with detrital quartz silt inclusions, represents thin microbial mat (N-09. 1725.83 m). **C)** Crenulated carbonaceous microbial mat (N-09 1768.93 m). **D)** Microbial mat encased radiolarite deposit. Possibly representing a "rolled up" and transported mat fragment encapsulating an overlying radiolarite deposit, that was re-suspended and transported during erosive storm currents (N-09 1725.83 m). **E)** Microbial mat rip up fragment. Likely generated during erosive bottom currents, and encased in a thin clay-dominated storm bed (N-09 1710.08 m). **F)** Example diagram of microbial mat features. Shows a nice illustration of the "rolled up" mat feature in (D) (Schieber, 1999).

Diagenetic

Discontinuous Horizontal Pyritization

Thin discontinuous horizontal pyritization. Generally formed from pyrite framboids, rarely made up of euhedral pyrite.

These features may represent diagenetic alteration of remnant bedding surfaces under poorly oxygenated waters, or pyritization of thin microbial mats.

I-78 1860.16 m, Thin section scan showing abundant discontinuous pyritization of possible remnant bedding planes.

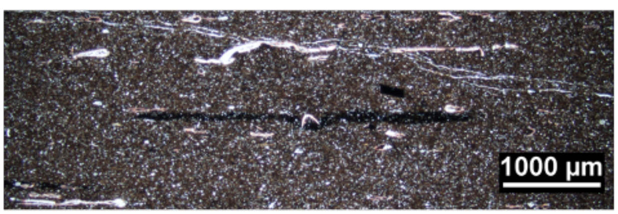

I-78 1945.69 m, Discontinuous pyrite stringer in a fossiliferous matrix. Deformation by fossil fragment suggests very early diagenetic pyritization.

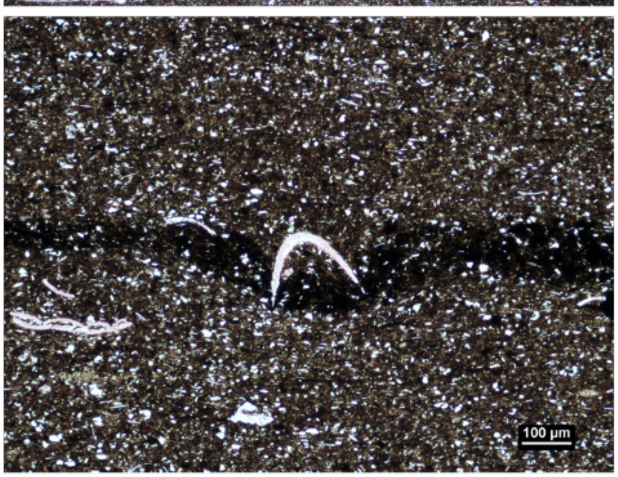

Zoomed in image of deformation in above photo.

Dolomitization

Diagenetic dolomitization can be rhombic, microcrystalline, or replacement of microbody fossils (e.g. replacement of siliceous radiolarians or intragranular cementation of tentaculitid cavities). Ferroan dolomite, formed during early diagenesis may be a good indicator of poorly oxygenated bottom waters (Raiswell, 1971; Schieber, 1999; Hickey and Henk, 2007; Macquacker et al., 2007; Aplin and Macquaker, 2011)

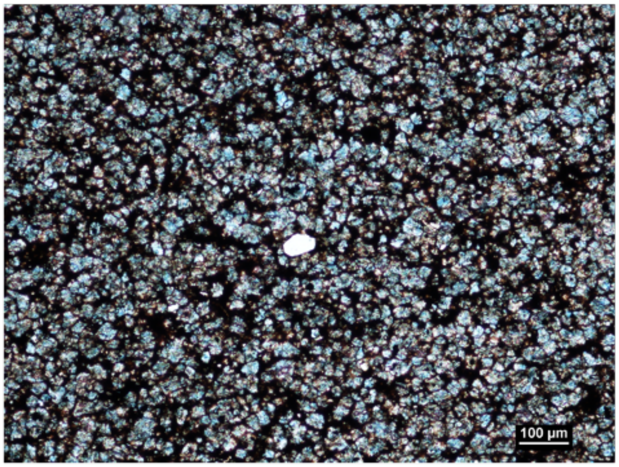

N-09 1813.76 m, Abundant rhombic diagenetic dolomite. Ferroan composition indicated by blue staining.

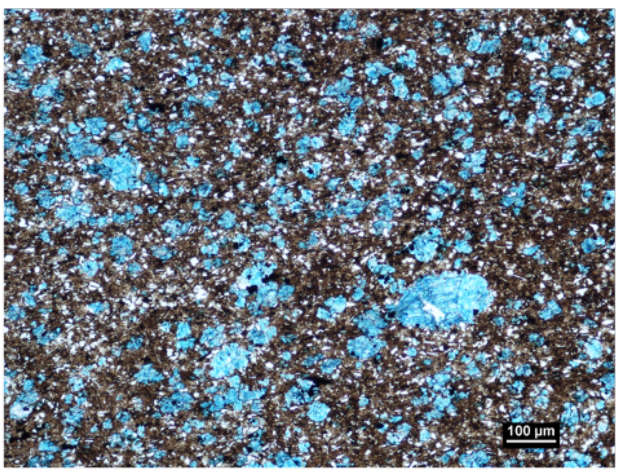

N-09 1749.21 m, Abundant microcrystalline diagenetic dolomite. Ferroan composition indicated by blue staining.

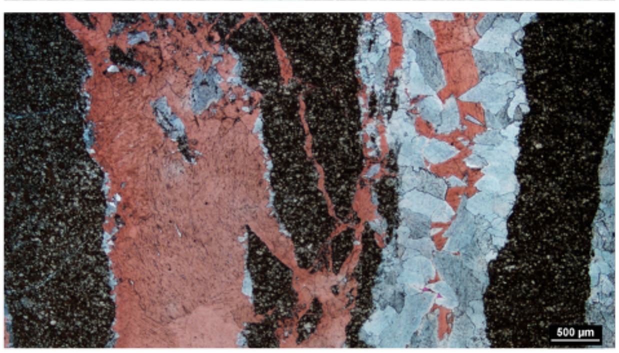

H-64 1250.52 m, Calcite (pink) and dolomite (blue) fracture infill of a brecciated rhombically dolomitized (silt-sized blue stained crystals) mudstone.

Composite Grains

Composite grains represent the part of the matrix made up of aggregates of detrital, biogenic and/or diagenetic components. Several composite grain types exist within the HRG.

Phytodetritus

Aggregates of organic matter, detrital sediment, and micro-organism tests. Such phytodetritus is generated in the overlying water column and delivered to the sediment surface through suspension settling or re-transportation in low density flows (e.g. surge-like flows).

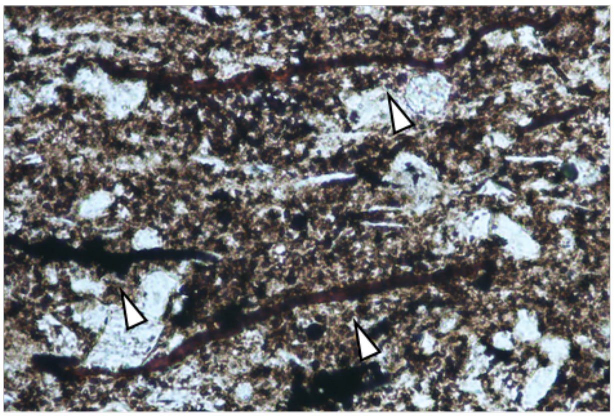

N-09 1722.36 m, Elongate phytodetritus (arrows) in clay and silt matrix.

Rafted Silt Aggregates

Formed by entrapment of detrital silt within the EPS membranes of benthic microbial mats or cyanobacteria, which subsequently detach from the seafloor creating a buoyant silt raft (Olsen et al., 1978; Schieber, 1999; Schieber, 2007).

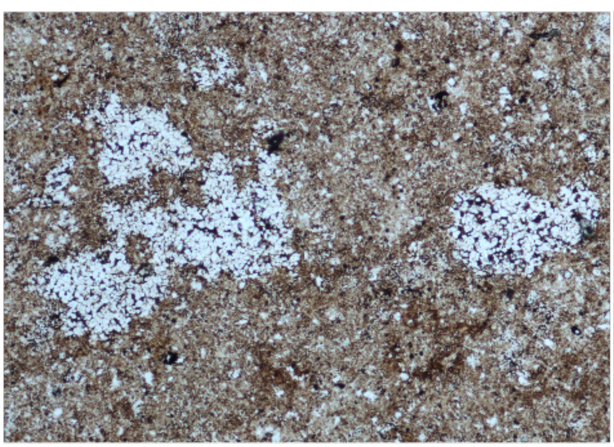

I-78 1835.00 m, Bedding plane view of several rafted silt aggregates.

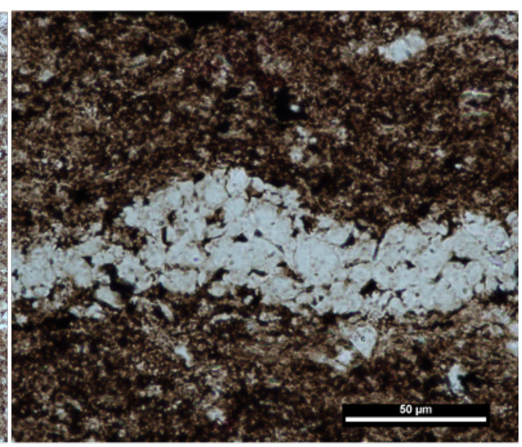

N-09 1734.54 m, Cross section through a silt raft. Shows amalgamation of distinct individual quartz grains in an otherwise clay-rich matrix.

Intrabasinal Rip-up Clasts

Intrabasinal rip-up clasts are horizontal elongate lenticular, generally lighter-in-colour, coloured lenticular features composed of dominantly clay; in some instances they are silt-bearing. Clasts are generally organic-poor and lack pyrite. These clasts form through up-dip erosion and bed-load transport of previously deposited semi-consolidated water-rich clay and mud clasts, and adopt their lenticular shape as a result of compaction (Schieber et al., 2010).

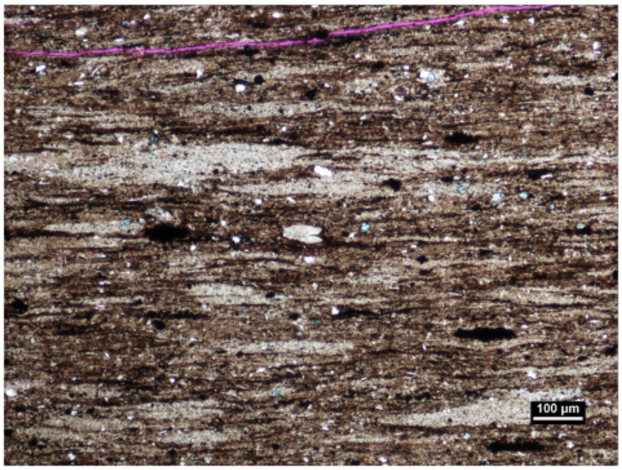

N-09 1812.72 m, Abundant intraclasts throughout matrix, showing clear horizontal orientation. Dark horizontal streaks are organic matter.

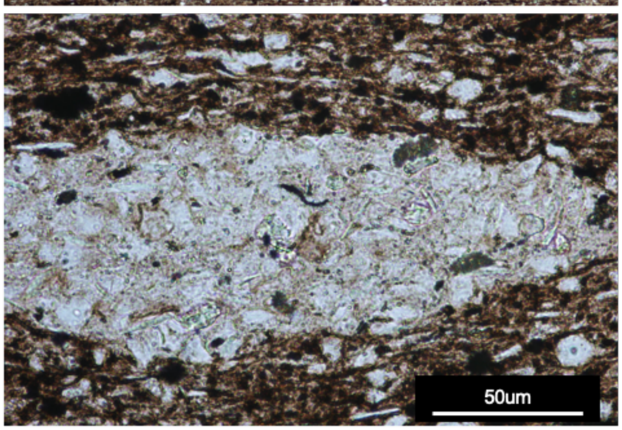

N-09 1703.64 m, Close up image of a silt-bearing intraclasts showing OM and pyrite poor composition.

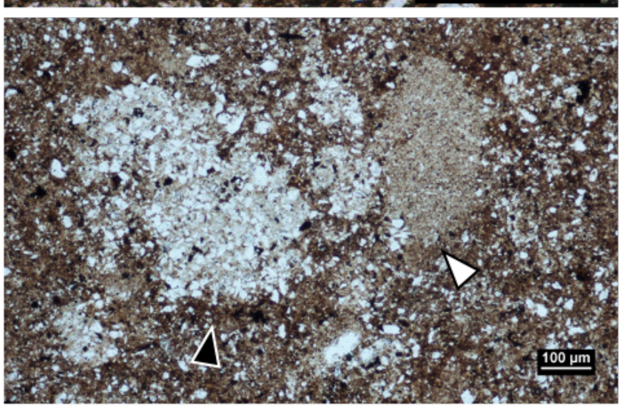

I-78 1822.00 m, Bedding plane view of a silt-bearing intraclast (black arrow) and clay intraclast (white arrow).

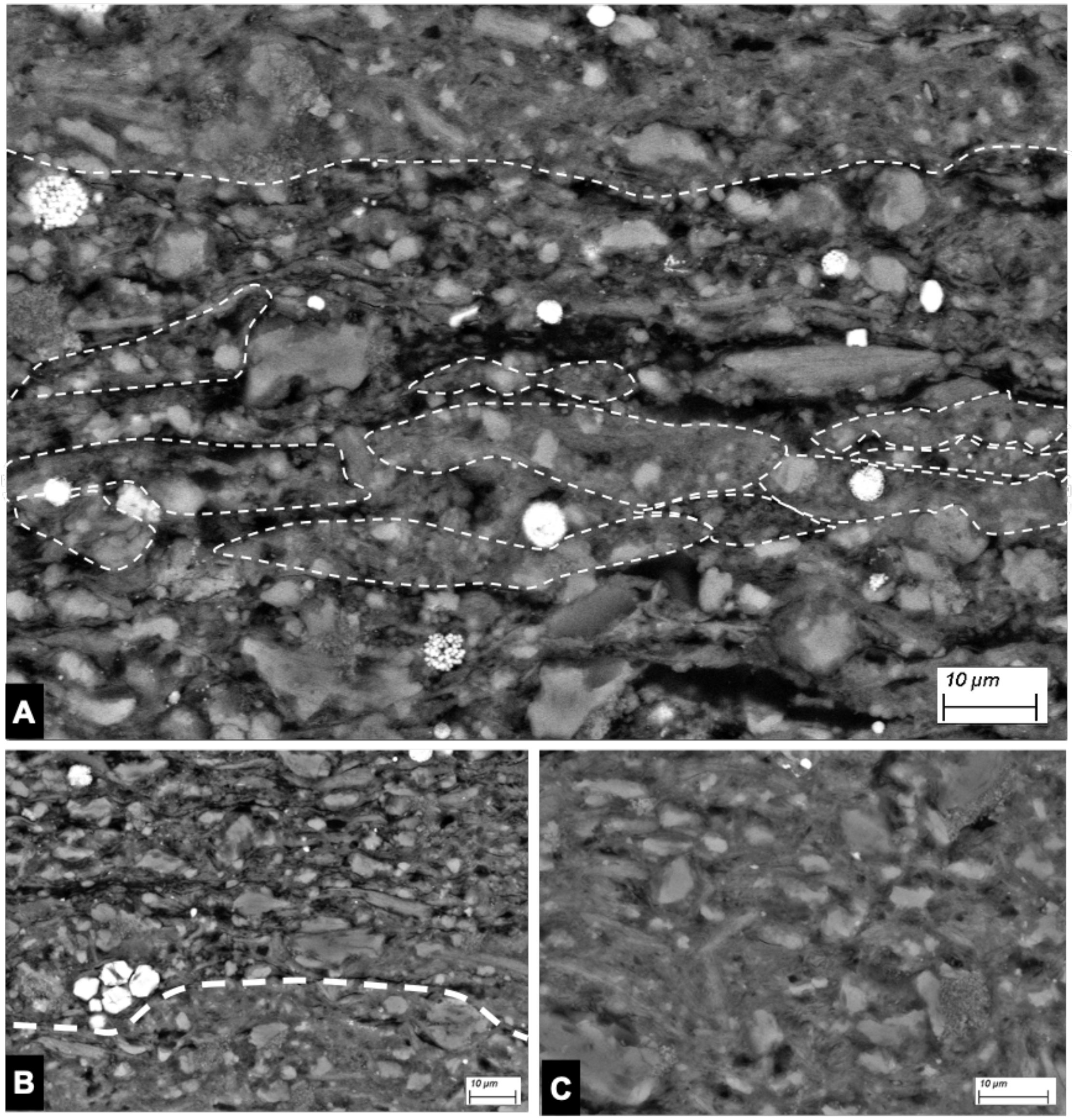

Scanning Electron Microprobe Back Scatter Electron (SEM BSE) photographs of intrabasinal rip up clasts. **A)** Image showing a thing layer of intraclasts near center (intraclasts are outline in dashed lines). Intraclasts show homogenized internal structure when compared to the clear horizontal structure of the surrounding matrix and OM. Matrix is made up of clay (intermediate interference colours - n), quartz silt (smooth intermediate n), organic matter (black) and pyrite framboids (bright n). **B)** Image showing contact (dashed line) between an intraclast (below) and the surrounding matrix (above). **C)** image showing internal homogenization of an intraclast. No apparent internal structure or organization.

Sedimentary Structures

There are a variety of sedimentary structures present in the HRG at the petrographic level that have gone unnoticed at the macroscopic level. These structures provide valuable evidence for the conditions during deposition of these mudstones.

Depositional Structures

Unidirectional Current Ripples

Silt laminae show low angle inclines and downlap the lower beds. The very low angle relief of the forsets can be attributed to post depositional dewatering and compaction of the water-rich clay matrix portion (Schieber et al., 2007). These structures are good evidence for bottom water currents and bedload traction transport of detrital components.

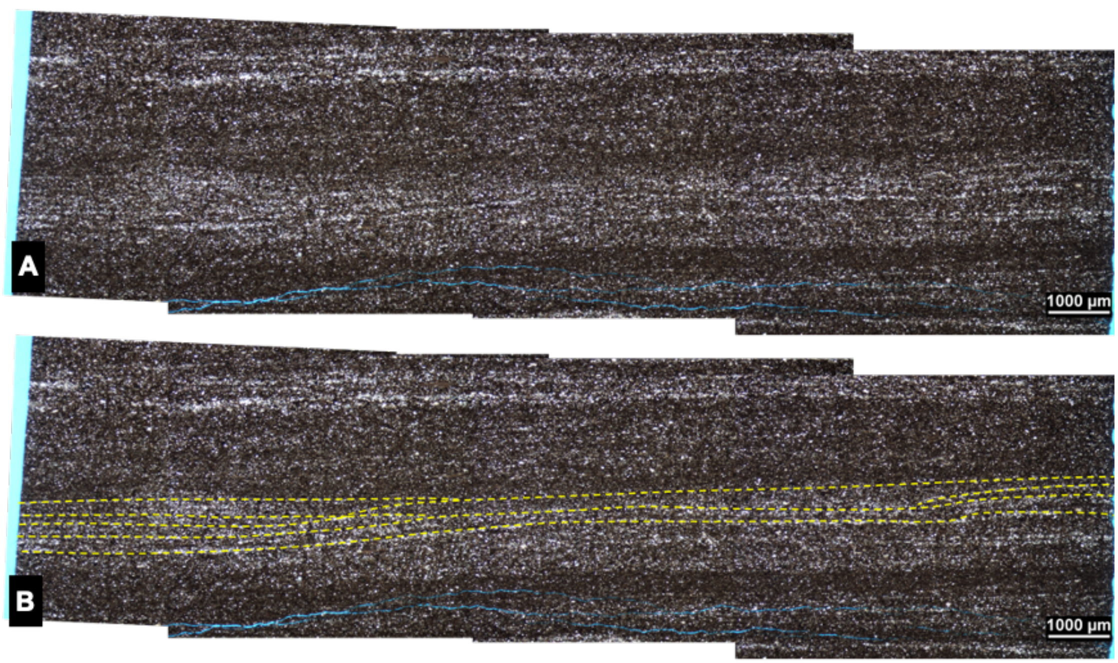

A) Photomicrograph showing a cross section of a unidirectional current ripple (flow is from right to left). **B)** Same photo as A), with forsets outlined in dashed yellow.

Discontinuous Silt Laminae

Thin silt laminae may form from two different processes: 1) increased bottom current energy resulting in deposits of coarser-grained silt, or 2) high energy erosive bottom currents resulting in winnowing and deposition of thin silt accumulations.

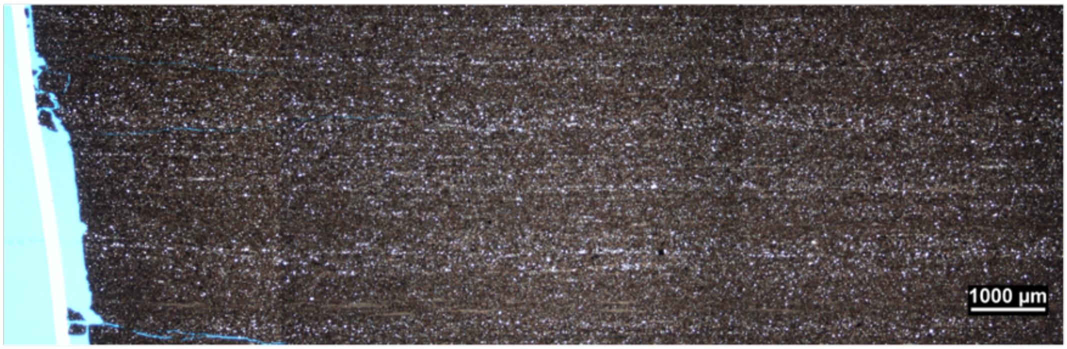

Photomicrograph showing stacked winnowed shell lags (fossil shell material is made of calcite tentaculitid shells). Clay beds (dark beds) represent a return to fair weather conditions.

Wave Enhanced Sediment Gravity Flows (WESGF)

Gravity-driven sediment flows where energy is provided by agitation from orbital motion of surface waves (Maquaker et al., 2010). WESGF's have a three-part layering: A) erosion and deposition, B) laminar sediment gravity flow, C) waning flow portion. Lack of soft sediment deformation beneath the bases of the A portion (silt beds) indicates that the bottom current removed the upper water-rich portion of the sediment and scoured into de-watered pre-compacted material. (also evident by the truncation of thin silt beds below)

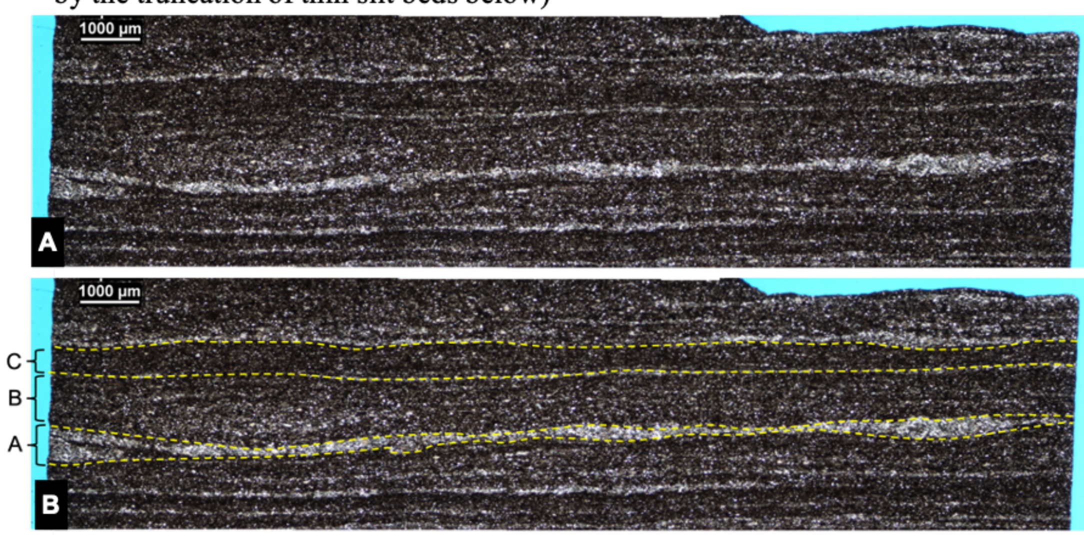

A) Photomicrograph of a wave enhanced sediment gravity flow (WESGF). **B)** Same photo as A), depositional surfaces have been outlined to show three-part layering (A, B, C described above).

Plug-like Flows (Low Density Turbidites)

Plug-like flows represent deposition from fine-grained cohesive sediment gravity flows travelling along the distal sediment-water interface (Baas et al., 2009). The cohesive nature of the flows results in variable thickness (but thin, <1 mm) massive-appearing accumulations of clay and silt matrix, as grain-grain interaction is too high to allow preferential settling of the coarser grained fraction (e.g. silt).

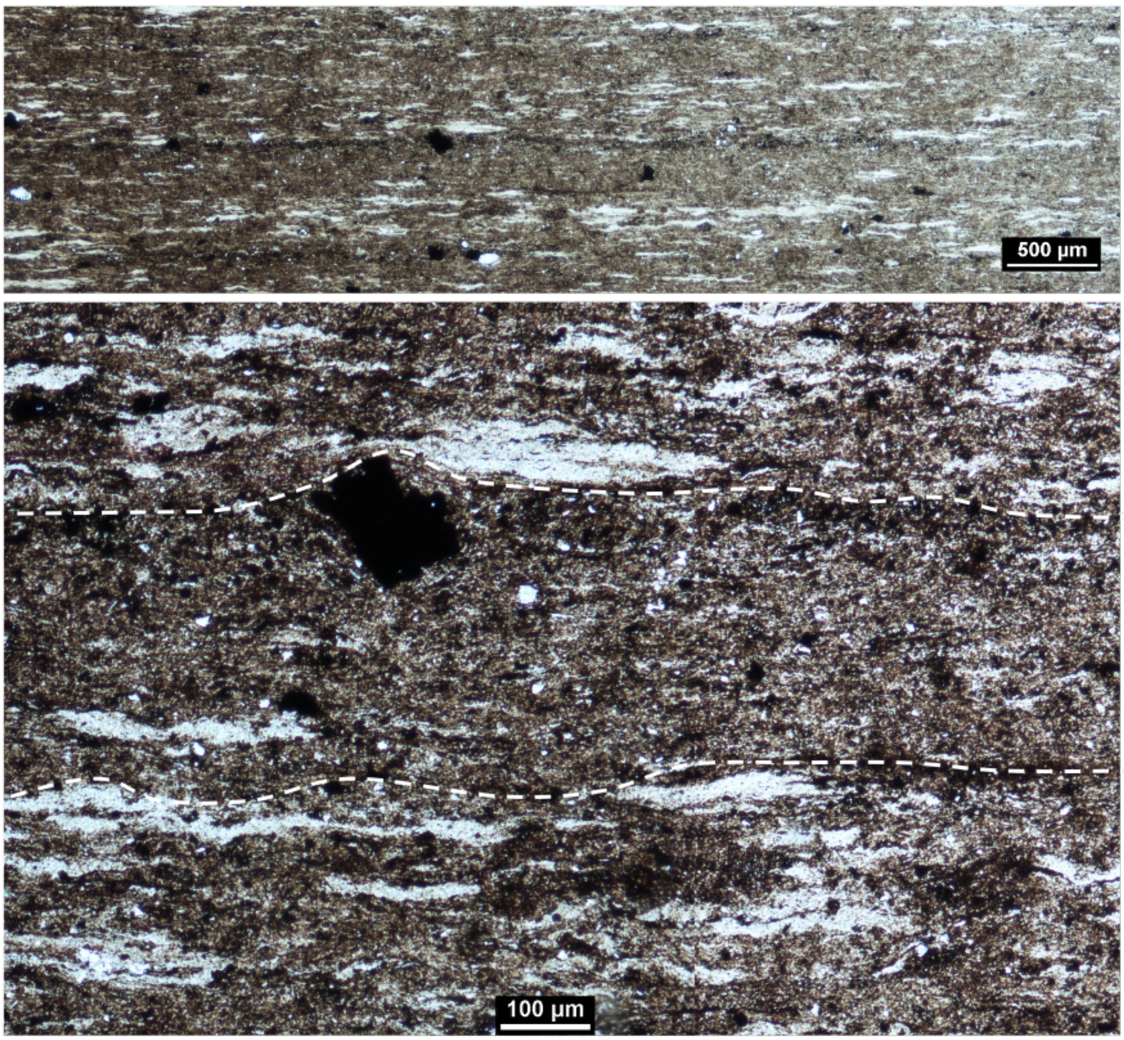

N-09 1706.58 m, **Upper:** Photomicrograph of massive-appearing plug-like flow deposit bound by intraclast rich beds. **Lower:** zoomed in photo of above. Relatively large black feature is a pyrite fragment.

Normal Grading

Normally graded beds are present through the HRG. They can be composed of declining abundances of intraclasts, elongate organic matter (phytodetritus), silt, or bioclastic debris. Such beds can be deposited from the low density turbidite surge and surge-like flows. These flows are non-cohesive and the lack of grain-grain contact allows for the preferentially settling of the coarser grained flow fraction first (Mulder and Alexander, 2001).

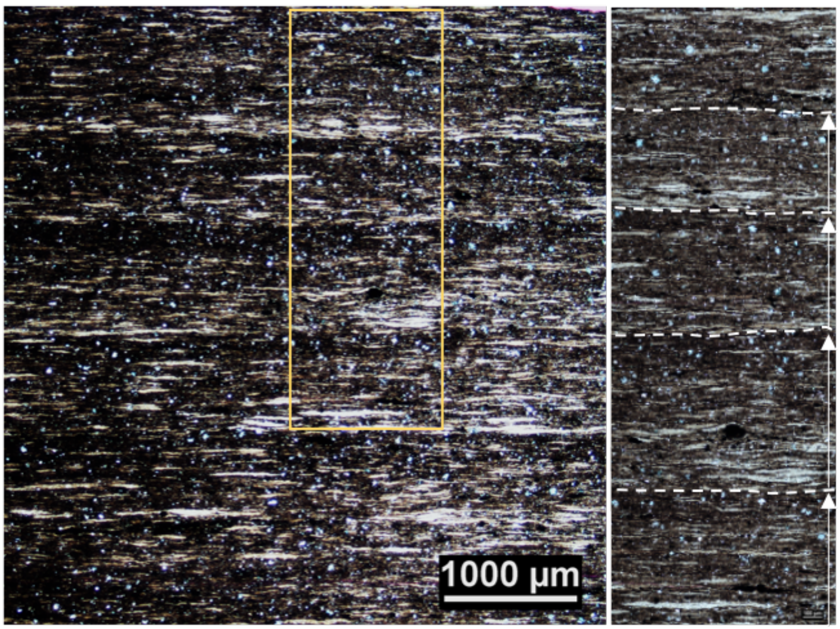

N-09 1807.35 m, Photomicrograph showing stacked normally graded beds, fining upwards from intraclastic rich bases to clay rich tops.

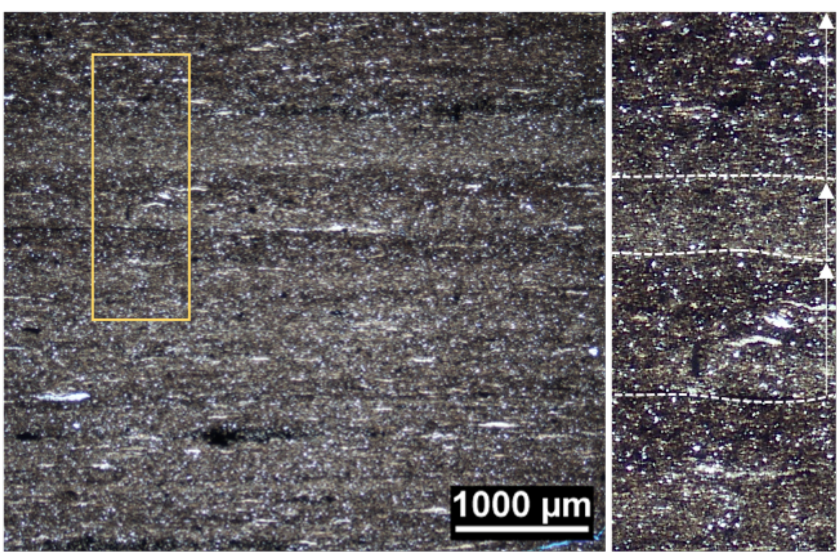

N-20 1710.08 m, Photomicrograph showing stacked normally graded beds, fining upwards from phytodetritus and silt rich bases to clay rich tops.

Debrites

Variable thickness accumulations of fossil shell debris and clay matrix. The random dispersal and orientation of fossil fragments within the clay matrix indicates rapid deposition of a cohesive sediment. Such deposits are common of debrites.

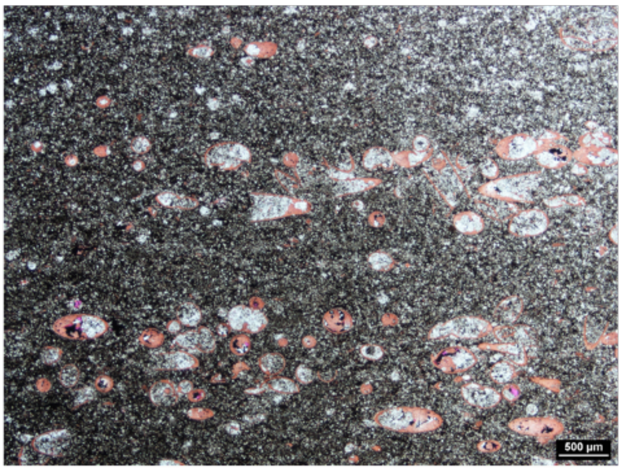

N-09 1777.48 m, variably dispersed and oriented calcite-filled tentaculitid fragments.

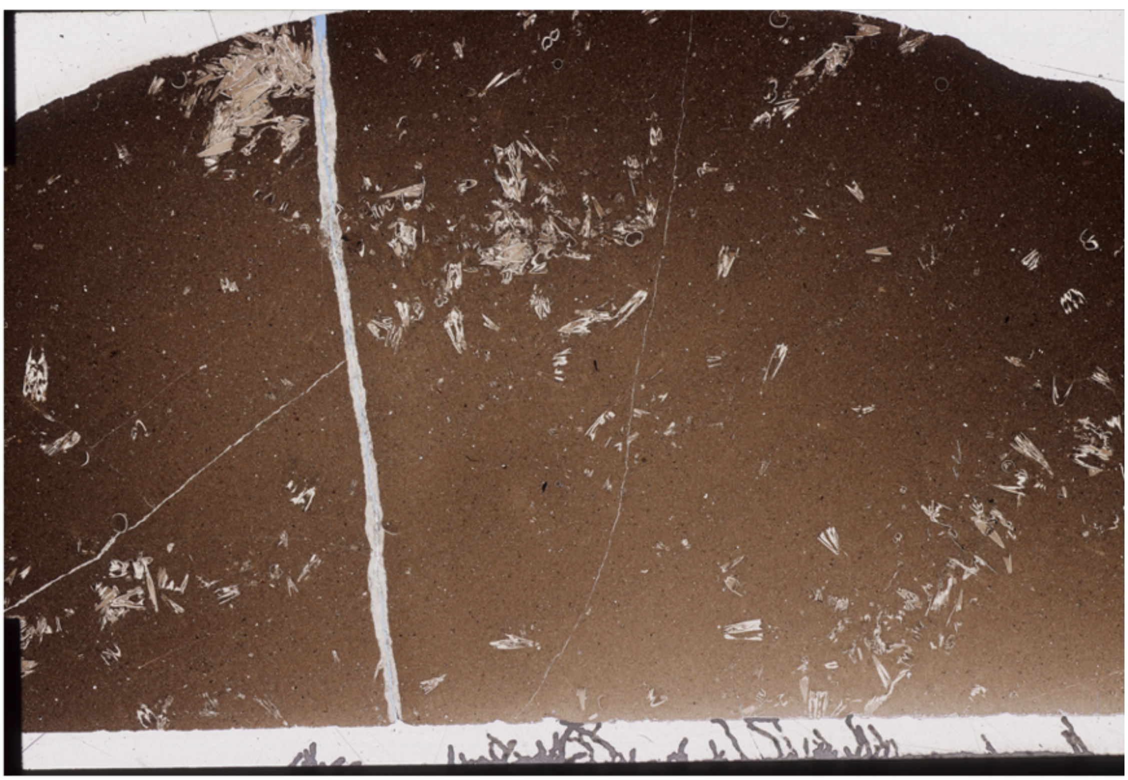

I-78 1945.00 m, Bedding plane thin section scan showing random orientation and accumulations of tentaculitid shells.

Intraclastic Lags

Thin continuous or discontinuous horizontal accumulations of intraclasts. Indicate likely bedload traction transport of the more proximally generated intraclasts.

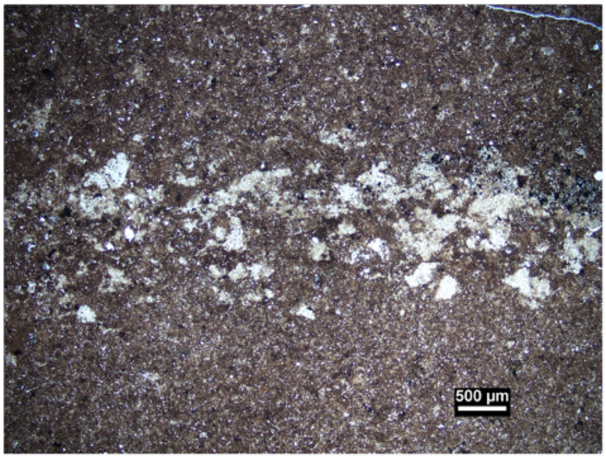

I-78 1846.00 m, an oblique-cut bedding plane photomicrograph of an intraclastic lag.

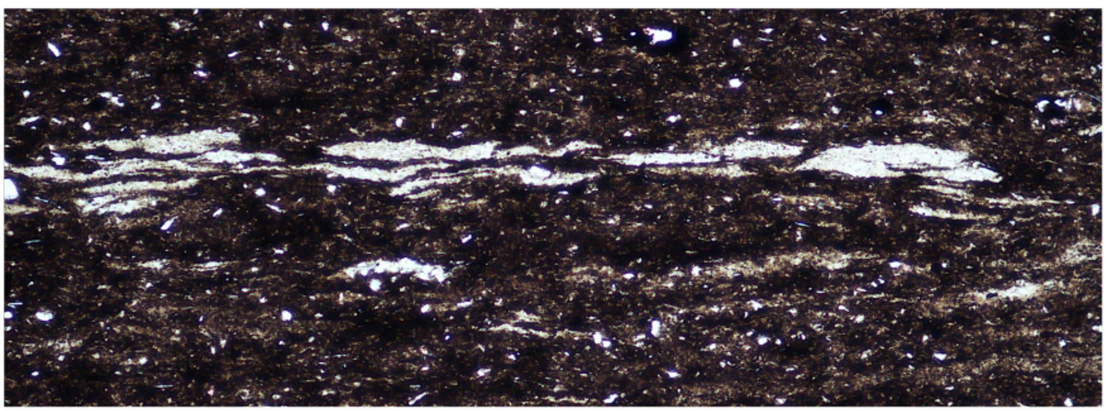

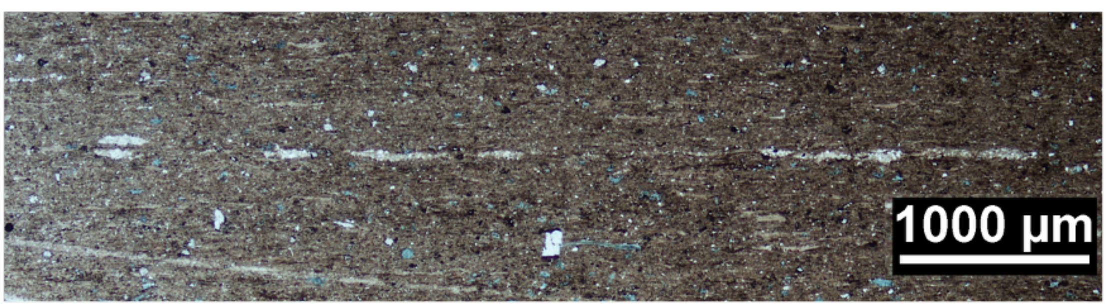

Photomicrograph showing intraclastic lags. **Upper:** undulating thickness continuous intraclastic lag (N-09 1798.67 m). **Lower:** discontinuous intraclastic lag. Lag dictates an otherwise unidentifiable bed contact (N-09 1699.77 m).

Winnowed Shell Lags

Variable thickness accumulations of fossil shell debris. Fossils can be intact or fragmented. The clay-poor nature of the beds indicates winnowing of the matrix portion by erosive bottom currents.

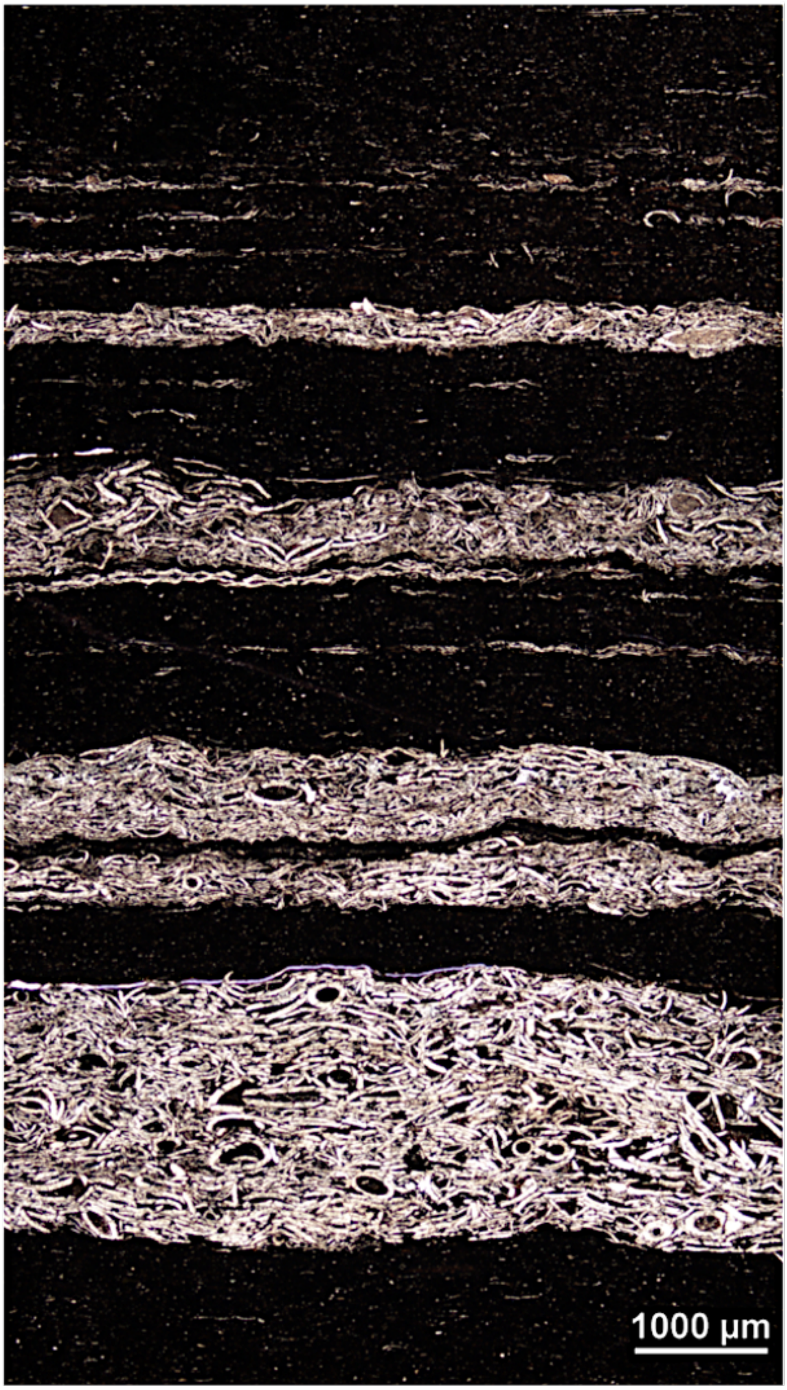

N-20 2092.95 m, Photomicrograph showing stacked winnowed shell lags (fossil shell material is made of calcite tentaculitid shells). Clay beds (dark beds) represent a return to fair weather conditions. In this case the winnowed beds may represent winnowed debrites.

Deformation Structures

Soft Sediment Deformation

Soft sediment deformation in the Horn River group is restricted to the Bell Creek member of the Hare Indian Formation. Deformation was only documented within the Intraclastic rich claystone microfacies.

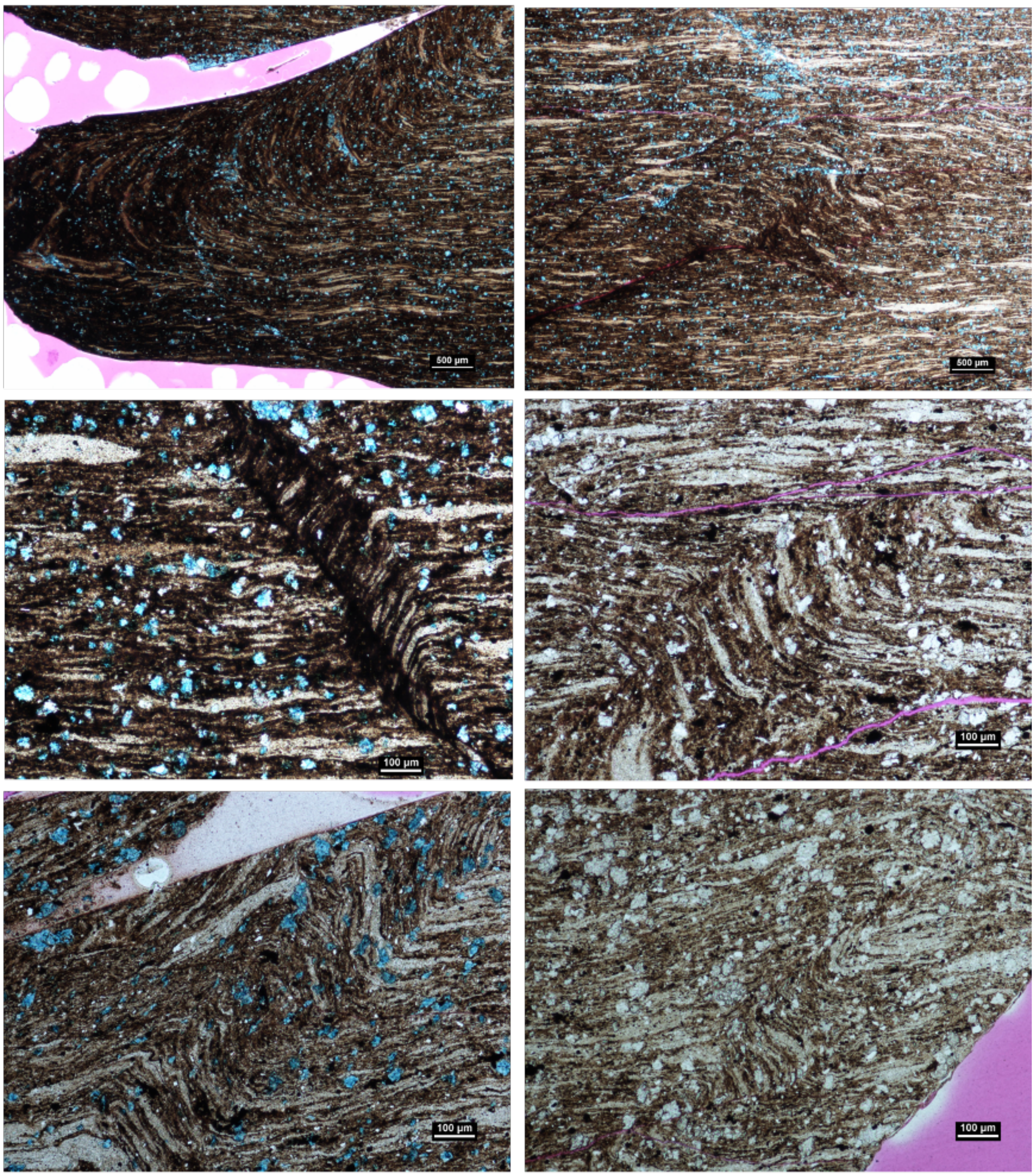

H-64 1275.38 m, Photomicrographs showing soft sediment deformation. All photos are from the same thin section.